

5-2013

## Targeting Histone Deacetylases (Hdac) For The Treatment Of Soft Tissue Sarcoma

Gonzalo Lopez

Follow this and additional works at: [https://digitalcommons.library.tmc.edu/utgsbs\\_dissertations](https://digitalcommons.library.tmc.edu/utgsbs_dissertations)



Part of the [Cancer Biology Commons](#), and the [Medicine and Health Sciences Commons](#)

---

### Recommended Citation

Lopez, Gonzalo, "Targeting Histone Deacetylases (Hdac) For The Treatment Of Soft Tissue Sarcoma" (2013). *Dissertations and Theses (Open Access)*. 351.  
[https://digitalcommons.library.tmc.edu/utgsbs\\_dissertations/351](https://digitalcommons.library.tmc.edu/utgsbs_dissertations/351)

This Dissertation (PhD) is brought to you for free and open access by the MD Anderson UTHealth Houston Graduate School at DigitalCommons@TMC. It has been accepted for inclusion in Dissertations and Theses (Open Access) by an authorized administrator of DigitalCommons@TMC. For more information, please contact [digcommons@library.tmc.edu](mailto:digcommons@library.tmc.edu).

**Targeting Histone deacetylases (HDACs) for the treatment of genetically  
complex soft tissue sarcoma**

by  
*Gonzalo Lopez,*

APPROVED:

---

Dina Lev, MD, Supervisory Professor

---

David J. McConkey, PhD

---

Juan Fueyo-Margareto, MD

---

Alexander J. F. Lazar, MD, PhD

---

Raphael E. Pollock, MD, PhD

APPROVED:

---

Dean, The University of Texas  
Graduate School of Biomedical Sciences at Houston

**Targeting Histone deacetylases (HDAC) for the treatment of soft tissue sarcoma**

A

DISSERTATION

Presented to the Faculty of  
The University of Texas  
Health Science Center at Houston

and

The University of Texas  
M.D. Anderson Cancer Center  
Graduate School of Biomedical Sciences

in Partial Fulfillment  
of the Requirements  
for the Degree of

DOCTOR of PHILOSOPHY

by

Gonzalo Lopez, MS

Houston, Texas

May 2013

## **Dedication**

I dedicate this work to my parents who have been a loving inspiration and support in my life, my sister and niece for their love and support during the good and bad times, and the rest of my family (aunts, uncles, cousins) and friends whom are also vital in my life.

I would also like to dedicate this work to loved ones and those whom I will never meet, who suffer or have suffered from cancer.

## **Acknowledgments**

I would like to personally thank Dr. Dina Lev for her consummate mentorship and loving support. She has not only been a huge inspiration, but a parental figure and friend.

Dr. Raphael Pollock has been a great mentor and has played a crucial supportive role. His dedication toward assisting in our writing and presentations are deeply appreciated.

My committee members (Dr. David McConkey, Dr. Juan Fueyo, Dr. Alexander Lazar, Dr. Dennis Hughes, Dr. Khandan Keyomarsi) have all been very supportive and extremely helpful in my work and during my development as a graduate student.

Dr. Keila Torres and Dr. Alexander Lazar have both been a joy to work with and I truly appreciate their exceptional support.

Sarcoma Research Center lab members, past and present, made the lab a pleasant place to work and grow as a student. Many life-long friends were made.

I would also like to acknowledge Dr. John C. Perez and Dr. Elda Sanchez for their mentorship and support during my time as an undergraduate and graduate student at the Natural Toxins Research Center. I had considered various majors from engineering to veterinary until I met these wonderful people whom guided me towards my current career.

And Shohrae Hajibashi for her loving friendship, even though was for a short time, will last forever in my heart.

**Targeting Histone deacetylases (HDAC) for the  
treatment of genetically complex soft tissue sarcoma**

Publication No. \_\_\_\_\_

Gonzalo Lopez, MS

Supervisory Professor: Dina Lev, MD

Histone deacetylase inhibitors (HDACi) are a new class of anticancer therapeutics; however, little is known about HDACi or the individual contribution of HDAC isoform activity in soft tissue sarcoma (STS). We investigated the potential efficacy of HDACi as monotherapy and in combination with chemotherapy in a panel of genetically complex STS. We found that HDACi combined with chemotherapy significantly induced anti-STS effects *in vitro* and *in vivo*. We then focused our study of HDACi in malignant peripheral nerve sheath tumor (MPNST), a subtype of highly aggressive, therapeutically resistant, and commonly fatal malignancies that occur in patients with neurofibromatosis type-1 (NF1) or sporadically. The therapeutic efficacy of HDACi was investigated in a panel of NF1-associated and sporadic MPNST cell lines. Our results demonstrate the NF1-associated cohort to be highly sensitive to HDACi while sporadic cell lines exhibited resistance. HDACi-induced productive autophagy was found to be a mode of resistance and inhibiting HDACi-induced autophagy significantly induced pro-apoptotic effects of HDACi *in vitro* and *in vivo*. HDACs are not a single enzyme consisting of 11 currently known isoforms. HDACs used in these studies inhibit a variety of these isoforms, namely class I HDACs which include HDAC1, 2, 3, and 8. Recently, HDAC8-specific inhibitors (HDAC8i) have been created and tested in

various cancer cell lines. Lastly, the potential therapeutic efficacy of HDAC8i was investigated in human (NF1-associated and sporadic) and NF1-associated murine-derived MPNST. HDAC8i abrogated cell growth in human and murine-derived MPNST cells. Similar to the pattern noticed with pan-HDACis NF1-associated cells, especially murine-derived, were more sensitive to HDAC8i compared to human sporadic MPNST cell lines. S-phase arrest was observed in human and murine MPNST cells, independent of p53 mutational and NF1 status. HDAC8i induced apoptosis in all cell lines tested, with a more pronounced effect in human and murine-derived NF1-associated cells. Most importantly, HDAC8i abrogated murine-derived MPNST xenograft growth *in vivo*. Taken together, these findings support the evaluation of pan-HDACi and isoform-specific inhibitors as a novel therapy to treat MPNST, including in combination with autophagy blocking combination regimens in particular for patients with sporadic MPNST.

## Table of contents

Approval signatures.....	i
Title page.....	ii
Dedication.....	iii
Acknowledgments.....	iv
Abstract.....	v
Table of contents.....	vii
List of Figure.....	x
List of Tables.....	xiii
Abbreviations.....	xiv
Chapter I: Introduction.....	1
Section 1: Genetically complex soft tissue sarcoma (STS).....	1
1.1    Epidemiology and etiology.....	1
1.2    Biological features of STS; patterns of disease.....	3
1.3    Histological classification.....	3
1.4    Diagnosis and treatment.....	4
1.5    Outcome.....	5
Section 2: Malignant peripheral nerve sheath tumors (MPNSTs); an aggressive subset of genetically complex STS.....	7
2.1    Epidemiology.....	7
2.2    Diagnosis and treatment.....	8
2.3    Outcome.....	9



<b>Section 3: HDACs and the role of broad spectrum and isoform-specific</b>	
<b>HDAC inhibitors in cancer .....</b>	<b>10</b>
<b>Chapter II: Hypothesis.....</b>	<b>17</b>
<b>Chapter III: Aims.....</b>	<b>18</b>
<b>Chapter IV: Significance.....</b>	<b>19</b>
<b>Chapter V: Materials and Methods .....</b>	<b>20</b>
<b>Chapter VI: Results.....</b>	<b>40</b>
<b>Section 1: The potential effects of HDACis on STS.....</b>	<b>40</b>
1.1 Effects as monotherapy.....	41
1.2 Combining HDACis with conventional chemotherapy.....	44
1.3 HDAC down-stream targets potentially contributing to the anti- STS and chemosensitivity effects of HDACis.....	60
<b>Section 2: HDACis elicit anti-MPNST effects.....</b>	<b>63</b>
2.1 The effects of HDACis on MPNST growth in vitro and in vivo.....	63
2.2 Potential mechanisms of sensitivity.....	71
<b>Section 3: (Macro)Autophagy as a mechanism of HDACi resistance in</b>	
<b>MPNST.....</b>	<b>74</b>
3.1 HDACis induce autophagosome accumulation in MPNST cells.....	74
3.2 HDACis induce productive autophagy in MPNST cells in vitro and in vivo.....	78
3.3 Autophagy is a mechanism of therapeutic resistance in MPNST.....	81

<b>Section 4: Molecular mechanisms underlying HDACi induced autophagy in MPNST.....</b>	<b>88</b>
4.1 Autophagy gene array results and confirmation.....	88
4.2 IRGM as an HDACi target enhancing autophagy.....	90
<b>Section 5: Aim 3 Effects of HDAC8 inhibition on MPNST.....</b>	<b>92</b>
5.1 Effects of HDAC8is on human and murine MPNST cells in vitro.....	92
5.2 Effects of PCI4 on the growth of human and murine MPNST in vivo.....	99
<b>Chapter VII: Discussion.....</b>	<b>103</b>
<b>Chapter VIII: Conclusions and future directions.....</b>	<b>119</b>
<b>References.....</b>	<b>122</b>
<b>Vita.....</b>	<b>145</b>

## List of figures

Figure 1. Anatomic distribution sarcomas.....	1
Figure 2. Cross-section of leg showing sarcoma differentiation.....	3
Figure 3. Natural history of MPNST development.....	7
Figure 4. Diagnosis of MPNST.....	8
Figure 5. Schematic depiction of HDAC isoforms and their sub-cellular localization.....	11
Figure 6. HDACi induces time- and dose-dependent increase in histone 3, histone 4, and tubulin acetylation in STS cells.....	40
Figure 7. STS cells are highly sensitive to HDACis.....	41
Figure 8. HDACi induces G2 arrest and apoptosis in STS cells.....	43
Figure 9. HDACi sensitizes STS cells to chemotherapy in vitro.....	44
Figure 10. Combining PCI2 with low-dose doxorubicin results in significant reduction SKLMS1 xenograft growth in SCID mice.....	47
Figure 11. Combining PCI2 with low-dose doxorubicin results in significant reduction HT1080 xenograft growth in SCID mice.....	49
Figure 12. Combining PCI2 with low-dose cisplatin or doxorubicin results in significant reduction of HT1080 pulmonary metastatic growth in nude mice.....	52
Figure 13. PCI2 induces p21 expression independent of p53 status in STS cells.....	54
Figure 14. PCI2 induces decreased Rad51 expression in STS cells.....	55
Figure 15. ChIP showing decreased Pol II binding to RAD51 gene and increased Pol II binding to P21 gene in response to PCI2.....	56
Figure 16. PCI2 regulates RAD51 and P21 promoter activity.....	57

Figure 17. PCI2-mediated transcriptional repression of Rad51 may be through E2F binding.....	58
Figure 18. PCI2 induces changes in gene expression in STS cell lines.....	62
Figure 19. MPNST642 cell line characterization.....	63
Figure 20. Growth-inhibitory effects of HDACis in MPNST cell lines.....	65
Figure 21. HDACis have an effect on MPNST cell line clonogenic potential... ..	66
Figure 22. HDACi induces apoptosis in a subset of MPNST cell lines.....	68
Figure 23. HDACi induces a time- and dose-dependent increase in target acetylation in MPNST cell lines.....	69
Figure 24. PCI2 inhibits the growth of MPNST xenografts exhibiting significant sensitivity in vivo.....	70
Figure 25. MPNST sensitivity to HDACi is not mediated through p53.....	72
Figure 26. NF1 knockdown sensitizes sporadic MPNST cells to PCI2.....	73
Figure 27. TEM images showing ultrastructural changes in MPNST cells in response to PCI2.....	74
Figure 28. HDACi induces and increase in LC3-II expression in MPNST.....	75
Figure 29. Cells stably transduced to express GFP-LC3 exhibited increased GFP puncta in response to HDACi.....	76
Figure 30. PCI2 induces autophagy in MPNST in vivo.....	76
Figure 31. TEM shows PCI2-induced autophagy and apoptosis in NF1-associated MPNST cells.....	77
Figure 32. HDACi induces autophagy in NF1-associated MPNST cells.....	77
Figure 33. PCI2 induces an increase acridine orange positive cells in MPNST cells.....	78
Figure 34. PCI2 induces productive autophagy in MPNST cells.....	79

Figure 35. HDACi induces productive autophagy in vitro and in vivo.....	80
Figure 36. Beclin1 knockdown sensitizes MPNST cells to PCI2.....	81
Figure 37. ATG5 knockdown sensitizes MPNST cells to PCI2.....	82
Figure 38. ATG7 knockdown sensitizes MPNST cells to PCI2.....	82
Figure 39. Pharmacological inhibition of autophagy sensitizes MPNST cells to PCI2.....	83
Figure 40. Pharmacological inhibition of autophagy enhances PCI2-induced apoptosis in MPNST cells.....	84
Figure 41. PCI2 combined with CQ reduces MPNST tumor growth in vivo.....	85
Figure 42. PCI2 combined with CQ enhances apoptosis in MPNST in vivo.....	85
Figure 43. PCI2 combined with CQ reduces lung metastases in vivo.....	87
Figure 44. PCI2 induces changes in autophagy-related genes in MPNST in vitro.....	89
Figure 45. PCI2 induces changes in autophagy-related genes in MPNST in vivo.....	89
Figure 46. HDACi increases IRGM mRNA and protein expression in MPNST.....	90
Figure 47. IRGM knockdown sensitizes MPNST cells to PCI2.....	91
Figure 48. PCI3/PCI4 do not increase histone and tubulin acetylation in MPNST.....	93
Figure 49. PCI3/PCI4 inhibits MPNST cell growth in vitro.....	94
Figure 50. PCI3/PCI4 abrogates MPNST cell colony formation capacity.....	96
Figure 51. PCI3/PCI4 induces S-phase cell cycle arrest in MPNST.....	97
Figure 52. PCI3/PCI4 induces apoptosis in MPNST.....	98
Figure 53. PCI4 had no effect on MPNST642 xenograft growth in vivo.....	100
Figure 54. PCI4 inhibits murine MPNST xenograft growth in vivo.....	101

**List of tables**

**Table 1. Antibodies.....22**

**Table 2. HDAC inhibitors.....24**

**Table 3. Kits.....25**

**Table 4. Primer sequences.....26**

**Table 5. Codelink oligo microarray analysis of PCI2-induced gene changes in  
STS cell lines.....60**

**Table 6. Human MPNST cell line panel characterization.....65**

## **Abbreviations**

ACD: autophagic cell death

ac.H3: acetylated histone 3

ac.H4: acetylated histone 4

BFA: Bafilomycin A1

BLI: bioluminescence

CQ: Chloroquine

ChIP: chromatin immunoprecipitation

DMSO: dimethyl sulfoxide

FACS: fluorescence-activated cell sorting

FDA: Food and Drug Administration

GFP: green fluorescent protein

HAT: histone acetyltransferase

HBSS: Hank's balanced salt solution

HDAC: histone deacetylase

HDACi: histone deacetylase inhibitor

HDACis: histone deacetylase inhibitors

HMBA: hexamethylene bisacetamide

IHC: immunohistochemistry

i.m.: intramuscular

i.p.: intraperitoneal

MPNST: Malignant peripheral nerve sheath tumor

NHF: normal human fibroblast

NLS: Nuclear localization sequence

NSC: normal human Schwann cells

PCI2: PCI-24781

PCI3: PCI-34051

PCI4: PCI-48012

PI: propidium iodide

qRT-PCR: quantitative real-time polymerase chain reaction

RT-PCR: reverse transcriptase polymerase chain reaction

SAHA: Suberoylanilide hydroxamic acid

s.c.: sub-cutaneous

SCID: Severe combined immunodeficiency

SEER: Surveillance Epidemiology and End Results



STS: Soft tissue sarcoma

TEM: transmission electron microscopy

TSA: Trichostatin a

TUNEL: Terminal deoxynucleotidyl transferase dUTP nick end labeling

WB: Western blot

## Chapter I: Introduction

### Section 1: Genetically complex soft tissue sarcoma (STS)

#### 1.1 Epidemiology and etiology

“Cancer” as a disease has been described and treated with methods of the time that date back to ancient Egypt around 1500 B.C. In the campaign against cancer it is important to identify that malignant disease is not a single entity. Sarcoma and carcinoma make up most solid tumors; however, sarcoma is not equal to carcinoma. Sarcomas are heterogeneous tumors that are different from other cancers based on

their germ layer origin, sarcoma arises from mesenchymal tissues and carcinoma arise epithelial tissues (1). Sarcoma is divided into sarcoma of the bone and soft tissue sarcoma (STS) which entail numerous subclasses based on the tissue of origin. STS have a ubiquitous distribution throughout the body with a higher propensity to develop in the lower extremities (**Fig. 1**). STS constitute 1% of all adult cancers and occur at a higher frequency in children at about 15% of all neoplasms. The incidence of this disease is about 10 – 12,000 new cases per year in

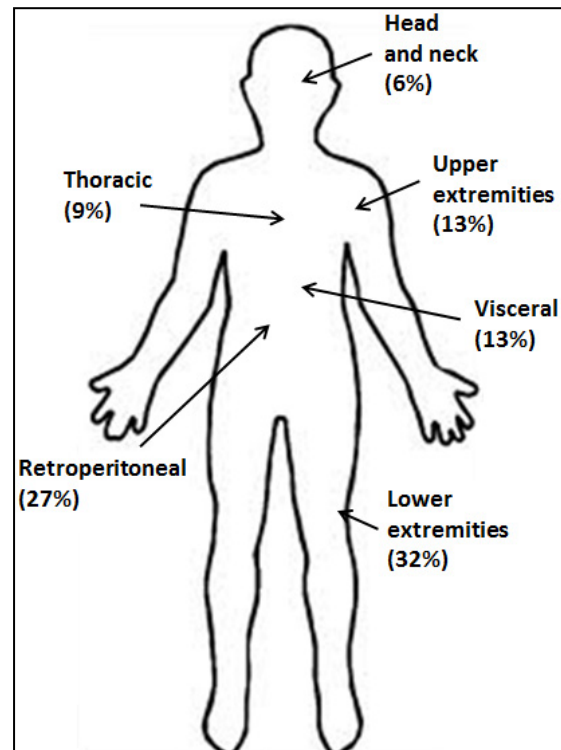


**Figure 1.** Anatomic distribution of sarcomas. Sarcomas can arise anywhere in the human body. This data is from UTMDACC Sarcoma Surgical Database (1996–2005). Modified from Figure 3, Lahat et al. Surg Clin N Am 2008 88,451–481.

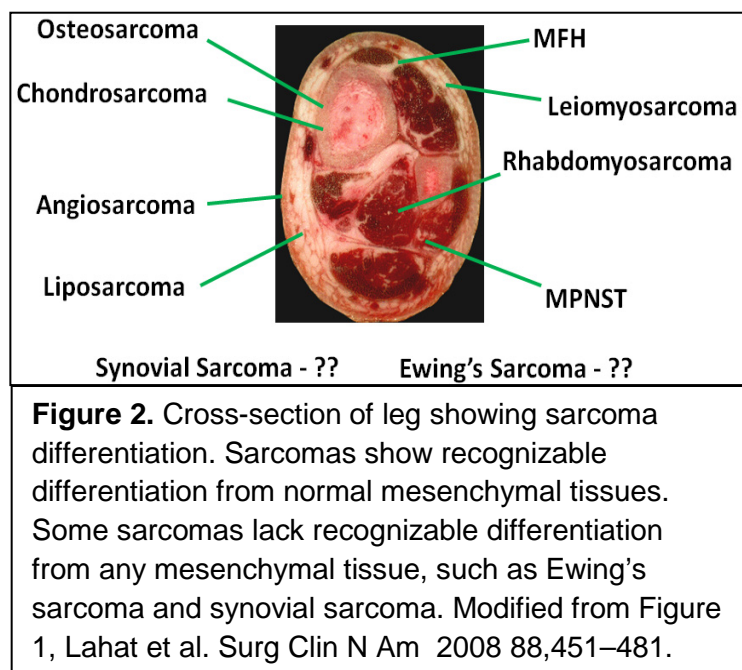
the US; where about 4,000 of these patients succumb to the disease (1). According to the Surveillance Epidemiology and End Results (SEER) database the incidence ratio of STS men are more likely to develop the disease compared to women (2). Relative to other cancers; not much is known about the epidemiology of STS (2). Sarcomas in general are a main cause of neoplastic-related deaths throughout the first two decades of life and account for the 5th leading cause of in men under 20 years old and the 4th leading cause of malignancy-related deaths in women under 20 years of age (3). STS are believed to arise spontaneously with little known about causes of the disease. In rare occasions inherited conditions are known to predispose some individuals to developing STS. One such condition, Li-Fraumeni syndrome comprises a *TP53* gene (encodes the protein p53) mutation potentially leading to the predisposing of malignant disease (4, 5). Retinoblastoma is a malignancy initiated by a mutation in the *RB1* gene. Mutation of this tumor suppressor may occur spontaneously or hereditarily (6, 7). The loss of tumor suppressor NF1 is a common feature in patients with MPNST. NF1 loss can occur under heritable or spontaneous conditions. While *NF1* loss is a major driving force for the development of MPNST, this malignancy can develop in patients without NF1 (8, 9). As it is known to be a risk for the development of many cancers, ionizing radiation increases the risk for the future development of MPNST. It is well documented that women previously treated with radiation for breast cancer, have a high chance of developing angiosarcoma (10). In light of these potential risk factors, individuals diagnosed with STS have >15% risk of developing a second cancer in the future.

### 1.2 Biological features of STS; patterns of disease

The biological behavior of STS is exceedingly variable. The histological grade of the tumor is a major prognosticator on the behavior of the disease. Mitotic count, cellularity, necrosis, differentiation, and stromal content are factors used to determine histological grade (11). Low grade STS have low mitotic rates with a low risk of metastatic disease, however, these low grade tumors have a high risk for local recurrence (12). High grade STS have a high mitotic rate, exhibit invasiveness to local tissue and have a high risk of metastatic spread. For patients with high grade STS, metastatic disease most commonly occurs in the lungs. While lung metastases commonly arise from primary tumors of the extremities, they can occur from nearly any primary site or histology (12, 13).

### 1.3 Histological classification

As previously alluded to, STS is not a single entity and comprises about 50 histological subtypes (14) (**Fig. 2**). Sarcomas are molecularly grouped into two cohorts: sarcomas with specific reciprocal translocations and relatively



simple karyotypes, and sarcomas with complex, unbalanced karyotypes, with no specific translocations. Simple karyotypic sarcomas make up about 1/3 of all sarcomas with 15 of these sarcomas of various histologies. These simple karyotypic sarcomas possess over 25 different translocations with a majority of the derived fusion genes creating aberrant chimeric transcription factors with the latter producing aberrant kinases (2). These translocations biologically translate into transcriptional deregulation or aberrant signaling which entail an important determinant toward a specific therapy. Complex karyotypic sarcomas make up about 2/3 of all sarcomas in adults with a dynamic biology consisting of aberrations such as genetic gains and losses, chromosomal instability, and telomere dysfunctions. Diagnostically, the fusion genes of simple karyotypic sarcomas make for excellent molecular markers whereas complex karyotypic sarcomas; due to their multiple aberrations do not have bona fide diagnostic molecular markers.

#### *1.4 Diagnosis and Treatment*

STS is typically diagnosed in individuals at a median age of 56 years of age. A small percentage (about 10%) of patients less than 20 years of age are diagnosed with STS where patients over 55 years of age make up about 50% of STS diagnoses (2). The signs and symptoms of STS are not specific where most patients present with a painless and palpable mass. In a third of the presented cases, STS-induced pain is observed (15). Sarcomas growing in the abdominal and pelvic cavities may progress undetected over long periods of time barring symptoms resulting in a delayed diagnosis. Timely diagnosis and referral are advantageous, as the size of the tumor at

presentation is an incessant variable for the possibility of recurrence and metastasis (15).

To date, STS are typically treated using a multidisciplinary approach which includes surgery, chemotherapy, and radiation. As we continue to grasp a better comprehension on the diverse natural history, biology, and therapeutic response of STS; personalized therapy based on histology will be commonplace. Currently, surgical resection occasionally supplemented with radiotherapy, of the tumor remains the mainstay of therapy. While surgery and radiotherapy are used to treat localized tumors, chemotherapy is used to control manifestations of systemic disease. For metastatic disease, chemo- and/or radiotherapy are used to help with problems associated with metastasis, whereas surgery at this unfortunate stage is used for palliation.

### *1.5 Outcome*

The prognosis for patients with STS is predicted using nomograms established on tumor grade, tumor size, depth of the tumor, diagnosis, and age of the patient (16). Local recurrence is associated with tumor grade, margins (from surgical resection), and/or the use of radiation (14). Low grade STS have a chance of relapse beyond the 5 year diagnosis; where High grade STS usually occur within the first 5 years upon diagnosis (14).

More than 50% of STS patients that develop distant metastasis regrettably succumb to the disease. Patients diagnosed with metastases have a median survival of about 12 months from diagnosis (17, 18).

One of the more dismally aggressive complex karyotypic STS is malignant peripheral nerve sheath tumors (MPNST).

*Section 2: Malignant peripheral nerve sheath tumors (MPNSTs); an aggressive subset of genetically complex STS*

*2.1 Epidemiology*

MPNST make up about 3-10% of STS (19-21). More than 50% of patients that present with MPNST develop the disease within the background of an inherited disease known neurofibromatosis type I (NF1); the latter portion of MPNST patients develop the disease sporadically (22). The molecular hallmark of neurofibromatosis is the loss of

the tumor suppressor neurofibromin, known for its role as a regulator of Ras (23-25). The incidence rate of developing MPNST among NF1 patients occurs at 8 – 12% (22). Among NF1 patients, loss of heterozygosity of

the *NF1* gene occurs resulting in the development of benign superficial neurofibromas. Thirty to forty percent of the neurofibromas that develop grow deep (plexiform) within the NF1 patient and have an 8 – 13% lifetime risk of undergoing malignant transformation to become MPNST (25) (**Fig. 3**).

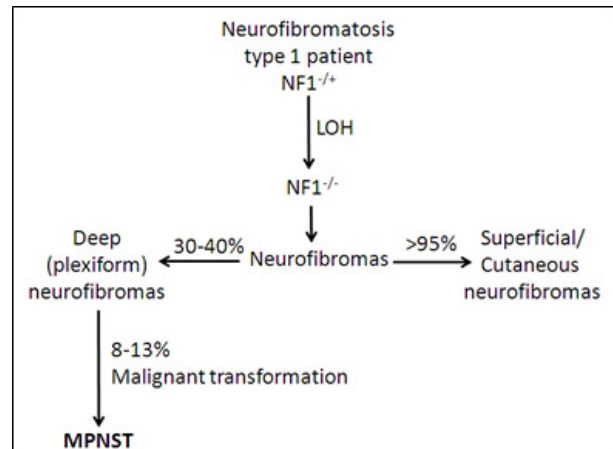


**Figure 3.** Natural history of MPNST development. In the natural history of this disease, a child is born with heterozygous loss of *NF1*. As they grow, there is a loss of heterozygosity in Schwann cells leading to formation of neurofibromas, which in most cases are superficial or dermal. About 30-40% will develop deep plexiform neurofibromas. 8-13% of these plexiform neurofibromas acquire the loss of other genes, such as p53 and undergo malignant transformation to become an MPNST.



Neurofibromin loss alone does not translate to the malignant transformation, as other molecular derangements must occur to induce malignant transformation (25).

## 2.2 Diagnosis and Treatment

Upon diagnosis of MPNST, patients undergo a physical examination with a thorough observation of their patient history. Prior to acquiring a biopsy of the potential tumor, a radiological image of the patient is obtained. A common imaging modality for MPNST is with the use of magnetic resonance imaging (MRI), which may differentiate neurogenic tumors from non-neurogenic tumors of the soft tissues. Despite the imperative diagnostic role of MRI, this method lacks the ability to distinguish benign

from malignant tumors, thus mandating the use of microscopic analysis of the tissue (**Fig. 4**). The criteria required to confirm the diagnosis of MPNST is based on one of the following settings: the tumor developed in association with a peripheral nerve or a plexiform neurofibroma, with features that are histologically compatible with MPNST. The

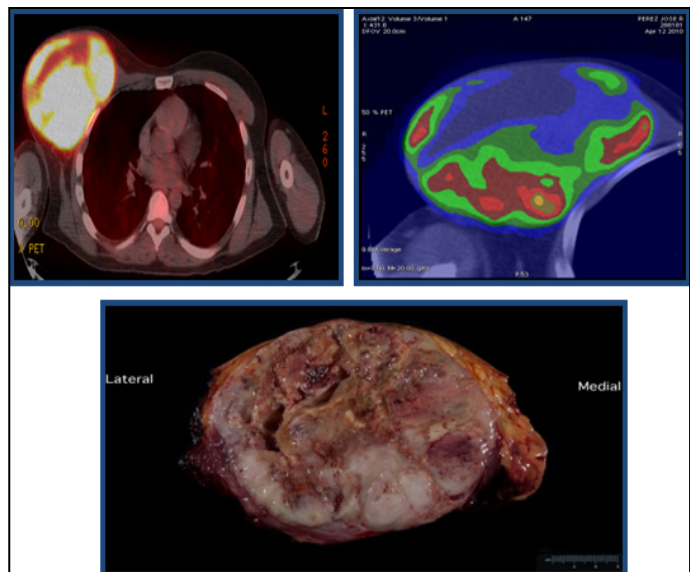


**Figure 4.** Diagnosis of MPNST . PET scan and gross cross-section of MPNST. (courtesy of Dr. Keila E. Torres, MD Anderson Cancer Center, Houston, TX)

tumor histologically resembles an MPNST which has developed in a NF1 patient, the tumor exhibits the definite histological characteristics of an MPNST (26, 27).

Complete surgical resection remains the primary mode of localized therapy. The aim of this front line treatment modality is complete surgical resection of the tumor with negative wide margins. Similar to its overall role in STS, systemic control of the disease by chemotherapy endures as a controversial therapy for MPNST (28-30).

### *2.3 Outcome*

Diagnosis of MPNST unfortunately translates into a dismal prognosis, where many of these patients have non-resectable disease upon presentation. Patients who are diagnosed with primary disease have a 10-year disease-specific survival at about 30%; however, this 10-year disease-specific survival drops to 26% in those with recurrent MPNST (28, 31). Patients with advanced disease (non-resectable and/or metastatic) respond poorly to chemotherapeutic intervention. The 5-year survival rate for patients with advanced disease is unfavorably at 20-50% (25), and the 10-year disease-specific survival is less than 8% (28).

Complex karyotypic sarcomas including MPNST have an array of molecular derangements, where targeting a single molecule among the vast derangements would not be a rational form of therapy. A therapeutic strategy to combat the heterogeneous nature of complex karyotypic STS would be ideal. Histone deacetylase

(HDAC) inhibition is one such strategy that has been shown to induce a multitude of anti-cancer effects.

### *Section 3: HDACs and the role of broad spectrum and isoform-specific HDAC inhibitors in cancer*

HDACs are a family of enzymes that deacetylate lysines on the core histones inducing the condensation of chromatin. Histone acetyltransferases (HAT) are the counterpart to HDACs as they acetylate lysine residues inducing an uncoiled conformation of chromatin. The balance of HDAC and HAT activity plays a significant role in epigenetics. This acetylation/deacetylation of lysine tails on histones was the initial consensus of HDACs and HATs (hence their name), however, various non-histone proteins, such as p53,  $\beta$ -catenin, Rb, NF $\kappa$ B, and E2F family members among various other protein substrates, were also discovered to be acetylated/deacetylated. Currently, eleven HDAC isoforms have been identified, including seven sirtuin isoforms (Nicotinamide adenine dinucleotide (NAD)<sup>+</sup>-dependent enzymes with deacetylase activity) in mammals (32, 33). HDACs have a catalytic domain that requires a metal ion (i.e. Zn, Fe) coordinates with oxygen of its carbonyl group to activate a water molecule with the support of histidine-aspartic acid for a nucleophilic attack resulting in the acetyl group to be removed from the target protein lysine residue. These isoforms (herein, only discussing HDAC isoforms), are organized into four classes based on sequence identity and domain organization (34, **Fig. 5**). Class I HDACs were initially believed to remain exclusively in the nucleus. However, HDAC3

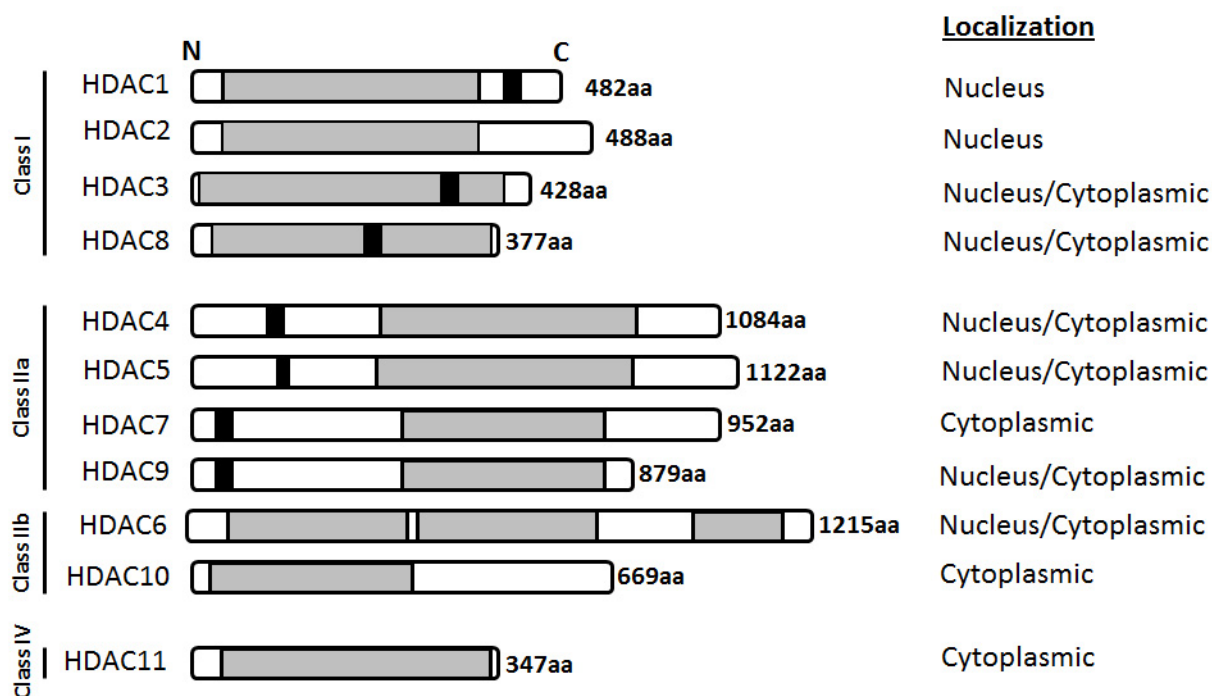


**Figure 5.** Schematic depiction of HDAC isoforms and their sub-cellular localization. Bars depict the length of each isoform. Amino acid (aa) length is depicted on the right of each bar. Grey depicts the metal ion-dependent catalytic domain. Black depicts the nuclear localization sequence (NLS). N = N-terminus, C = C-terminus. Left column represents the sub-cellular localization of each isoform.

and HDAC8 have been shown to be expressed in the nucleus and cytoplasm. Similar to HDAC3 and HDAC8, Class IIa and Class IIb HDACs have been shown to occur in both the nuclear and cytoplasmic compartments of various cells. HDAC6 and HDAC10 have both been shown to play a cytoplasmic role more so than a nuclear role. Class IV solely consists of HDAC11 which share similarities to Class I and II HDACs.

Mechanistically, HDACs work by chelating to the metal ion in the active site of individual HDAC isoforms inhibiting its deacetylation ability (35).

The first experiments with compounds shown to inhibit HDACs were conducted in murine erythroleukemia cells (MELC) by various groups. Differentiation of the MELC cells occurred when treated with DMSO (36), TSA (37) or hexamethylene

bisacetamide (HMBA) (38). Trichostatin A (TSA) is a natural, hydroxamate-based compound, which was first discovered to induce hyperacetylation of histones by inhibiting HDAC isoforms (37). From these observations, compounds that share structural similarity to TSA were created (38, 39).

Suberoylanilide hydroxamic acid (SAHA), similar in structure to TSA, is one of the early, synthetically available HDACis shown to hyperacetylate histones, induce differentiation and inhibit proliferation in cancer cells at nanomolar ranges (38). Since these initial evaluations, several other natural HDACi compounds have been discovered along with the development of various synthetic HDACis of different chemical backgrounds. Due to its efficacy in transformed cells, SAHA (Vorinostat/Zolinza) was the first HDACi approved by the FDA (Food and Drug Administration) for the clinical use against cutaneous T cell lymphoma (CTCL) (40, 41).

Since these promising effects, the monotherapeutic efficacies of HDACis are being evaluated in preclinical *in vitro* and *in vivo* models in a variety of malignancies of different histologies. Many preclinical studies have led way to the use of a variety of HDACis in clinical trials to evaluate the efficacy and toxicity of the drugs. Clinically, HDACis alone or in combination with another anti-cancer therapy (chemotherapy, radiotherapy) have generated promising anti-tumor activity. Currently, there are around 50 clinical trials evaluating the monotherapeutic efficacy of a variety of HDACis in cancers of various histology and more than 100 clinical trials evaluating the efficacy

of HDACis combined with various chemotherapeutic compounds

(<http://www.clinicaltrials.gov/>, <http://www.cancer.gov/clinicaltrials>).

The study of the efficacy of HDACis in sarcoma is limited. One of the earliest studies of HDACis in sarcoma occurred in 2002 where MS-275 was shown to have marked anti-cancer activity in pediatric osteosarcoma, malignant rhabdoid tumors, Ewing's sarcoma, and undifferentiated sarcoma (42). HDACis have also been shown to have superior efficacy in simple karyotypic soft tissue sarcomas including, synovial sarcoma (43-46), GIST (47), rhabdomyosarcoma (48-51) and complex karyotypic sarcomas such as fibrosarcoma (50, 52-54), leiomyosarcoma (50, 55), and MPNST (56, 57).

Most of the HDACis currently used are broad-spectrum/pan inhibitors and target many HDAC isoforms with a high affinity to Class I HDACs, namely HDAC1, 2, 3. Due to the broad spectrum inhibition of these compounds, not much is known regarding the individual contribution of each HDAC isoform toward various malignancies. Inhibiting a multitude of HDACs has side effects where isoforms important for the tumorigenic nature are inhibited while redundant HDAC isoforms are also blocked resulting in undesirable effects on normal physiology. Park et al. (58) showed that by specifically inhibiting (via siRNA KD) HDAC1, 6, and 8 but not HDAC4 decreased matrix metalloproteinase 9 (MMP9) expression and the invasive capacity of breast cancer cells. This observation further illustrates the importance of individual HDACs and their contribution toward certain malignancies; owing toward the development of inhibitors for individual HDAC isoforms.

Recently, the development of HDAC8-specific inhibitors has paved a way to understanding the contribution of certain isoforms individually. Currently, specific inhibitors for HDAC6 (e.g. tubacin, tubastatin a) and HDAC8 are the only two isoform specific compounds, where the development of specific inhibitors for isoforms are underway. HDAC8's structural uniqueness (59) from other class I HDAC isoforms has resulted in its isolation and subsequent crystallography structure, allowing for the development of specific inhibitors.

The *HDAC8* gene, located on the Xq13 chromosome, encodes a 377 amino acid long protein. Where classical class I HDACs are phosphorylated by casein kinase proteins, HDAC8 is phosphorylated at serine 39 by cyclic AMP-dependent protein kinase A (PKA) (60). Similar to other class I HDAC isoforms, HDAC8 possesses a nuclear localization sequence (NLS) in its catalytic domain. Unlike the ubiquitous distribution and expression of the other class I HDACs, HDAC8 has varying distribution among human tissues. HDAC8 has been shown to be at a higher expression in the brain and pancreas compared to HDAC1 and HDAC3, but at a lower expression level in other organs (i.e. heart, placenta, kidney, liver) compared to other class I HDACs (61, 62). Similar to other class I HDACs, HDAC8 expression is elevated in cancers of various histologies (61, 62).

To date, little is known about the role of HDAC8 in normal physiology and cancer. Its role in the hyperacetylation of histones remains controversial where HDAC8 has been shown to deacetylate histones 3 and histone 4 in certain cells types, but not in others (63, 64). Among the few deacetylation targets, HDAC8-mediated deacetylation of

estrogen-related receptor alpha (ERR $\alpha$ ) enhanced its DNA binding affinity, thus enacting its role in transcriptional regulation of various processes (65). Non-deacetylation roles of HDAC8 have been identified. Phosphorylated-HDAC8 was shown to interact with human ever shorter telomeres 1B (hEST1B) by recruit Hsp70 to a complex that inhibits C-terminal heat shock protein interacting protein (CHIP), an E3 ubiquitin ligase. This pHDAC8-mediated protection of hEST1B was independent of its acetylation state. Recent studies have shown that cytoplasmic HDAC8 interacts with smooth muscle alpha-actin ( $\alpha$ -SMA) in muscle cells undergoing differentiation (66). Cytoplasmic HDAC8 has also been shown to have a diagnostic role in uterine mesenchymal tumors (67).

Recently, three compounds with high affinities toward HDAC8 have been developed and are in current cancer-related studies: compound 2/HDAC inhibitor XIX (commercially available), PCI-34051, PCI-48012.

HDAC8-specific inhibitor PCI-34051 (PCI3) is a potent inhibitor with a 4,200-fold selectivity over other HDAC isoforms. This compound was shown to induce apoptosis in T-cell lymphoma and leukemia cells lines, but not in cells derived from other B-cell or solid tumor cells lines (i.e. lung, colon, cervix, glioma, colon, breast ovarian). However, distinct from pan-HDACis, PCI3 did not induce the hyperacetylation of histones or tubulin in the cell lines tested (68).

In neuroblastoma, HDAC8 expression was shown to correlate with an unfavorable outcome (69). Compound 2, a linkerless hydroxamate HDAC inhibitor with high specificity to HDAC8 was recently created (70), and tested on neuroblastoma cell



lines. Knockdown of HDAC8 as well as with the use of compound 2 induced the differentiation of neuroblastoma cell lines by stimulating the outgrowth neuritic-like structures. Inhibition of HDAC8 either by knockdown or by compound 2 abrogated neuroblastoma cell line proliferation, but did not induce apoptosis. HDAC8 inhibition-induced expression of p21Waf1/Cip1 and NTRK1/TrkA was associated with the neuroblastoma cell line growth inhibition (69, 71). Interestingly, both neuroblastoma and MPNST derive from neural crest cell origins, suggesting a potential role for HDAC8 in the progression of these malignancies.

## Chapter II: Hypothesis

HDAC inhibition is a potentially novel therapy for the treatment of genetically complex STS.

## Chapter III: Aims

Aim 1: To preclinically determine the potential relevance of HDAC inhibition as a therapeutic modality for the treatment of genetically complex STS.

1.1: Determine the effect pan-HDACi as a single agent

1.2: Evaluate the role of pan-HDACi in combination with chemotherapy

Aim 2: To test the efficacy of pan-HDACi for the treatment of MPNST

2.1 Determine the efficacy of pan-HDACi *in vitro* and *in vivo*

2.2 Identify the mechanisms of sensitivity and resistance to HDACi

Aim 3: To assess the impact of HDAC8 inhibition on MPNST growth and pro-tumorigenic phenotype

3.1 Determine the effect of HDAC8 inhibition *in vitro*

3.2 Ascertain the effect of HDAC8 inhibition *in vivo*

## Chapter IV: Significance

There is a critical need for novel therapeutic strategies to improve the dismal outcome of patients suffering from high grade STS and aggressive subtypes such as MPNST. In this pre-clinical study we show the promising efficacy of pan- and isoform-specific HDAC inhibition in a panel of genetically complex STS, namely MPNST. This report also gives insight into the molecular contributors influencing therapeutic resistance that can be circumvented by rational combination therapies. Initial findings from this study have been factorial in the launch of clinical trials evaluating the effect of pan-HDAC inhibition combined with chemotherapy for patients with high grade sarcomas. This report emphasizes the importance of these preclinical models for the utility of HDAC inhibition in sarcoma, a malignancy with limited therapeutic avenues.

## Chapter V: Materials and Methods:

### *Cell lines*

Human HT1080 (fibrosarcoma), RD (rhabdomyosarcoma), and SKLMS1 (leiomyosarcoma) STS cells were obtained from the American Type Culture Collection. Primary normal human fibroblast (NHF) cultures were acquired from Promocell GmbH. MPNST cell lines utilized in these studies included the NF1-associated: ST88 (provided by Dr Jonathan Fletcher, Brigham and Women's Hospital, Boston, MA), T265 (provided by Dr George De Vries, Hines VA Hospital, Hines, IL), S462 (provided by Dr Brian Rubin, Cleveland Clinic, Cleveland, OH) and the MPNST642 isolated in our laboratory and the sporadic MPNST cell lines: STS26T (provided by Dr Steven Porcelli, Albert Einstein College of Medicine, Bronx, NY) and MPNST724 (provided by Dr Jonathan Fletcher) and were propagated and maintained as previously described (72). Murine-derived MPNST cell lines, NF1-TG-05 and -09 were established in our laboratory and MPNST6IEP and MPNST6IEP4 were provided by Dr. Luis Parada (The University of Texas Southwestern Medical Center, Dallas TX). Primary human adult Schwann cell (NSC) cultures, used as controls for MPNST experiments were established from human cauda equina nerves were provided by Dr Patrick Wood (Miami Project, University of Miami, Miami, FL) and maintained as previously described (73). ST88, STS26T and MPNST724 cells were stably transfected to express GFP-LC3; overexpressing cells were FACS-sorted on the basis of green fluorescent protein (GFP) expression. Cells were cultured in DMEM

supplemented with 10% FBS (Life Technologies). DNA fingerprinting (short tandem repeat) was conducted for all cell lines less than 6 months prior to the conduct of the studies, confirming that no cross-contamination has occurred.

## Antibodies

<u>mAb Name</u>	<u>Company</u>	<u>Application</u>	<u>Ref</u>
Rad51	Santa Cruz	WB	50
Ac.H3	Millipore	WB	50
Ac.H4	Millipore	WB	50
Ac.tubulin	Sigma	WB	50
$\beta$ -actin	Santa Cruz	WB	50
CD31	BD Biosciences	IHC	50
PCNA	Dako Cytomation	IHC	50
E2F1	Santa Cruz	ChIP	50
E2F4	Santa Cruz	ChIP	50
RNA polymerase II	Covance	ChIP	50
IgG	Santa Cruz	ChIP	50
CTGF	Santa Cruz	WB	50
CHK1	Cell signaling	WB	50
Mouse IgG	Santa Cruz	ChIP	50
Rabbit IgG	Santa Cruz	ChIP	50
LC3B	Cell Signaling	WB	56
GFP	Santa Cruz	WB	56
Beclin 1	Santa Cruz	WB	56
p53	Santa Cruz	WB	56
Ki67	MIB-1	IHC	56

IRGM	Abcam	WB	56
PARP	Abcam	WB	56
Caspase 3	Cell signaling	WB	56
NF1	Santa Cruz	WB	56

Table 1. Antibodies

Antibodies were used for WB, ChIP, and IHC. Secondary antibodies included horseradish peroxidase–conjugated (Universal kit HRP; Biocare Medical) and fluorescent secondary antibodies (anti-rabbit Alexa488 and anti-mouse Alexa 594; Jackson Immuno Research). Other reagents included CytoQ FC Receptor block (Innovex Bioscience), Hoechst 33342 (Polysciences), and propyl gallate (ACROS Organics).



### Drugs/compounds

Compound	Class	Specificity
PCI-24781 (PCI2)	Hydroxamate	Broad spectrum
SAHA	Hydroxamate	Broad spectrum
MS-275	Benzamide	Class I
PCI-34051 (PCI3)	Hydroxamate	HDAC8
PCI-48012 (PCI4)	Hydroxamate	HDAC8

Table 2. HDAC inhibitors used in this study were reconstituted in DMSO for *in vitro* studies. For *in vivo* use, PCI2 was dissolved in 50mM Sodium lactate, pH 4.2; PCI4 was dissolved in 0.5% methylcellulose.

Chemotherapeutic agents used in this study: Doxorubicin (Ben Venue Lab) and cisplatin (Sicor) were obtained from the MD Anderson Cancer Center Pharmacy. Autophagy inhibitors: Bafilomycin A1 (Sigma; B1793) was reconstituted in DMSO and was only used for *in vitro* studies; Chloroquine (Sigma; C6628) was reconstituted in sterile deionized water and used for *in vitro* and *in vivo* studies.

## Kits

Kit	Company	Ref.
CellTiter96 Aqueous Non-Radioactive Cell Proliferation Assay kit	Promega	50, 56
Annevin V	BD Biosciences	50, 56
cDNA 1st strand synthesis	Roche	50, 56
Qiagen RNeasy® Mini Kit	Qiagen	50
TUNEL	Promega	50, 56
ChIP	Upstate	50
Stratagene Quick Change mutagenesis kit	Stratagene	50
Ras activity assay	Cell Biolabs	56
Autophagy RT2 Profiler PCR Array	SA Biosciences	56

Table 3. Kits used in these studies were utilized per the manufacturer's instructions.

## Cell culture based assays

### Western Blot

Western blot analysis was performed by standard methods. Briefly, 25 - 50µg of proteins extracted from cultured cells were separated by SDS-PAGE and transferred onto nitrocellulose membranes. Membranes were blocked and blotted with relevant antibodies. HRP-conjugated secondary antibodies were detected by enhanced chemiluminescence (Amersham Biosciences, Plc.).

### Reverse transcriptase PCR (RTPCR) and Real time PCR (qRTPCR)

These experiments were conducted as we have previously described (74). Primers used are depicted in the table below:

Gene	Forward primer	Reverse primer
<i>*Rad51</i>	TGGCCCACAACCCATTTTAC	TCAATGTACATGGCCTTTCTTCAC
<i>GAPDH</i>	GAGCCACATCGCTCAGAC	CTTCTCATGGTTCACACCC
<i>Rad51</i>	GAGGTGAAGGAAAGGCCATGT	GGGTCTGGTGGTCTGTGTTGA
<i>p21</i>	GGAAGACCATGTGGACCTGT	AATCTGTCATGCTGGTCTGC
<i>Actin</i>	CAGCCATGTACGTTGCTATCCAGG	AGGTCCAGACGCAGGATGGCATG
<i>IRGM</i>	CCCTTCGAAACACAGGACAT	AGTTCTCCAGGGTTGTGGTG
<i>CXCR4</i>	GGTGGTCTATGTTGGCGTCT	TGGAGTGTGACAGCTTGGAG
<i>TMEM74</i>	TGACCAGGCAGATACAGCAG	GTGGAGAAGTCCTGGTGGAA
<i>NFkB1</i>	CCTGGATGACTCTTGGGAAA	TCAGCCAGCTGTTTCATGTC
<i>ATG5</i>	TGGGGTGGATATAGGGCATA	GACCTGGAGCCAATGAAAAA
<i>ATG7</i>	ACCCAGAAGAAGCTGAACGA	CTCATTTGCTGCTTGTTCCTCA

Table 4. Primer sequences used in these experiments. PCR primers for both assays

were designed using primer 3 software. Total RNA was isolated from cultured

STS/MPNST cells using TRIzol reagent (Invitrogen) per manufacturer's instructions.

Total RNA (1µg) was reverse transcribed using SuperScript III reverse transcriptase (Invitrogen) and 2µL of the product were used as templates. The PCR reaction mixture contained 2× PCR Master Mix (Promega), 0.2µM of primers (each 0.5µM), and 2µL cDNA. \**Rad51* primers for RT-PCR. All other primers were designed for qRT-PCR.

### *Tumor growth assays*

#### *MTT (3-(4,5-dimethylthiazol-2-yl)-2,5-diphenyltetrazolium bromide) assay*

Cell growth assays used CellTiter96 Aqueous Non-Radioactive Cell Proliferation Assay kit (Promega) per the manufacturer's instructions. Growth rates were analyzed 48 - 96 h after HDACi (pan-HDACis: PCI-24781/SAHA/MS-275; HDAC8is: PCI-34051, PCI-48012) treatment and with doxorubicin or cisplatin alone or combined with HDACi; several administration sequences were evaluated: 24 h pretreatment with PCI2 followed by the addition of chemotherapy for 24 h and conversely, pretreatment with chemotherapy followed by PCI2 as well as treatment with both compounds concomitantly for 24 h. Absorbance was measured at 490 nm wavelength; treated cell absorbance values are presented as a percentage of untreated cell absorbance.

### *Clonogenic assay*

STS and MPNST cells were plated at 100-200 cells per well in 6-well culture plates. 24 h after plating, the cells were treated with DMSO (control) and varying concentrations of HDACi (pan-HDACis: PCI-24781/SAHA/MS-275; HDAC8is: PCI-34051, PCI-48012) for 24 h or continuous treatment. In combination studies, MPNST cells were first treated with an autophagy inhibitor (BFA/CQ) for 24 h then combined with HDACi for an additional 24 h. After combination therapy the drugs were removed and fresh media was added to the test wells; cells remained in fresh media (changed every 48 h) for 10 days. After 10 days, the cells were stained with a 6% glutaraldehyde, 0.5% crystal violet solution for 30 min. Staining solution was decanted from each well and cells washed with deionized H<sub>2</sub>O. Individual colonies retaining staining solution were counted.

### *Cell cycle FACS analysis*

Cells were treated with pan-HDACis (PCI-24781/SAHA) or HDAC8is (PCI-34051/PCI-48012) for varying periods. Propidium iodide/fluorescence-activated cell sorting (FACS) analysis was conducted as described (75).

### *Apoptosis assays*

Apoptosis was measured using the Apoptosis Detection kit I (BD Biosciences, San Jose, CA) per manufacturer's recommendations. As a standard,  $1 \times 10^6$ /mL of cells per treatment condition (time and dose as indicated) were fixed and stained with 5  $\mu$ L Annexin V–FITC (BD PharMingen, San Diego, CA) and 5  $\mu$ L propidium iodide (Sigma, St Louis, MO). Flow cytometric analysis was performed for  $1 \times 10^4$  cells and analyzed by FACScan (Becton Dickinson, Franklin Lakes, NJ) using a single laser emitting excitation light at 488 nm. Data were analyzed by CellQuest software (Becton Dickson, Franklin Lakes, NJ). To confirm annexin V-FITC FACS results, WBs were conducted on samples similarly used for annexin V-FITC FACS. Westerns were blotted for apoptotic markers: cleaved caspase 3 and/or cleaved PARP.

### *Transfection procedures*

siRNAs (pools targeting: beclin, ATG5, ATG7, IRGM, p53, and control non-targeting constructs, Thermo Scientific, Dharmacon) were introduced into cells using X-tremeGENE (Roche) per manufacturer's instructions. Briefly,  $2 \times 10^5$  cells were plated in each well of a six-well plate and incubated overnight. A mixture of siRNA (20nM) and X-tremeGENE diluted in Dulbecco's modified Eagle medium (DMEM) was added for 24 h, followed by incubation in regular medium. Cells were harvested at indicated time points for specific experiments.

### *p53 transfection*

Adp53 and AdLacZ adenoviruses were produced and titered by the Vector Core Laboratory at M.D. Anderson Cancer Center. Transfection procedures were conducted as we have previously described (76).

### *Autophagy assays*

### *Transmission electron microscopy (TEM)*

MPNST cells were grown in 6-well culture plates and treated with PCI2 (1 $\mu$ M) or DMSO alone for 24, 48, or 72 h and then fixed for one hour with a solution containing 3% glutaraldehyde plus 2% paraformaldehyde in 0.1M cacodylate buffer (pH 7.3). After fixation, the samples were post-fixed in 1% OsO<sub>4</sub> in the same buffer for 30min then stained with 1% uranyl acetate. Representative areas were chosen for ultrathin sectioning and electron microscopic viewing (JEM 1010 transmission electron microscope; JEOL, Peabody, MA), as previously described (77). Digital images were also obtained (AMT imaging system; Advanced Microscopy Techniques Corp., Danvers, MA). Three replicates were performed for each experiment.

### *Acridine orange staining and FACS analysis*

Autophagy was evaluated in MPNST cell lines by the staining of acidic vesicular organelles as previously described (78, 79). Briefly, MPNST cell lines were treated with pan-HDACis or DMSO (control). 48 h later, cells were stained with acridine orange (1 µg/mL; Sigma-Aldrich) for 15 min; samples were examined and images were taken using a fluorescence microscope. For further quantification, cells were treated and stained as above, trypsinized, and analyzed via flow cytometry. Green (510-530nm) and red (>650nm) fluorescence emission from  $2 \times 10^4$  cells illuminated with blue (488nm) excitation light was measured using FACS Calibur (Becton Dickinson) using CellQuest software.

### *LC3 conversion*

Conversion of soluble LC3-I to lipid bound LC3-II is associated with the formation of autophagosomes. Cleavage of LC3 at the carboxy terminus immediately following synthesis yields the cytosolic LC3-I form. During autophagy, LC3-I is converted to LC3-II through lipidation by a ubiquitin-like system involving Atg7 and Atg3 that allows LC3 to become associated with autophagic vesicles. The presence of LC3 in autophagosomes and the conversion of LC3 to the lower migrating form LC3-II have been used as indicators of autophagy. WB for LC3 demonstrating enhanced expression of LC3B-II (normalized to actin) is an indicator of increased number of autophagosomes. The inhibitors chloroquine and bafilomycin block the last stages of



productive autophagy thus will result in autophagosome accumulation; WB for LC3B-II in the presence of these inhibitors is expected to show increased LC3B-II levels (normalized to actin). Combining chloroquine or bafilomycin with compounds that enhance productive autophagy is expected to show further increase in LC3B-II expression.

#### *GFP-LC3 puncta*

MPNST cells were stably transfected to express GFP-LC3 (STS26T, MPNST724, ST88); overexpressing cells were FACS-sorted on the basis of green fluorescent protein (GFP). The presence and images of GFP-LC3 puncta was observed using fluorescent microscopy.

#### *GFP cleavage assay*

When GFP-LC3 is delivered to a lysosome the LC3 part of the chimera is sensitive to degradation, whereas the GFP protein is relatively resistant to hydrolysis. Therefore, the appearance of free GFP on WB (blotted for GFP) can be used to monitor lysis of the inner autophagosome membrane and breakdown of the cargo, indicative of productive autophagy (79). Lysate preparation and western blotting of GFP-LC3 cells samples were conducted as mentioned above.

## *Therapeutic animal experiments*

### *Effect of monotherapy on local xenograft growth*

All animal procedures and care were approved by the MD Anderson Cancer Center Institutional Animal Care and Usage Committee. Animals received humane care as per the Animal Welfare Act and the NIH "Guide for the Care and Use of Laboratory Animals." Animal models were utilized as previously described (78). Trypan blue staining confirmed viable cells (SKLMS1 or HT1080 cells  $1 \times 10^6$ /0.1 mL HBSS/mouse; STS26T, MPNST724, or MPNST642 cells  $1-2 \times 10^6$ /0.1 mL HBSS/mouse; MPNST6IEP4 cells  $1 \times 10^6$ /0.1 mL HBSS/mouse) were injected into the flank (SKLMS1 i.m., HT1080, STS26T, MPNST724, MPNST642, MPNST6IEPVI s.c.) of 6-wk-old female SCID mice (MPNST cells were injected into hairless SCID mice), growth was measured twice weekly. When average tumor volumes reached 100 mm<sup>3</sup>, the mice were assigned to treatment groups (7-8 mice/group). STS/MPNST cells were allocated into 2 treatment arms: Vehicle; HDACi/HDAC8i (PCI2 [25-50mg/kg BID 5X d/wk, i.p.]; PCI4 [20mg/kg BID 5X d/wk, i.p.]). PCI2/PCI4 dose and treatment schedules were determined per company recommendations. The mice were followed for tumor size and body weight and sacrificed when control group tumors reached 1.5 cm average largest dimension. Tumors were resected, weighed, and frozen or fixed in formalin and paraffin-embedded for immunohistochemical studies.

### *Effect of monotherapy on autophagy*

MPNST724 and STS26T GFP-LC3 cells were injected into the flank of hairless SCID mice s.c. When palpable tumors reached average diameter ~10mm, STS26T GFP-LC3 xenografts were treated with either vehicle or PCI2 (25mg/kg), and mice were euthanized 2, 4, and 6 h after treatment. MPNST724 GFP-LC3 xenografts (when average diameter ~10mm) were allocated into four treatment arms: Vehicle, PCI2 (25mg/kg), chloroquine (50mg/kg), PCI2 + CQ. Mice were treated with CQ a day prior to combining with PCI2. Mice from these groups were euthanized after 24 h treatment (groups receiving CQ were treated with this compound for 48 h). Resected tumors were processed for lysate and analyzed on WB.

### *Effect of monotherapy on metastatic growth*

HT1080GL (for studies in Lopez et al. 2009) or STS26TGL (for studies in Lopez et al. 2010) cells (stably expressing green fluorescent protein/Luciferase; GL) were tail vein injected, resulting in experimental lung metastases that could be followed by bioluminescence. A similar experimental design used for local growth experiments were used for lung metastasis experiments. Treatment was initiated when bioluminescence showed established lung metastases. The mice were followed and euthanized when bioluminescence suggested control group had significant pulmonary tumor load. Lungs were resected, weighed, and fixed in formalin for the creation of paraffin blocks.

### *Combined HDACis with conventional chemotherapy*

For local growth studies, SKLMS1 or HT1080 cells ( $1 \times 10^6$ /0.1 mL HBSS/mouse) were injected s.c. into the flank of 6-wk-old female SCID mice; growth was measured twice weekly. When average tumor volumes reached  $100 \text{ mm}^3$ , the mice were assigned to treatment groups (7-8 mice/group). STS cells were allocated into 4 treatment arms: 1) vehicle; 2) doxorubicin/cisplatin (1.2mg/kg/biweekly and 2 mg/kg/biweekly, respectively, i.p.); 3) PCI2 (50mg/kg BID 5X d/wk, i.p.); and 4) PCI2 + chemotherapy (PCI2 initiated 24 h before chemotherapy in all cases). PCI2 dose and treatment schedules were determined per company recommendations. The mice were followed for tumor size and body weight and sacrificed when control group tumors reached 1.5 cm average largest dimension. Tumors were resected, weighed, and frozen or fixed in formalin and paraffin-embedded for immunohistochemical studies.

For lung metastasis model, HT1080GL cells were used. Lung metastasis models were conducted as mentioned above.

### *Combined HDACi with autophagy blockade*

For experiments evaluating effect of treatment on local tumor growth trypan blue staining confirmed viable MPNST cells (MPNST642, MPNST724 and STS26T;  $1-2 \times 10^6/0.1$  mL HBSS/mouse) were used. Cell suspensions were injected subcutaneously into the flank of six week old female hairless SCID mice (n =10/treatment group) and growth was measured twice weekly; after establishment of palpable lesions (average diameter >5mm) mice were assigned to treatment groups as described below. An experimental lung metastasis MPNST model was used to evaluate metastases' growth. STS26T cells ( $1 \times 10^6/0.1$  mL HBSS/mouse) were injected into the tail vein of female SCID mice. Ten days after injection (a time-point by which 95-100% of mice develop established lung metastases) mice were allocated to treatment groups as per below. Therapeutic regimens included a four armed study: 1) DMSO; 2) PCI2 (25mg/kg/d for five days/week); 3) chloroquine (50mg/kg/d for five days a week); and, 4) combination of PCI2 and chloroquine. In the latter studies, including a chloroquine arm, this drug was initiated a day prior to PCI2 treatment. Mice were followed for tumor size, well-being, and body weight and sacrificed when control group tumors reached an average of 1.5 cm in their largest dimension. Tumors were resected, weighed, and frozen or fixed in formalin and paraffin-embedded for immunohistochemical studies. For lung metastasis studies mice were followed for body weight and well-being and sacrificed after two weeks of treatment. Lungs were resected, evaluated macroscopically for tumor load and weighed.

## *Tissue based experiments*

### *Immunohistochemistry (IHC)*

IHC and terminal deoxyribonucleotide transferase–mediated nick-end labeling (TUNEL) assays were conducted on paraffin and frozen sections, respectively. Conventional H&E staining was done (MD Anderson core facility) and examined by light microscopy. IHC was done using anti-Ki67 (1:500; DAKO Carpinteria, CA), anti-PCNA (1:500; DAKO Carpinteria, CA), and anti-CD31 (1:50; PharMingen, San Diego, CA). Fluorometric TUNEL System (Promega; Madison, WI) was used to detect DNA fragmentation on frozen sections as per the manufacturer's protocol.

### *WB and RTPCR/qRTPCR (from in vivo tissues)*

For protein lysates; cells were washed twice with cold PBS. Whole cell lysate was added to the cells and the plate remained at 4°C for 20 min. The cells were then scraped using a cell scraper and the lysate was placed in a 1.5mL pre-chilled Eppendorf tube. The lysate was then placed on a rotator at 4°C for 20 min. The lysate was then centrifuged at 140,000 rpm at 4°C for 10 min. The supernatant was transferred to a fresh, 1.5mL pre-chilled Eppendorf tube and stored at -80°C until further use.

For mRNA-based experiments, cells were washed twice in cold PBS. TRIzol was added to the cells and the plate was placed on a rocker for 10 min at room temperature. After 10 min, samples were placed in a 1.5mL pre-chilled Eppendorf tube.

### *High throughput experiments*

#### *Autophagy qRT-PCR array*

Total RNA was isolated from MPNST724 and STS26T cells (PCI-24781 treated [0.5 $\mu$ M/24h] and untreated) using TRIzol. After DNase treatment, RNA was further cleaned up using Qiagen RNeasy® Mini Kit (Qiagen, Valencia, CA). cDNA was synthesized by RT2 First Strand kit (SABiosciences, Frederick, MD) following manufacturer's instructions. Gene expression profiling using the Autophagy RT2 Profiler™ PCR Array (SABiosciences, Frederick, MD) was conducted. This platform is designed to profile the expression of 84 key genes involved in autophagy (for a comprehensive list of included genes see [www.sabiosciences.com](http://www.sabiosciences.com)). qRT-PCR was conducted using Mastercycler Eppendorf realplex (Eppendorf AG, Hamburg, Germany) based on array manufacturer's instructions. Relative gene expression was determined using the  $\Delta\Delta$ CT method. Data were further analyzed by PCR Array Data Analysis Web Portal ([www.SABiosciences.com/pcrarraydataanalysis.php](http://www.SABiosciences.com/pcrarraydataanalysis.php)). All experiments were repeated twice.

## *Statistics*

### *Statistical analysis for tissue culture based experiments*

Cell culture-based assays (and Western blot analyses) were repeated at least three times; mean  $\pm$  SD was calculated. Cell lines were examined separately. For outcomes that were measured at a single time point a two-sample t-test was used to assess differences; a linear mixed model was used to assess treatment effects and association between compounds.

### *Statistical analysis for animal experiments*

For STS and MPNST-based *in vivo* experiments (50, 56) the average (AVG), standard deviation (STDV)/standard error mean (SEM), and range for all *in vivo* experiment group variables were calculated and recorded. Tumor weights (g) and lung weights (g) for each treatment group were measured for the following: 1<sup>st</sup> quartile, 3<sup>rd</sup> quartile, maximum, minimum, median. All tumor weight and lung weight data are depicted as box plots. The number of lung metastases for (56) are depicted as a dot plot. For outcomes that were measured at a single time point, 2-sample t-tests were used to assess the differences. Differences in xenograft growth (tumor/metastases) *in vivo* were assessed using a 2-tailed Student's t-test. IHC analysis (Ki67, TUNEL) were assessed using 2-tailed Student's t-test. Significance was set at  $p \leq 0.05$ .



Chapter VI: Results

Section 1: Aim 1: The potential effects of HDACis on genetically complex STS

1.1 Effects as monotherapy

The goal of this initial set of studies was to evaluate the effects of pan-HDAC inhibitors on the growth of genetically complex human STS cells *in vitro*. The hydroxamic acid-based pan-HDACis used were PCI2 and suberoylanilide hydroxamic acid (SAHA/Vorinostat). To first confirm that these compounds truly inhibit HDAC activity in our cell lines and induce protein acetylation *in situ*. The expression of acetylated histone 3 and histone 4 and acetylated tubulin was via western blot. A time- and dose-dependent increase in acetylated histones 3, 4 and tubulin was observed using both compounds in human STS cell lines of diverse histology and differential p53 status: Fibrosarcoma (HT1080, wild type p53), rhabdomyosarcoma (RD, mutated p53), and leiomyosarcoma (SKLMS1, mutated p53) (**Fig. 6**).

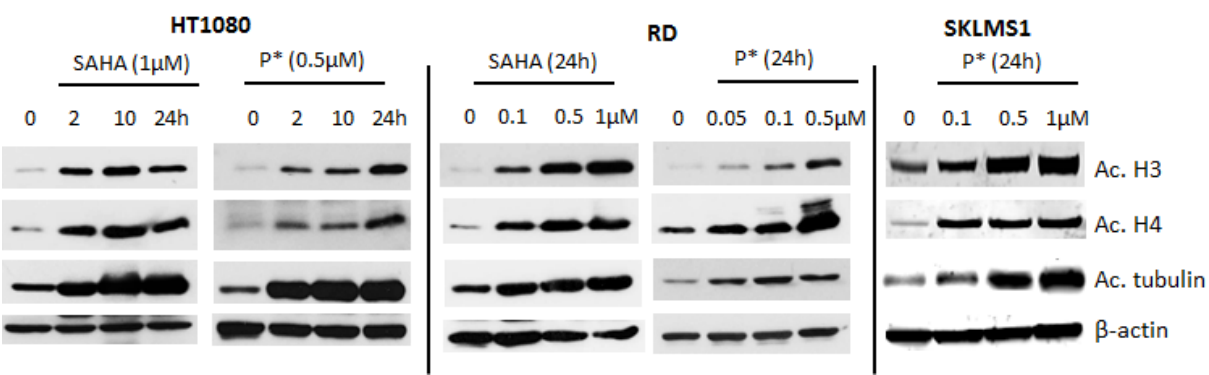


**Figure 6.** Western blot analysis showing HDACi (PCI2 and SAHA) induced time- and dose-dependent increase in histone 3, histone 4, and tubulin acetylation in STS cells. This increase in acetylation is a marker for the HDAC inhibitory effect of these compounds. Modified from Figure 1, Lopez et al. Clin Cancer Res 2009;15:3472-3483.

We next evaluated the effects of HDAC inhibition on STS cell growth *in vitro*. Both HDACis induced a dose-dependent decrease in cell growth after 48 h treatment, with all three cell lines showing more sensitivity to PCI2 compared to SAHA when assayed via MTS (**Fig. 7A**). No significant effect on the growth of normal human fibroblasts (NHF) was observed. Resistance of normal cells to the effects of HDACi has been previously reported (81), and our data repeated these findings. A marked effect on STS clonogenic capacity was noted with both compounds (**Fig. 7B**). These

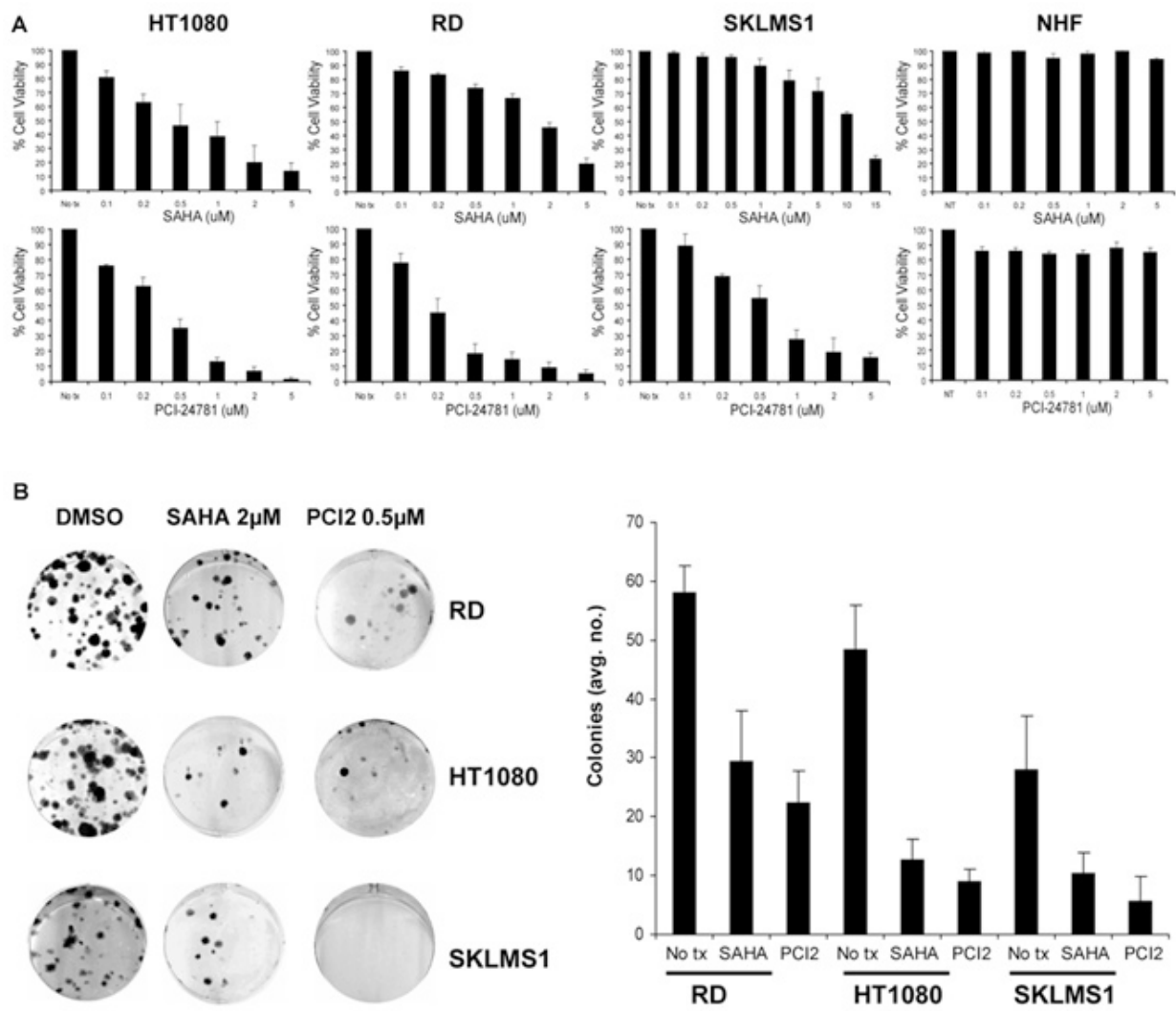


**Figure 7.** A, MTS assays demonstrating the effect of HDAC inhibition (48 h) on STS cell growth. Although STS cell growth inhibition was seen with both agents, a more significant response to PCI2 was observed in cells tested. No effect was seen after treatment of normal human fibroblasts (NHF). B, HDACis abrogate STS cell colony formation capacity. Right panel, number of colonies counted in experiments repeated three times. Results represent the average of a minimum of three replications ( $\pm$  SD). Modified from Figure 1, Lopez et al. Clin Cancer Res 2009;15:3472-3483.

later assays were conducted using a 24 h treatment, the compounds were removed and the cells were grown in normal media for 14 days.

Together these data suggest that HDACis inhibit the growth of genetically complex STS cell lines regardless of histological subtype and differential p53 status, supporting additional investigation on the impact of HDACis on STS *in vitro* and *in vivo*.

Next we aimed to determine whether HDACi-induced growth inhibition is secondary to abrogated cell cycle progression and/or cell death. First, to assess the effect of HDACis on the cell cycle, STS cell lines were treated with IC50 doses of both drugs for 48 h and propidium iodide (PI) staining/FACS were conducted. Both drugs were found to induce G2/M cell cycle arrest, in the cell lines tested, independent of p53 mutational status (**Fig. 8A**). For example, PCI2 (0.5 $\mu$ M) treatment for 48 h, resulted in decreased proportion of S-phase cells from  $42 \pm 6.4\%$  to  $26 \pm 9.1\%$  and from  $34 \pm 5\%$  to  $17 \pm 5\%$ , in RD (p53 mut.) and HT1080 (p53 wt) cells, respectively. Whereas G2/M phase cells increased from  $22 \pm 1.7\%$  to  $64 \pm 3.6\%$  and from  $30 \pm 6.4\%$  to  $49 \pm 5.7\%$ , respectively ( $p < 0.05$ ). Similarly, SAHA induced S-phase depletion and G2/M arrest in both cell lines. Cell cycle analyses also demonstrated an increase in the sub-G1 fraction in cell lines treated with either HDACi, indicative of fragmented DNA, suggesting HDACi-induced cell death. To test whether increased sub-G1 fraction is the result of

apoptosis, annexin V/PI staining FACS analyses were conducted. PCI2 induced marked apoptosis in a dose- and time-dependent manner (**Fig. 8B**). Although only minimal apoptosis was seen 24 h after exposure to PCI2, 74%  $\pm$  14 and 64%  $\pm$  25 Annexin V positivity was observed in HT1080 and RD cells, respectively, after 96 h of PCI2 (0.5 $\mu$ M) treatment. In brief, HDAC inhibition abrogated STS growth by inducing G2/M cell cycle arrest and apoptosis *in vitro*.

Prior to testing the effects of HDACis on STS growth *in vitro* we opted, as depicted in

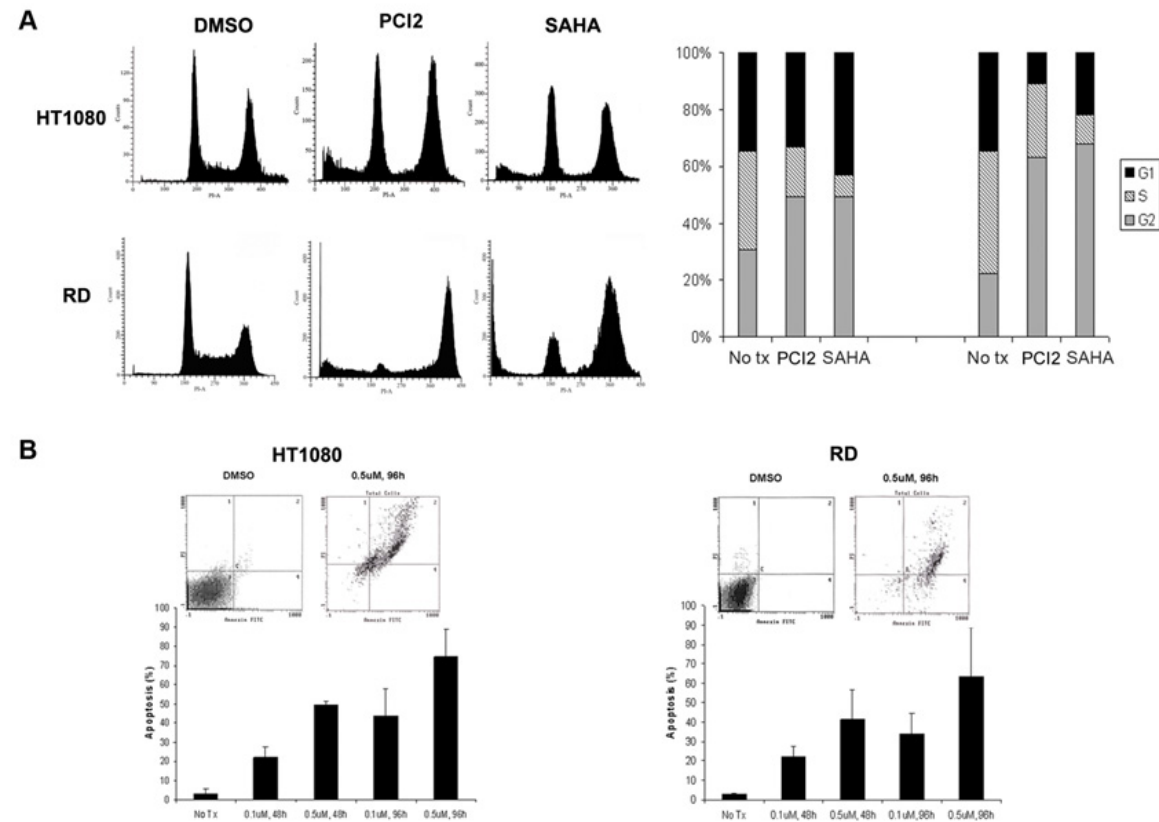


**Figure 8.** A, PI staining/FACS analyses showing the effect of HDACis (PCI2 0.5  $\mu$ M/48 h, SAHA 2  $\mu$ M/48 h) on STS cell cycle progression. A significant ( $p < 0.05$ ) reduction in S phase cells and G2 arrest is seen. Additionally, an increase in sub G1 population is observed, suggesting cell death. B, PCI2 induced STS cell apoptosis in a time- and dose-dependent manner (Annexin V/PI staining FACS analyses). Modified from Figure 2, Lopez et al. Clin Cancer Res 2009;15:3472-3483.

the next section to identify HDACi-based therapeutic combinations that demonstrate superior anti-STS effects as compared to monotherapy.

*1.2 Combining HDACis with conventional chemotherapy*

Multiple lines of evidence suggest that combining HDACis with conventional chemotherapy and/or radiation, result in synergistic anti-cancer effects (82-84). We

aimed to determine if these findings can be recapitulated in STS. To that end we examined the efficacy of low dose PCI2 (0.1M) in combination with low doses of

two different chemotherapeutic drugs commonly used as a treatment for STS: the anthracycline drug doxorubicin (0.5μM) and the DNA cross-linking drug, cisplatin (1μM). Cells were pretreated with PCI2

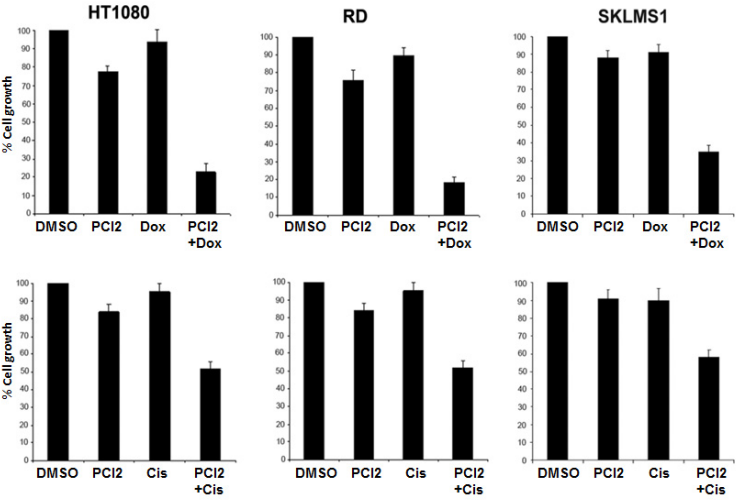


**Figure 9.** Pretreatment of STS cells with PCI2 (0.1μM/24h) sensitizes STS cells to chemotherapy. A superior effect was shown when combining PCI2 and doxorubicin (0.5μM/24 h;  $p < 0.0001$ ) or cisplatin (1μM/24h;  $p < 0.05$ ) as compared with each agent alone. When sequencing was reversed, i.e. pretreatment with chemotherapy (24 h) followed by the addition of PCI2 (24 h), or when the drugs were administered concomitantly for 24 h, no such superior effect was observed (data not shown). Modified from Figure 2, Lopez et al. Clin Cancer Res 2009;15:3472-3483.

alone for 48 h, chemotherapy alone for 24 h, or by sequential combination of PCI2 and

chemotherapy (cells pretreated with PCI2 for 24 h, then chemotherapy was added for an additional 24 h). MTS assays were conducted at 48 h (**Fig. 9**). The combination of PCI2 (0.1 $\mu$ M) and doxorubicin (0.5 $\mu$ M) caused growth reductions of 77%  $\pm$  4.7, 81%  $\pm$  3.1, and 65%  $\pm$  3.5 in HT1080, RD, and SKLMS1 cells, respectively. In contrast, low dose PCI2 alone resulted in 23%  $\pm$  3.2, 24%  $\pm$  5.6, and 12%  $\pm$  4.4 growth inhibition of HT1080, RD, and SKLMS1 cells, whereas low dose doxorubicin alone caused 6%  $\pm$  9.5, 10%  $\pm$  4.5, and 9%  $\pm$  4.5 growth reduction, respectively. Statistical analysis showed a statistically significant, superior effect for combination compared with each compound alone (PCI2 plus doxorubicin  $p < 0.001$ ; PCI2 plus cisplatin,  $p < 0.05$ ; **Fig. 10**). A similar pattern was seen when PCI2 was combined with cisplatin. Interestingly, this effect was lost when drugs were administered together for 24 h or when cells were pretreated with chemotherapy for 24 h prior to PCI2 treatment (data not shown), suggesting that PCI2 possibly sensitizes STS cells to the effect of chemotherapy.

Recognizing the anti-STC effects of HDACis as monotherapy and more so in combination with chemotherapy *in vitro* we next aimed to assess whether this impact can also be observed *in vivo*. Three human xenograft SCID mouse models were utilized: two local growth models, SKLMS1 growing intramuscular and HT1080 growing subcutaneous, and an experimental lung metastasis model, using HT1080. Each of these models were used in a four-armed study to evaluate the efficacy of PCI2 alone, doxorubicin or cisplatin alone, and the combination of PCI2 with either chemotherapy. Of note, PCI2 was administered first and chemotherapy was

administered on day 2. For local growth models, the therapy commenced when tumors were at  $\sim 100\text{mm}^3$ . Bioluminescence was used to identify the establishment of lung metastases for the experimental lung metastasis model; once the mice had a comparable establishment of bioluminescence in the chest cavity, the treatment was started. The mice were followed for tumor size and body weight and sacrificed when control group tumors reached 1.5 cm average largest dimension or when bioluminescence suggested control group had significant pulmonary tumor load. Effects of tumor growth were statistically assessed using a linear mixed model. To determine the impact of treatments on tumor weights at termination of study, a linear regression model was used.

In the first experiment, SKLMS1 xenografts were used and the effects of PCI2, doxorubicin and their combination were evaluated (**Fig. 10A**). Treatment with low-dose doxorubicin alone or PCI2 alone did not significantly affect SKLMS1 xenograft growth ( $p = 0.06$  and  $p = 0.015$ , respectively). Combining PCI2 with low dose doxorubicin resulted in significant growth inhibition compared to either drug alone ( $p < 0.0001$ ) (**Fig 11A**). Tumor volume at study termination was: control  $1738\text{mm}^3 \pm 334$ , doxorubicin  $1253.1\text{mm}^3 \pm 281.5$ , PCI2  $1182\text{mm}^3 \pm 329$ , combination  $460.3\text{mm}^3 \pm 240$ . Similarly, PCI2 and more so PCI2 + doxorubicin resulted in significant reduction in tumor weights at study termination as compared to control and doxorubicin alone treatment groups ( $p = 0.026$ ,  $< 0.0001$ ,  $= 0.0023$ ,  $= 0.047$ , respectively) (**Fig 10B**). Average group tumor weights at study termination were  $1.62\text{g} \pm 0.47$  for control,  $1.34\text{g} \pm 0.43$  for doxorubicin,  $1.11\text{g} \pm 0.26$  for PCI2, and  $0.64\text{g} \pm 0.24$  for combination. H&E staining of

different treatment arm tumors revealed marked tumor necrosis in PCI2 and combination treatment groups (**Fig 10C**); viable tumor sections were immunohistochemically evaluated for the impact of different therapies on STS cell proliferation (PCNA) and apoptosis (TUNEL). Average PCNA and TUNEL-positive

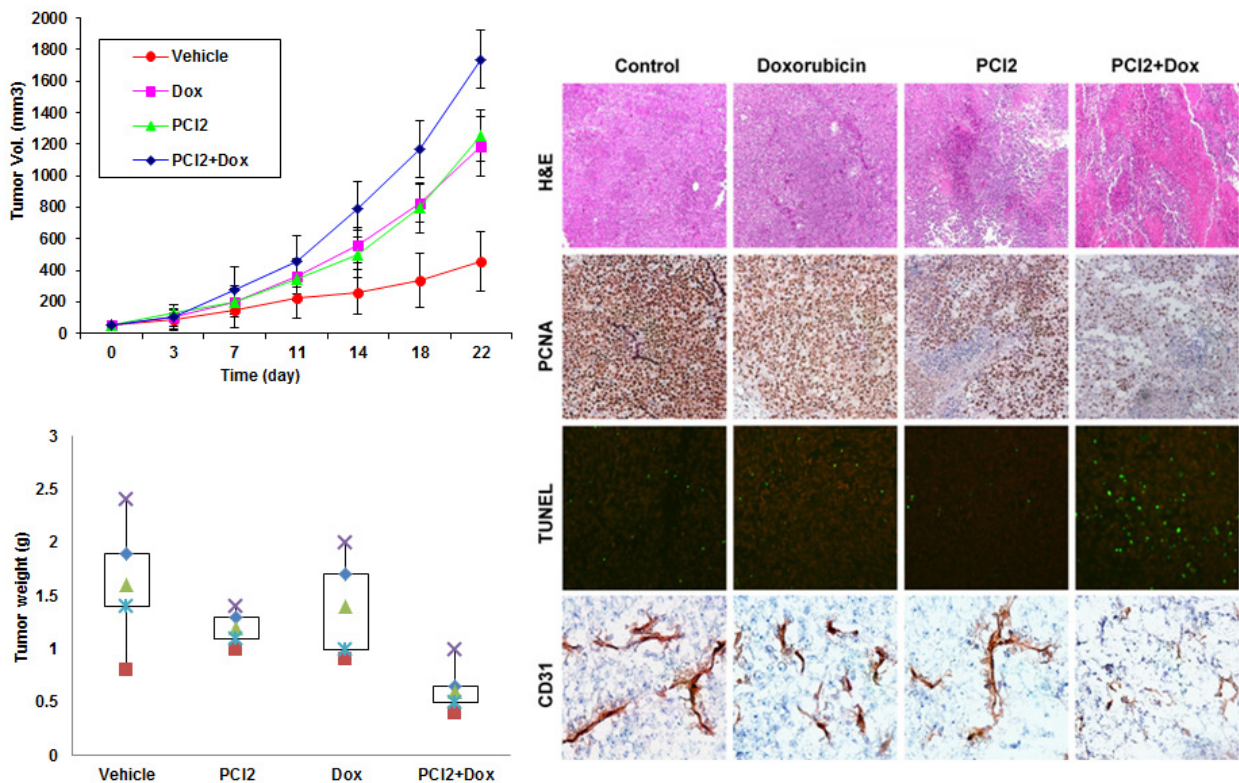


**Figure 10.** Combining PCI2 (50mg/kg/d) with low-dose doxorubicin (1.2mg/kg/biweekly) results in significant reduction SKLMS1 xenograft growth in SCID mice. A, tumor growth curves showing a significant synergy between the two drugs ( $p < 0.0001$ ). B, PCI2 alone effects on tumor weight were statistically significant ( $p = 0.026$ ) compared with controls. Most importantly, the reduction in tumor weight due to combined PCI2/chemotherapy was very statistically significant compared with the other treatments ( $p < 0.0001$ ,  $= 0.0023$ , and  $= 0.047$  versus control, doxorubicin, and PCI2 groups, respectively). C, IHC analysis of xenograft specimens showing enhanced tumor necrosis in PCI2-treated tumors, and most significantly in combination therapy specimens (H&E), decreased tumor proliferation (PCNA) and increased apoptosis (TUNEL). No significant differences in CD31 counts were seen; however, a marked decrease in the number of large, patent blood vessels was discernible in the combination group. Modified from Figure 3, Lopez et al. Clin Cancer Res 2009;15:3472-3483.



staining nuclei revealed  $88 \pm 2$  and  $20 \pm 2.4$  for control,  $85 \pm 1.2$  and  $16 \pm 1.4$  for doxorubicin,  $71 \pm 2.3$  and  $19 \pm 1.1$  for PCI2, and  $57 \pm 4.6$  and  $61 \pm 18.4$  for combination, respectively. Together these data suggest that combination therapy had the strongest anti-proliferative and apoptosis-inducing effects ( $p < 0.05$ ). Sections were also stained for CD31 to examine therapy effects on tumor-associated vasculature. No significant differences in CD31 counts were seen; however, markedly decreased numbers of large, patent blood vessels was discernible in the combination group (**Fig 10C**).

The second mice experiment evaluated the effects of PCI2, cisplatin and their combination on the growth of established HT1080 xenografts (**Fig. 11A**). Cisplatin and PCI2 when administered as single agents had only minimal effects on HT1080 tumor growth. However, significant tumor growth delay was observed with combined therapy ( $p < 0.001$  versus all other treatment groups; **Fig. 11A**). This was also reflected in a significantly reduced tumor volume at study termination for xenografts treated with therapeutic combination. Tumor volumes were: control  $1437.1\text{mm}^3 \pm 419$ , cisplatin  $1031.5\text{mm}^3 \pm 574.8$ , PCI2  $1078.7\text{mm}^3 \pm 567.7$ , combination  $254.8\text{mm}^3 \pm 200$  ( $p < 0.001$  for combination compared to all other therapeutic arms). Average group tumor weights at study termination were  $1.23\text{g} \pm 0.15$  for control,  $1.01\text{g} \pm 0.39$  for cisplatin,  $1.09\text{g} \pm 0.54$  for PCI2, and  $0.36\text{g} \pm 0.22$  for combination (**Fig 11B**). Statistical analysis determined that combination therapy significantly reduced tumor weight as compared to control, cisplatin, and PCI2 alone ( $p = 0.0003$ ,  $= 0.0038$ , and  $= 0.0011$ , respectively). IHC results were similar to those for the SKLMS1-treated

tumors described above, showing increased necrosis in PCI2 and combination groups (**Fig. 11C**). Decreased proliferation and enhanced apoptosis were most pronounced in the combination-treated group (average PCNA and TUNEL-positive staining nuclei were  $83 \pm 7.1$  and  $18 \pm 0.3$  for control,  $62 \pm 2.8$  and  $17 \pm 2.5$  for cisplatin,  $50 \pm 2.8$

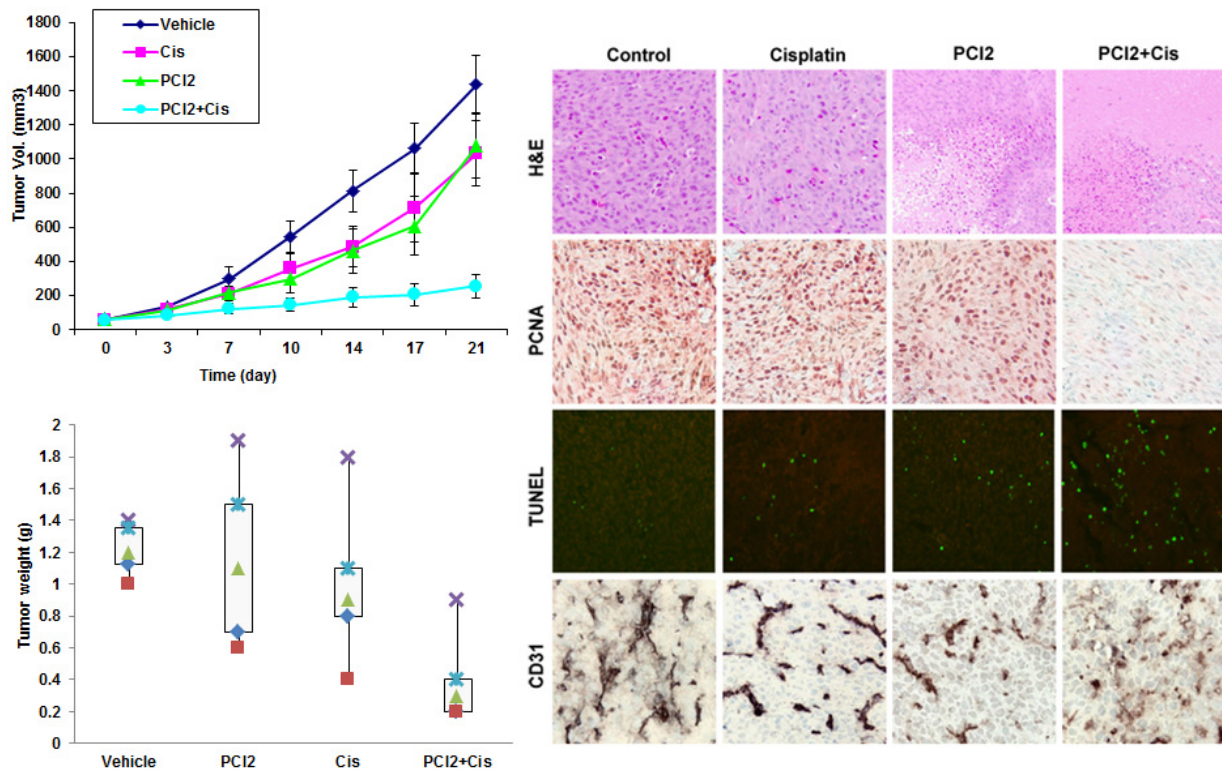


**Figure 11.** Combining PCI2 (50mg/kg/d) with low-dose cisplatin (2mg/kg/biweekly) results in significant reduction of HT1080 xenograft growth in nude mice. A, tumor growth curves showing a significant synergy between PCI2 and cisplatin in vivo ( $p < 0.001$ ). B, a highly statistical significant tumor weight reduction was observed with combined treatment compared with the other three groups ( $p = 0.0003$ ,  $= 0.0038$ , and  $= 0.0011$  versus control, cisplatin, and PCI2 groups, respectively). C, as observed in SKLMS1 xenografts, enhanced tumor necrosis in PCI2-treated tumors, and most significantly in combination therapy specimens was observed in HT1080 tumors (H&E). Decreased tumor proliferation (PCNA) and increased apoptosis (TUNEL) was also seen. No significant differences in CD31 counts were shown; however, a marked decrease in the number of large, patent blood vessels was discernible in the combination group. Modified from Figure 4, Lopez et al. Clin Cancer Res 2009;15:3472-3483.

and  $21 \pm 5.9$  for PCI2, and  $38 \pm 14.1$  and  $33 \pm 8.6$  for combination, respectively;  $p < 0.05$ ). No significant difference in CD31 positivity was seen among groups, whereas a reduction in large blood vessels was observed in the combination group.

Together, both these studies suggest that PCI2 alone while highly effective *in vitro* does not induce dramatic anti-growth effects *in vivo* using the dose and regiment selected. However, combining PCI2 with chemotherapy markedly improves ant-STs effects *in vivo*.

While previous studies focused on the effects of PCI2 ± chemotherapy on local growth it is even more important to evaluate whether this therapeutic regiment can impact the growth of STS metastasis which is the cause for STS patient death. A major limitation to being able to assess the effects of therapy on STS metastatic development and growth is the current lack of spontaneous STS metastasis models. To that end, for our studies, we utilized an experimental STS lung metastasis model where HT1080 cells are injected i.v. into mice tail vein. Lung metastases are commonly visible at ~2 weeks after injection. To be able to follow-up the development and growth of lung metastases in these mice, we utilized HT1080 cells stably transduced to express GFP/luciferase (GL) and metastasis volume was determined using bioluminescence (BLI). Mice were allocated into six treatment arms after pulmonary metastases were confirmed per BLI and treatment was initiated (**Fig. 12**). Drug combination sequencing was done similar

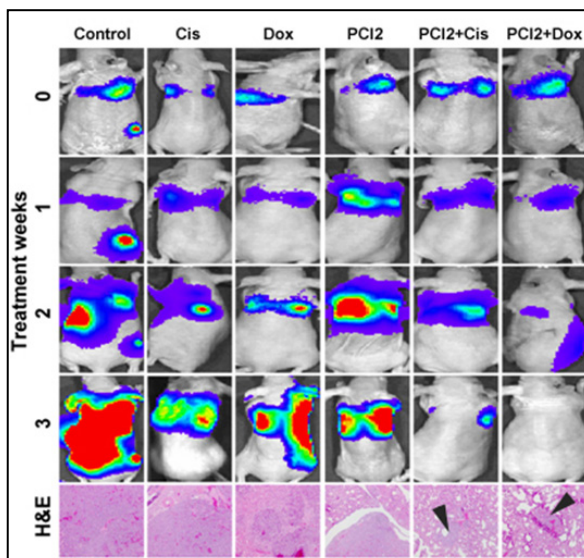


**Figure 12.** Combining PCI2 (50mg/kg/d) with low-dose cisplatin (2mg/kg/biweekly) or doxorubicin (1.2mg/kg/biweekly) results in significant reduction of HT1080 pulmonary metastatic growth in nude mice. Nude mice injected with HT1080 cells ( $1 \times 10^6$ /mouse) through tail vein were followed using bioluminescence. Treatment (as recorded) was initiated after bioluminescence suggested established lung metastases ~3 weeks after cell injections. Sequential bioluminescence imaging of mice from each treatment arm show a substantial increase in luciferase readout in control, cisplatin-, doxorubicin-, and PCI2-treated groups; decreased readouts were noted in combination therapy groups. H&E staining demonstrated only limited lung metastatic deposits in combination-treated groups (microscopic metastasis are marked by arrow heads) as compared to large metastatic load in other treatment arms. Modified from Figure 4, Lopez et al. Clin Cancer Res 2009;15:3472-3483.

to the previously mentioned therapeutic experiments. Experiment was terminated when BLI readout in control treated mice suggested an extensive metastatic load (~3 weeks after therapy initiation). At this time point, as depicted in **Fig. 12**, readout demonstrated a markedly reduced

pulmonary tumor load in mice treated with combination therapies as compared to vehicle, PCI2, or chemotherapy arms alone. Lung metastases load was also enhanced on H&E staining of the lungs. Vehicle and monotherapy-treated lungs demonstrated massive tumor load replacing almost entirely the lung parenchyma, whereas combination treated lungs demonstrated no or only microscopic results. These differences were also notable per lung weights (treated lung metastases weights were calculated by deducting the estimated average normal mouse lung weight from

actual lung weight at study termination), where combination therapy-treated lungs

were significantly smaller in weight compared to vehicle and monotherapy. Average lung metastases weight per group was  $0.55\text{g} \pm 0.14$  for control,  $0.62\text{g} \pm 0.26$  for cisplatin,  $0.48\text{g} \pm 0.33$  for doxorubicin,  $0.33\text{g} \pm 0.20$  for PCI2 group,  $0.15\text{g} \pm 0.19$  for PCI2 + cisplatin, and  $0.13\text{g} \pm 0.14$  for PCI2 + doxorubicin. Statistical analysis revealed a trend toward reduced metastatic load in PCI2 alone treated mice but it did not reach statistical significance, whereas PCI2 combined with either chemotherapy resulted in significant lung metastases weight reduction ( $p < 0.05$ ).

Combined, these data further demonstrates that PCI2/chemotherapy combinations induce significant effects on the growth of STS lung metastasis and support consideration of this therapeutic regimen in the clinical setting. Importantly, these data formed the basis for a currently on-going phase I/II clinical study evaluating “PCI-24781 in Combination With Doxorubicin to Treat Sarcoma” (ClinicalTrials.gov identifier: NCT01027910).

Continuing our pre-clinical studies, as presented next, we sought to identify potential mechanisms contributing to HDACi sensitivity and especially to the noted chemosensitivity effects induced in response to HDAC inhibition.

Studies from our lab have previously demonstrated that Rad51 is commonly overexpressed in genetically complex STS contributing to the resistance of these malignancies to conventional chemotherapy; particularly doxorubicin (85). RAD51, a member of the RecA/Rad51 family of proteins, is a critical regulator of DNA double strand repair through homologous recombination (86, 87). Hypothesizing that modified Rad51 expression potentially contributes to the observed chemosensitivity effects of HDACis in STS, we set to confirm the effects of PCI2 on Rad51 expression. *p21* mRNA expression has been shown increase in response to HDAC inhibition with a variety of HDACi compounds in numerous cell lines of different histologies (50, 88). As a control, we opted to identify *p21* mRNA expression in response to PCI2 in STS. qRT-PCR and RTPCR demonstrated an early (4 h treatment) increase in *p21* mRNA expression in SKLMS1 (p53 mut.) cells when treated with PCI2 (**Fig. 13**). We then verified Rad51 expression in response to PCI2. qRT-PCR and RTPCR and WB analysis validated that PCI2 decreased

*RAD51* RNA and protein expression in STS cell lines, respectively (**Fig. 14**).

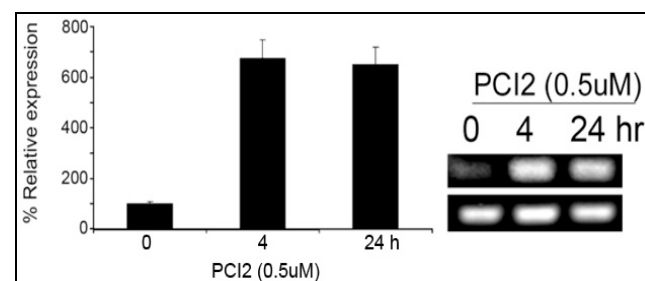
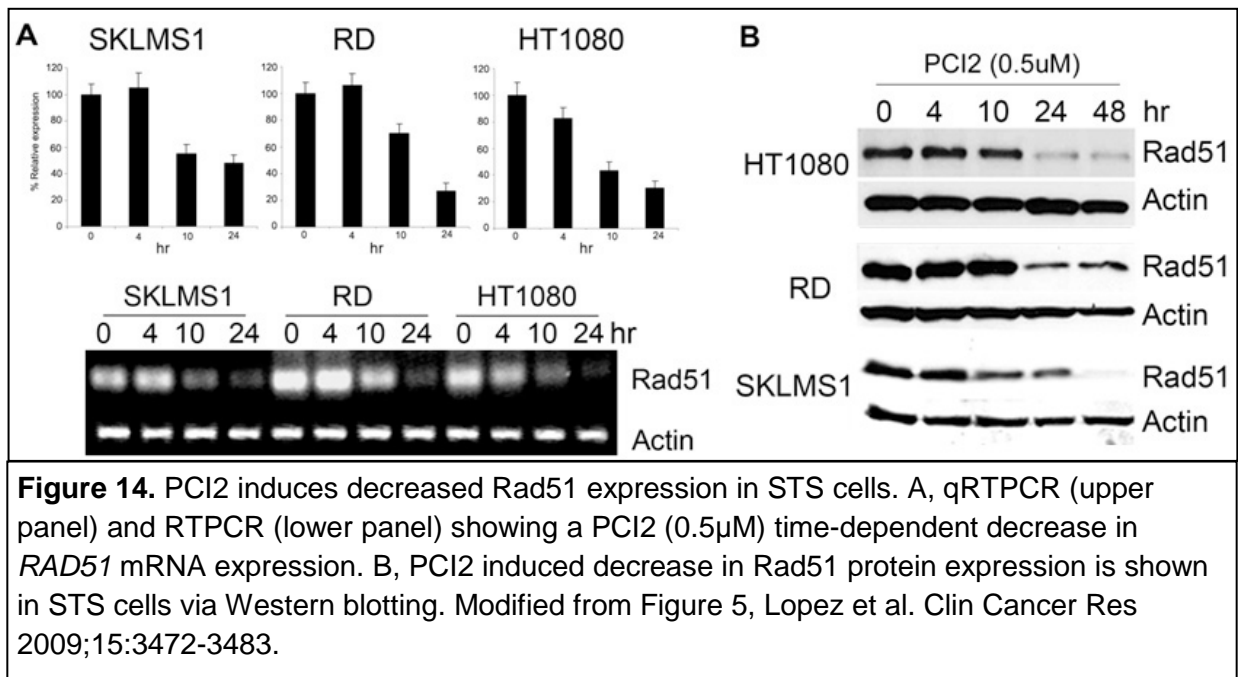


**Figure 13.** PCI2 induces *p21* expression independent of p53 status in STS cells. qRT-PCR and RT-PCR showing a relatively early (4h treatment) increase in *p21* mRNA expression in SKLMS1 (mutated p53) cells in response to PCI2. Modified from Figure 5, Lopez et al. Clin Cancer Res 2009;15:3472-3483.



Next, we aimed to define the mechanism by which HDACis inhibit RAD51 expression. First, to identify whether PCI2 affects *RAD51* mRNA stability the, transcriptional inhibitor actinomycin D was used and *RAD51* mRNA levels are determined with or without PCI2 treatment. *RAD51* mRNA half-life was found to be comparable between treated and untreated cells, signifying that PCI2 does not have a direct effect on *RAD51* mRNA degradation (data not shown). To further identify the effect of PCI2 on *RAD51* transcription, we evaluated the recruitment of Poly II (RNA polymerase II) to the *RAD51* gene. The recruitment of Poly II to the *p21* gene was used as a control as we initially showed that PCI2 induced the upregulation of *p21* RNA expression (**Fig .13**). A chromatin immunoprecipitation (ChIP) assay using an anti-Poly II antibody was employed showing that PCI2 treatment decreased Poly II recruitment to the *RAD51*



gene while it increased the recruitment of Poly II to the *p21* gene (**Fig. 15**). ChIP assay was also used to determine the association of acetylated histone 3 (ac.H3) and histone 4 (ac.H4) to the *RAD51* and *p21* promoters after PCI2 treatment. In PCI2 treated cells increase of both ac.H3 and ac.H4 recruitment to the promoters of both genes were identified (**Fig. 15**). Together, these data

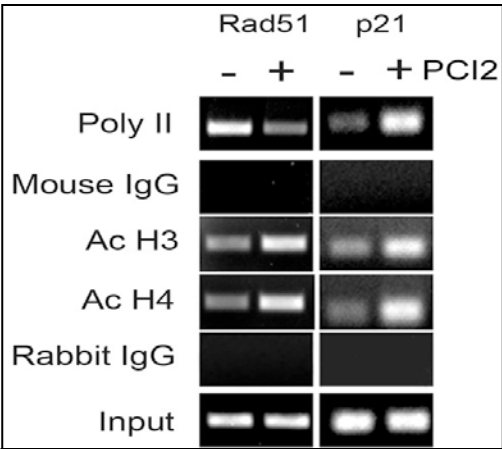


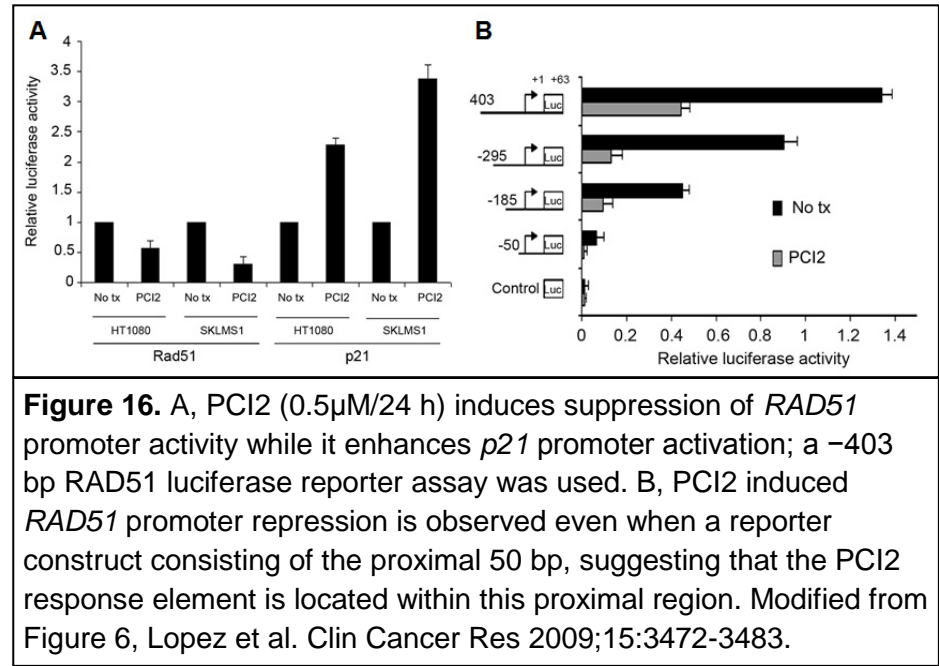
**Figure 15.** ChIP showing decreased Pol II binding to *RAD51* gene in response to PCI2 (0.5µM/24 h); in contrast increased Pol II binding to the *p21* gene is seen. Binding of acetylated histones 3 and 4 to the *RAD51* and *p21* promoters is enhanced. No significant nonspecific IgG binding was observed; input DNA was used as loading control. Modified from Figure 6, Lopez et al. Clin Cancer Res 2009;15:3472-3483.

indicate that PCI2 treatment induces the transcriptional repression of Rad51 accomplished by an increase of acetylated histone 3 and 4 at the *RAD51* promoter.

We next investigated the repressive effect of PCI2 on *RAD51* gene transcription using *RAD51* reporter assays. A luciferase reporter

construct of the *RAD51* promoter region -403 to +63 was transiently transfected into STS cells tested. Cells treated with PCI2 showed a significant reduction of *RAD51* promoter activity. In contrast, a *p21* reporter construct demonstrated increased *p21* promoter activity after PCI2 treatment (**Fig. 16A**). To further determine the *RAD51* promoter region required for PCI2-induced suppression, we utilized various 5' truncated promoter regions. All constructs treated with PCI2 significantly showed reduced luciferase expression (**Fig. 16B**). Luciferase expression was also significantly

reduced when the -50Luc region reporter was used, suggesting that the PCI2 response element is at the proximal region of the *RAD51* promoter. This promoter region was initially identified to include an E2F binding site which has been shown to be important in the transcriptional regulation of *RAD51* (89). To determine if PCI2 mediates its anti-Rad51 effects through this cis-regulatory element, the E2F binding



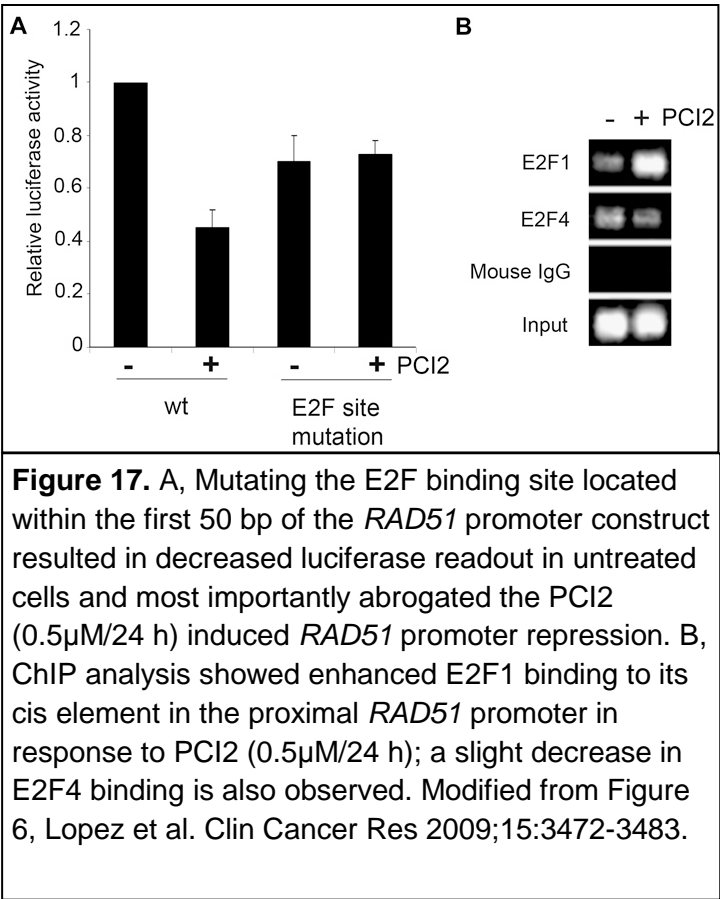
site within the *RAD51* reporter was mutated. DMSO treated cells

demonstrated a decrease in luciferase readout when the E2F

binding site was mutated, indicating that this site potentially mediates the transcription of Rad51. Interestingly, PCI2-induced reduction of luciferase expression noted when using a wild-type reporter construct was eliminated in cells transfected with the mutated E2F binding site construct (**Fig. 17A**). This data suggests that PCI2-mediated transcriptional repression of Rad51 occurs at the proximal region of the E2F binding site. E2F transcription factors consist of nine family members that can bind to this E2F site. Previously, E2F1 and E2F4 have been shown to bind the *RAD51* promoter (89). Thus, E2F1 and E2F4 binding to the *RAD51* promoter in response to PCI2 treatment was assessed. Using the ChIP assay, an increase in E2F1 binding was observed in

cells treated with PCI2, whereas a modest decrease of E2F4 binding was observed under this condition (**Fig. 17B**). Together, these data show that HDAC inhibition results in transcriptional repression of *RAD51* mRNA expression. PCI2-induced decrease of *RAD51* RNA represents a possible mechanism for the enhanced chemosensitivity observed in STS cells *in vitro* and *in vivo*.

In summary, studies presented above demonstrate that human STS cells are highly sensitive to the effects of HDACis *in vitro*, resulting in cell cycle arrest and enhanced cell death. Most importantly, HDAC inhibition sensitized STS cells to the effects of chemotherapy; a pre-clinical observation that is now being tested in the clinical setting. Multiple downstream



effectors might contribute to HDACi anti-STS impact; amongst such is Rad51. PCI2-induced decrease in Rad51 expression is a potential mechanism underlying HDACi chemosensitivity effects. While encouraging, it is important to recognize that genetically complex sarcomas are a heterogeneous malignancy cohort composed of multiple histologies. Taking this into account upon the completion of the studies above,

we decided to focus on a single histological subtype, MPNST and determine the effects of HDACi in this specific malignancy.

### 1.3 HDAC down-stream targets potentially contributing to the anti-STS and chemosensitivity effects of HDACis

HDACs operate by deacetylation of histone and other non-histone proteins resulting in changes in chromatin condensation. HDAC inhibition thus leads to enhanced protein acetylation which consequently results in changes in gene expression. In the following set of studies we sought to identify HDAC inhibition induced genes that their expression changes might modulate the functional effects observed in STS cells after HDACi treatment. To that end we conducted gene expression profiling comparing the expression of genes in STS cells treated with PCI2 (for 4 and 24 h) to those treated with DMSO (control) only. The custom Codelink oligo microarrays (GE Healthcare) platform was

utilized including probes for 2013 genes known to be highly involved in tumorigenesis.

A total of 33 genes (1.6%) exhibited changed expression in response to PCI2

Up-regulated			Down-regulated		
Gene Name	AVG	STDV	Gene Name	AVG	STDV
CTGF	16.24	0.64	TYMS	8.20	0.31
ROPN1L	14.45	5.45	HMGA1	7.93	1.09
SERPINI1	8.46	5.22	HDAC7A	7.75	2.21
FANK1	7.32	0.96	CCNA2	7.47	0.28
FTCD	7.06	3.54	CHK1	5.29	3.40
MAPK8IP1	5.20	1.61	UBE2C	4.94	0.06
CTSL2	5.06	2.71	CCNB1	4.86	0.29
MT1X	4.99	0.18	MGST1	4.30	1.20
SIRT4	4.82	3.14	RAD51	3.65	0.70
p21	4.62	0.18	PLK1	3.35	0.87

**Table 5.** Codelink oligo microarrays (GE Healthcare) containing a total of 2013 probes selected for known involvement in cancer to examine for PCI2-induced gene changes in STS cell lines. Cells were treated with PCI2 (0.5µM) or DMSO alone for 24 h, and RNA was subjected to analysis. A total of 33 genes exhibited reproducible change in expression (20 upregulated and 13 downregulated) in tested cell lines. Up-regulated genes are depicted in the upper panel (10 genes with the highest fold increase are shown), down-regulated genes are in the lower panel (10 genes with the highest fold decrease are shown).

treatment: 20 were found to be overexpressed in 13 to be down-regulated (**Table 5**).

Amongst the deregulated targets were included genes important for cell cycle progression: *CDKN1A*, *CHEK1*, *CDK4*; apoptosis: *BIRC5*, *CASP9*; transcription factors: *ID2*; DNA damage repair: *BRCA1*, *RAD51*.

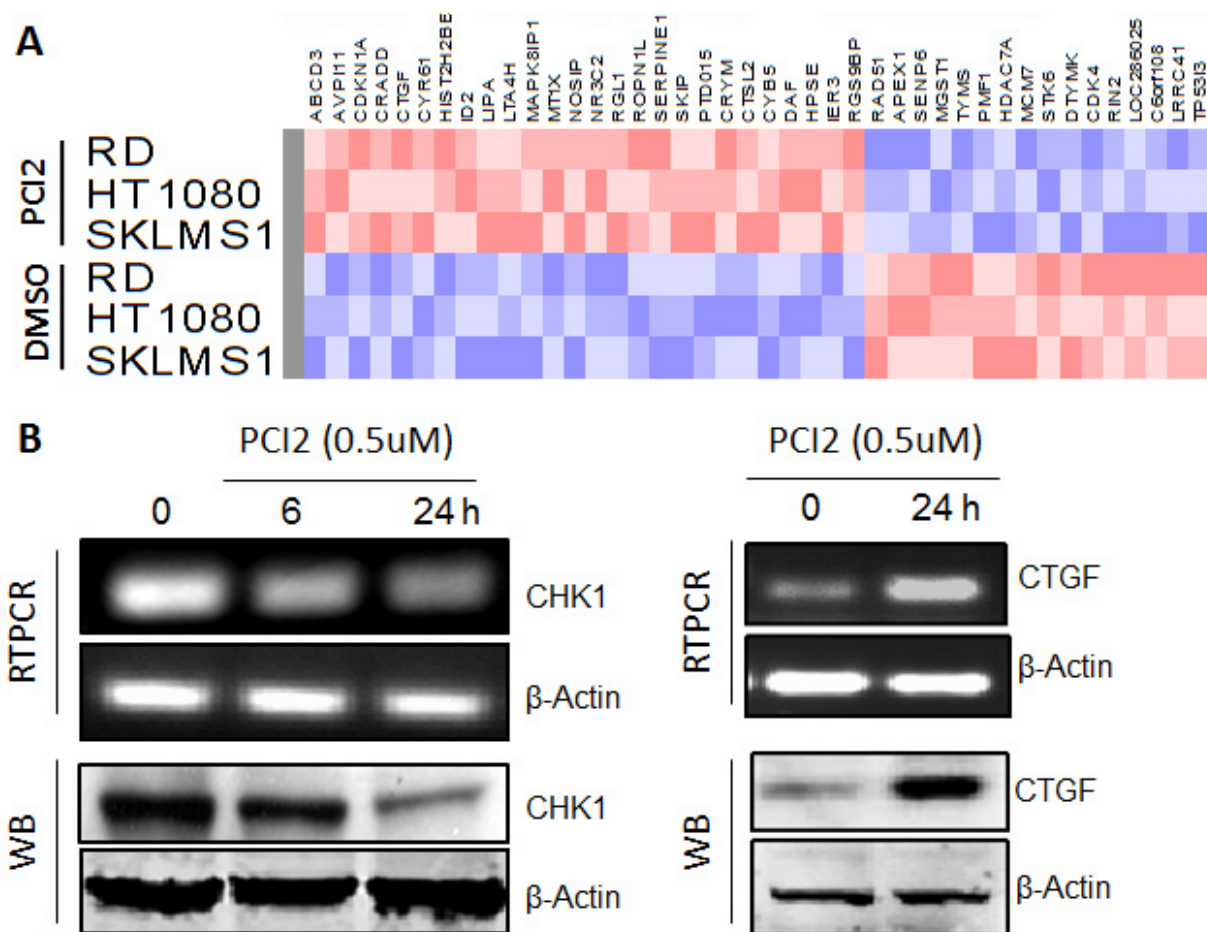


**Figure 18.** A, PCI2 induces changes in gene expression in a panel of STS cell lines. B, PCI2 induces decreased CHK1 and increased CTGF expression in STS cells. RT-PCR (upper panel) and western blot (lower panel).

Several genes were selected for array confirmation including *CDKN1A* (p21) and *CTGF* (demonstrating 4.6 and 16.2 fold increase, respectively) and *CHEK1* (demonstrating 5.3 fold decreased expression) (**Table 5**). RT-PCR and WB analyses confirmed the expected changes in the expression of these genes as was found by gene arrays (**Fig. 18**). Interestingly, one of the genes identified to be down-regulated in response to PCI2 treatment was *RAD51*.

Section 2: Aim 2: HDACis elicit anti-MPNST effects

2.1 The effects of HDACis on MPNST growth in vitro and in vivo

As described before, after showing the efficacy of HDAC inhibition in a panel of complex karyotypic STS subtypes, we then focused our studies of HDAC inhibition on a single, aggressive and dismal genetically complex STS subtype, MPNST. In this study, we used primary cultures of human normal Schwann cells (NSC) as a control, two sporadic MPNST cell lines (MPNST724 and STS26T), and four NF1-associated MPNST cell lines (S462, ST88, T265, and MPNST642). The MPNST642 cell line was established in our laboratory (Fig. 19). Prior to initiating our studies we have first characterized our cell line panel (Table 6).

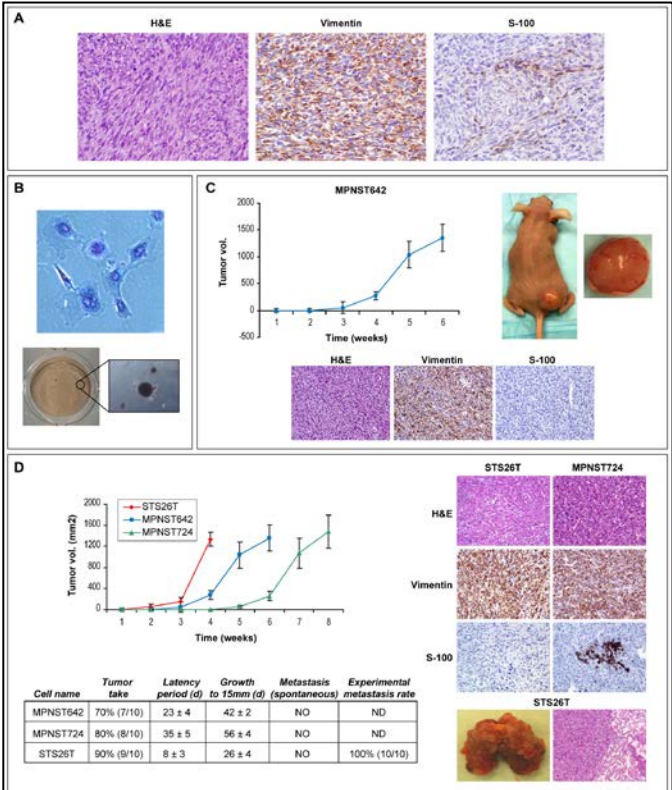


**Figure 19.** A, The cell line termed MPNST642 originated from a recurrent MPNST located in the forearm of a 21 year old male diagnosed with NF1 at childhood. IHC stains of original tumor are depicted (X200); H+E demonstrating the histomorphology of the tumor which stained positively for vimentin and focally for S100; B, MPNST642 cells have been growing in culture continuously for >60 passages (morphology is depicted, Geimsa staining, upper panel) and they exhibit anchorage independent growth (lower panel). DNA fingerprinting confirmed the cell origin to be from the human tumor and demonstrated that no cross contamination has occurred in culture; (continue to next page)



**Figure 19.** (Continued from previous page) C, MPNST642 cells ( $2 \times 10^6$ /mouse, s.c. injection) grow as xenografts in SCID mice: graph demonstrates growth rate (see also table below), histomorphology is similar to that of original patient tumor although S100 staining is negative (loss of S100 expression is known to occur with MPNST progression); D, Two additional MPNST cell lines of those used in our study (STS26T and MPNST724;  $1-2 \times 10^6$ /mouse) exhibit s.c. xenograft growth in SCID mice. Growth curves of all 3 available xenografts are shown together to enable comparison (left upper panel). H+E and IHC staining of xenografts are depicted (right upper panel) STS26T xenografts are negative for S100 while MPNST724 are focally positive. In addition, tail vein injection of STS26T ( $1 \times 10^6$ /mouse) results in reproducible lung metastasis – macroscopic and microscopic photographs are shown. The table summarizes the xenograft growth characteristics of all three human cell lines. STS26T are commonly used as a cellular model of sporadic MPNST and are widely accepted as a representative of this disease. MPNST724 have been kindly provided by Dr Jonathan Fletcher, the original diagnosis was made by a vastly experienced pathology team; S100 positivity in MPNST724 xenografts further supports the MPNST origin of these cells. Modified from Figure S1, Lopez et al. Cancer Res 2011;71:185-196.

Three pan-HDACis were used for this study: PCI2, SAHA, and MS275 to eliminate the possibility of compound specific off target effects. All three compounds induced a time- and dose-dependent growth inhibition that was most pronounced in a subset of MPNST cell lines tested. The graphs depict GI50s at 48 h; 4 MPNST cell lines were markedly sensitive to PCI2, with GI50s ranging between 0.1 and 0.35  $\mu$ M, whereas the 2 additional cell lines (STS26T and MPNST724) were relatively

Cell lines	doubling time (h)	NF1 associated	Ras active	p53 status	grow in mice	Lung metastases
S462	24	negative	Yes	mut.	No	No
ST88	36	negative	Yes	wt	No	No
MPNST642	38	negative	Yes	wt	Yes	No
T265	32	negative	Yes	mut.	No	No
STS26T	19	positive	No	null	Yes	Yes
MPNST724	27	positive	Yes	mut.	Yes	No

**Table 6.** Human NF1-associated MPNST cell lines: S462, ST88, MPNST642, T265. Human sporadic MPNST cell lines: STS26T, MPNST724. Doubling time is depicted in hours. All NF1-associated cell lines have been confirmed for loss of NF1. Sporadic cell lines retain NF1. Ras activity was detected in all NF1-associated cell lines and MPNST724; STS26T did not exhibit Ras activity (Ras activity was detected using a Ras Activity assay Kit, Table 4). Sequence analysis determined p53 mutation status in all cell lines. Only one NF1-associated MPNST cell line grows s.c. in SCID mice (MPNST642). Both sporadic cell lines grow s.c. in SCID mice, but only STS26T develops lung metastases in SCID mice after tail vein injection.

resistant exhibiting GI50s more than the clinically relevant dose ( $>1\mu\text{M}$ ). NSCs were resistant to PCI2 growth inhibitory effects. Higher doses of SAHA and MS-275 were needed to achieve PCI2-equivalent MPNST growth inhibition; however, a similar

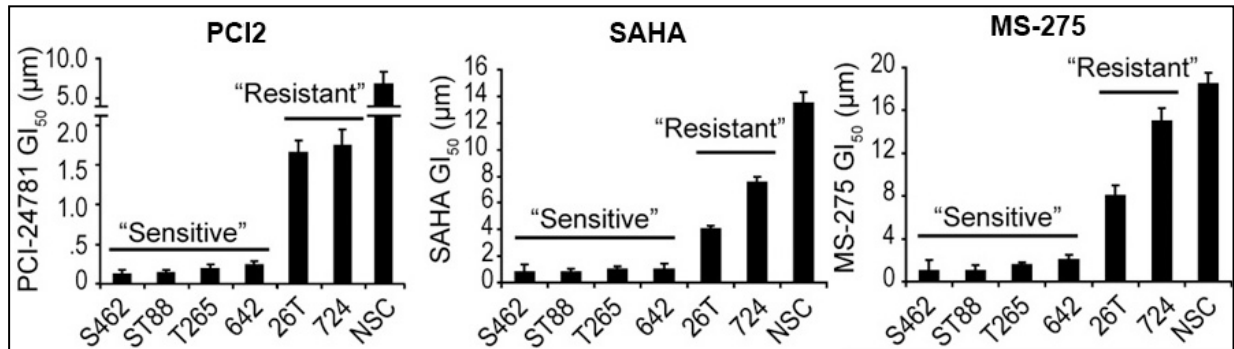


**Figure 20.** Growth-inhibitory effects (48 h) were determined via MTS assays, GI50s are depicted. One MPNST cell-line subset was highly sensitive to the effects of all 3 drugs (highest sensitivity to PCI2), whereas a second exhibited relative resistance. No significant effect on normal human Schwann cells' (NSC) growth was noted in clinically relevant therapeutic doses. Modified from Figure 1, Lopez et al. Cancer Res 2011;71:185-196.

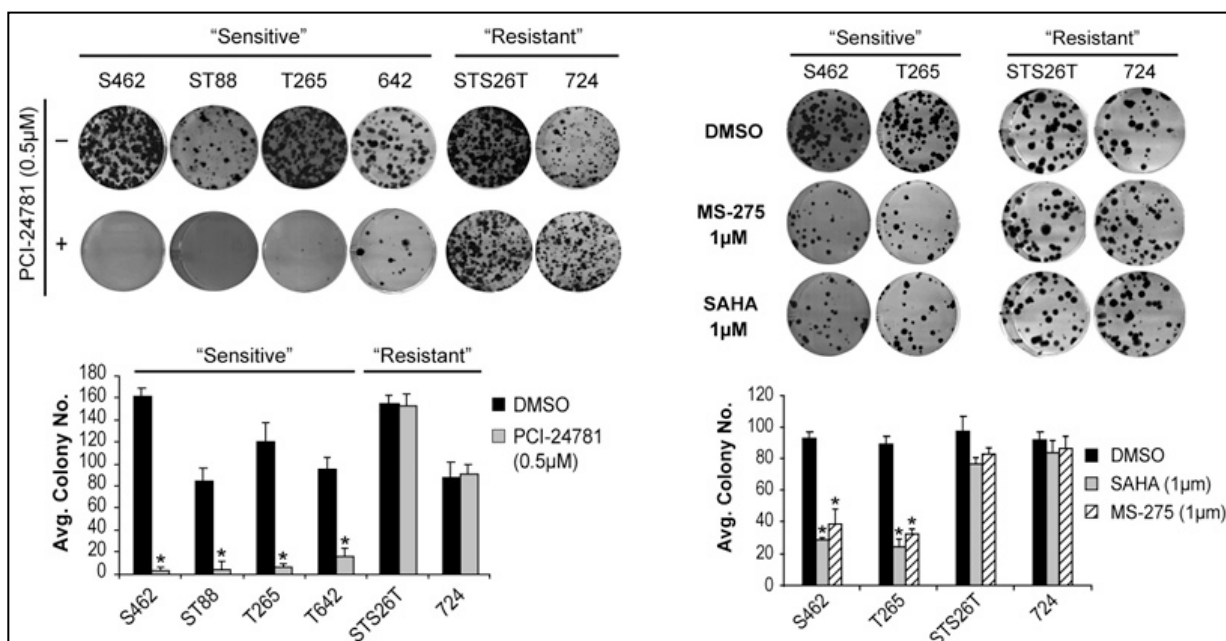
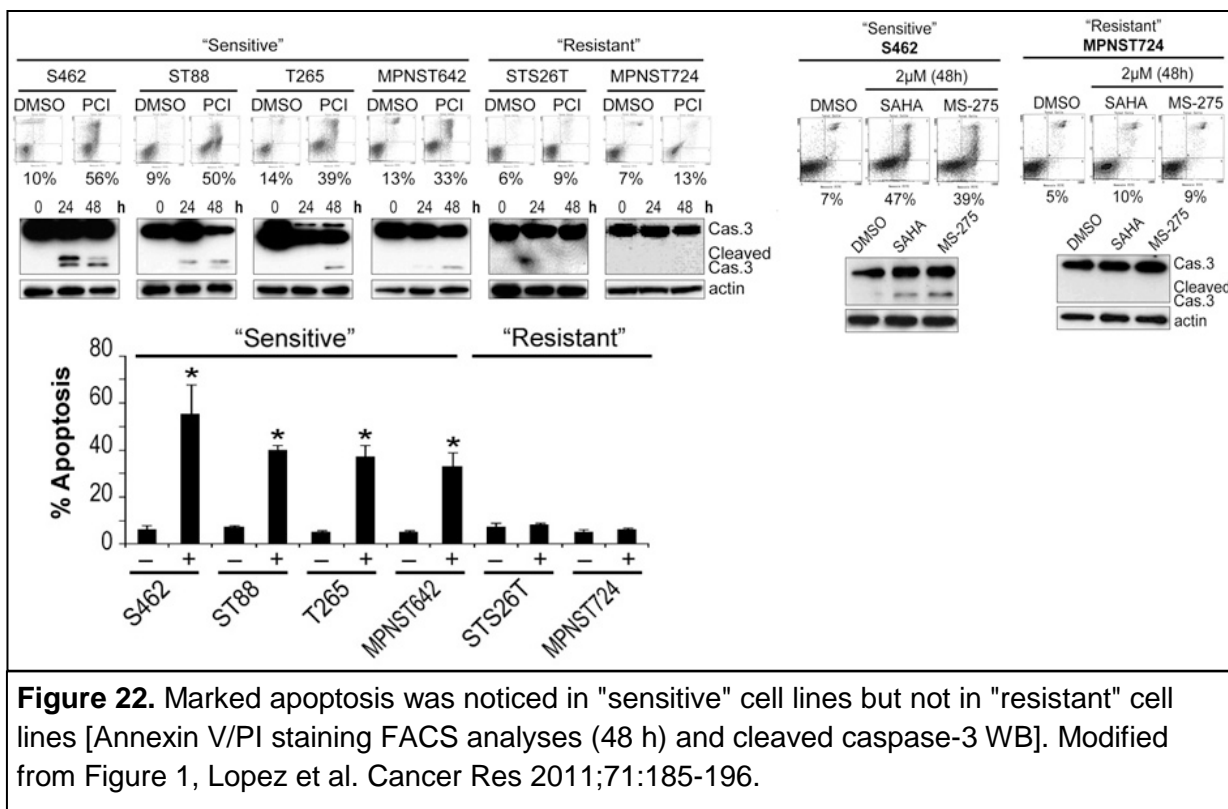


**Figure 21.** Clonogenic assays showed a similar pattern of response to HDACis. The respective graphs represent the number of colonies counted in experiments; repeated three times. Modified from Figure 1, Lopez et al. Cancer Res 2011;71:185-196.

response pattern was found for all these drugs, enabling MPNST cell designations to "sensitive" and "resistant" cohorts (**Fig. 20**).

This same pattern of sensitivity/resistance to the compounds was observed using clonogenic assays (**Fig. 21**). We then determined if this "sensitive" and "resistant" effect on growth was due to HDACi-induced apoptosis. All three compounds induced marked apoptosis (Annexin-V/PI staining FACS analysis and western blotting for cleaved caspase 3) in "sensitive" cell lines with little or no apoptosis in the "resistant" cells (**Fig. 22**). HDACi-induced acetylation of target proteins was observed in all cell lines including normal Schwann cells despite variations on the effect on growth (**Fig. 23**). Previous data have demonstrated that acetylation also occurs in normal cells (known to be resistant to HDACi effects), suggesting that even though HDACis reach

and inhibit their targets, additional mechanisms play a role in HDACi-mediated sensitivity and resistance (81).



We then tested the *in vivo* effect of PCI2 (this compound was selected due to its enhanced effect *in vitro*) on therapeutic "sensitive" and "resistant" human xenografts. Similar to the effects observed *in vitro*, MPNST642 xenografts were highly sensitive to the inhibitory growth effects of PCI2, while only a minimal effect on tumor growth occurred in MPNST724 and STS26T xenografts (**Fig. 24A**). Of note, marked effects on growth and tumor weight ( $p = 0.00016$  and  $0.0004$ , respectively) were noted in the MPNST642 experiment even when a relatively low therapeutic dose (25 mg/kg BID) was used. In contrast, no statistically significant impact ( $p > 0.05$ ) was found in

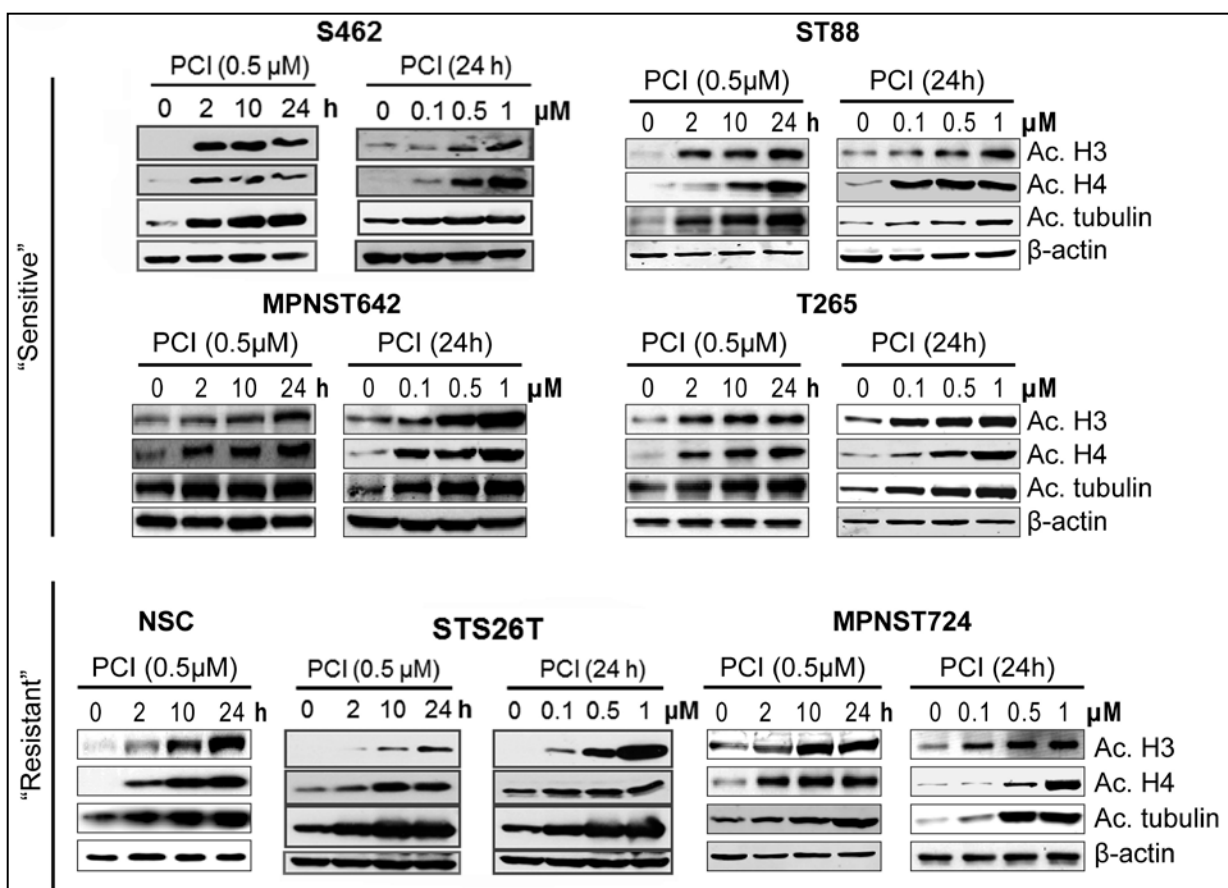


**Figure 23.** A time- and dose-dependent increase in target protein acetylation was shown after treatment with either of the compounds in all cell lines (including NSC) independent of growth inhibitory response (MS-275 is a selective HDAC1/HDAC2 inhibitor and does not affect tubulin acetylation). Modified from Figure 1, Lopez et al. Cancer Res 2011;71:185-196.

MPNST724 and STS26T experiments even when a high dose of PCI2 (50 mg/kg BID) was utilized (**Fig. 24A**). IHC analysis of the tumors from both xenografts reflected this difference in sensitivity and resistance (**Fig. 24B**). PCI2-treated MPNST642 xenografts had a decrease in Ki67 staining (cell proliferation) with an increase in TUNEL positive cells ( $p = 0.008$  and  $0.0008$ ). IHC analysis in the MPNST724 xenografts showed an opposite effect; no discernible change in Ki67 and TUNEL among vehicle and treated cohorts. This data further confirms HDACi-induced sensitivity and resistance in NF1-associated and sporadic MPNST cells, respectively.

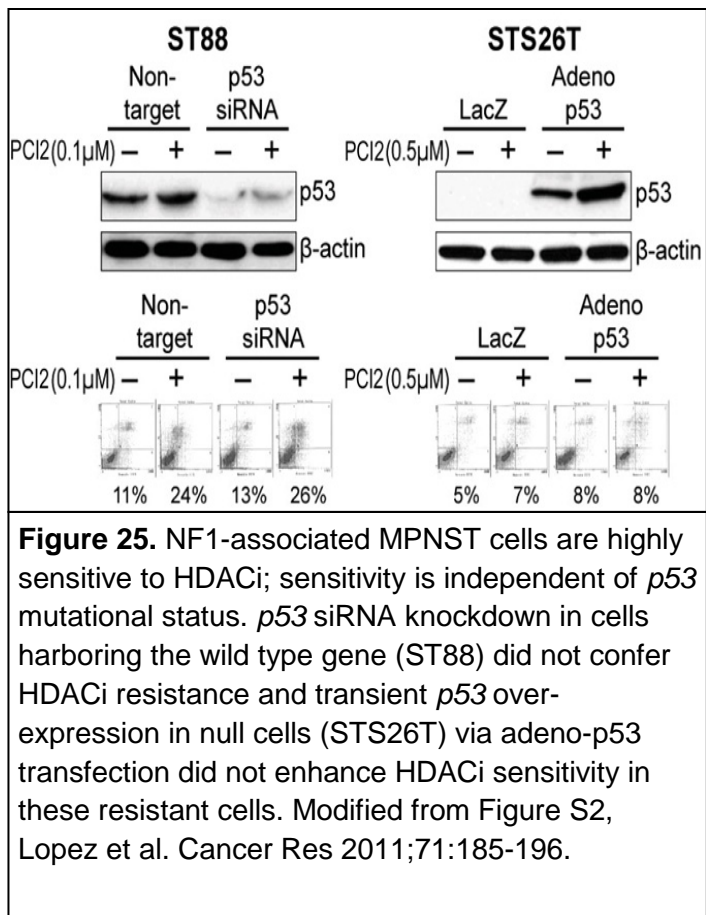


## 2.2 Potential mechanisms of sensitivity

Our results thus far suggest that a subset of MPNST cells are highly sensitive to HDACi effects. Unraveling the mechanism underlying this sensitivity is highly interesting from the biological/molecular perspective and can potentially be important for the appropriate selection of patients to HDACi-based “smart” clinical trials. First, we asked whether HDACi sensitivity is dependent of all tumor growth rates. **Table 7** depicts the average doubling times of our MPNST cell line panel. As can be ascertained from this data, no direct correlation between HDACi sensitivity and growth rate could be identified. Next, we sought to determine whether *p53* mutational status possibly correlates with HDACi sensitivity. HDACis are known to induce their effects, at least in part by *p53* activation (90). However, MPNSTs are known to commonly harbor *p53* mutations (91). To that end, we hypothesized that mutated *p53* cells might be more resistant to the effects of HDACis. *p53* mutational status of our panel of MPNST cell lines is depicted in **Table 7**. No direct correlation between *p53* status and HDACi sensitivity could be identified as the most sensitive cell line (S462) and the least sensitive cell lines (MPNST724 and STS26T) were found to harbor *p53* mutations. Furthermore, to evaluate whether the effects of HDACi in our cells are exerted at least in part through *p53*, wild-type *p53* ST88 and *p53* null STS26T cell lines were used. Knockdown of *p53* combined with PCI2 did not enhance apoptosis compared to non-target control in ST88 cells, suggesting that the absence of *p53* does not confer resistance to pan-HDACi. Overexpression of *p53* combined with PCI2 did



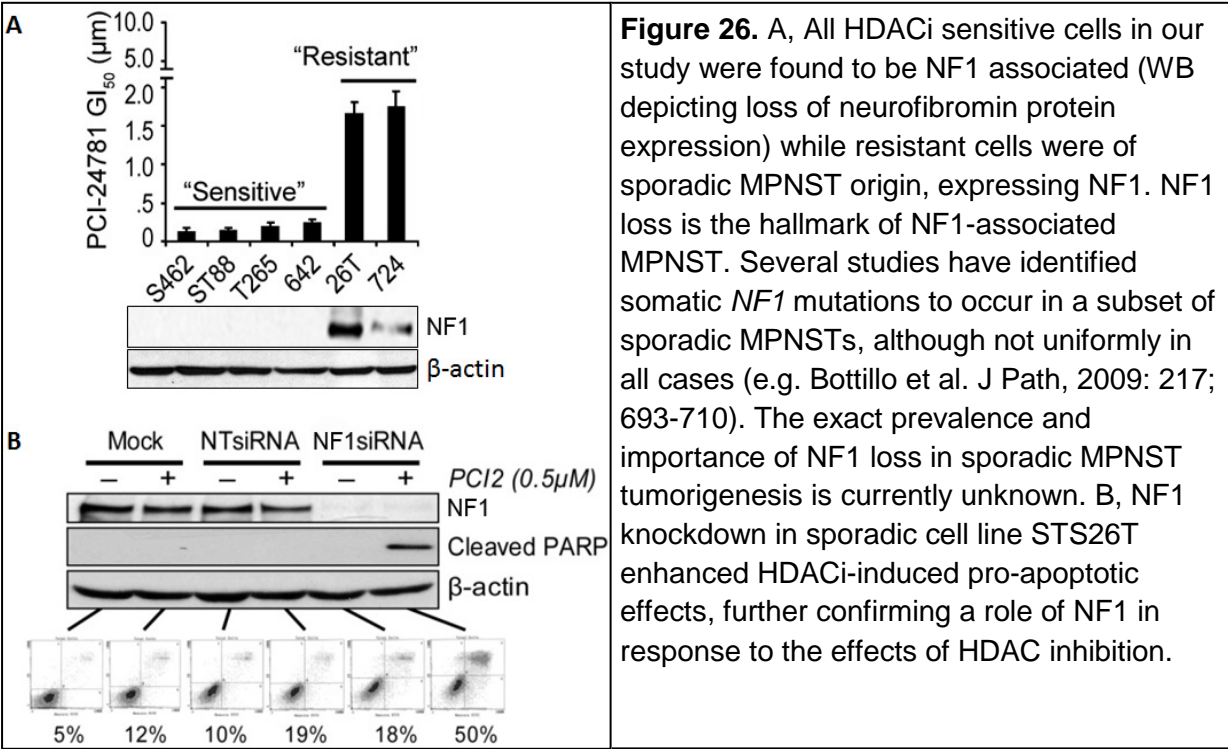
not enhance apoptosis compared to control in STS26T cells, suggesting that HDACi does not enhance sensitivity via p53 (**Fig. 25**).



Intriguingly, when we evaluated our results we noticed that all “sensitive” cell lines are NF1-associated while the “resistant” cells are sporadic MPNSTs (**Fig 26A**). While this observation has to be viewed with caution due to the limited cell line number available, we thought it is worthy of further investigation. Of note, this unique response pattern was not observed when we tested with doxorubicin or

other molecularly targeted anti-cancer therapies (e.g. the TKR inhibitor, XL184) (data not shown). Somatic NF1 loss has been suggested in another STS histological subtype, pleomorphic liposarcoma (PLS) (92); we evaluated our human PLS cell line cohort, finding that at least one of the three cell lines (Lisa2) exhibited NF1 expression loss (data not shown). Interestingly, this cell line was also the most sensitive to PCI2. While not directly related to these MPNST-focused studies, this observation further suggests a potential role for NF1 loss as an HDACi response biomarker and offers an

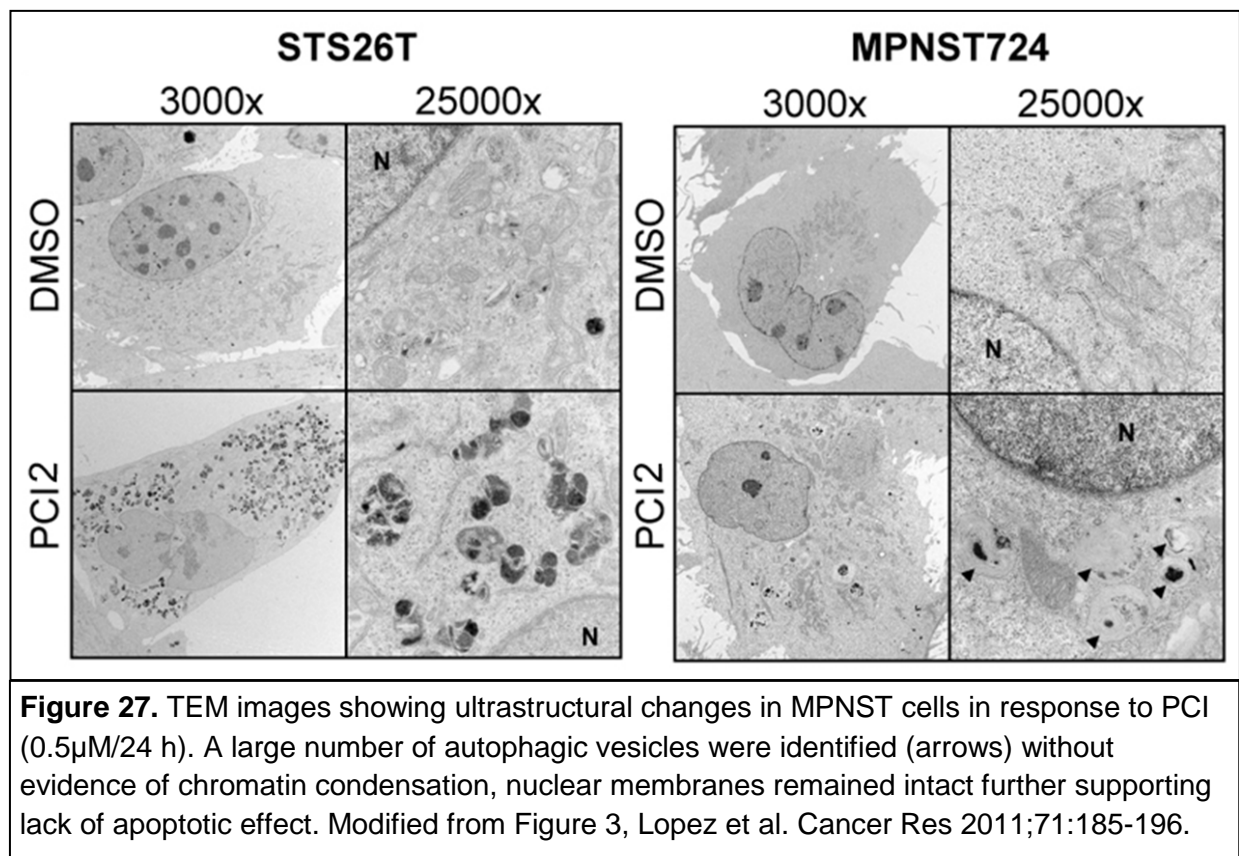
additional cellular model for basic NF1 studies. To determine whether NF1 loss does contribute to HDACi sensitivity, we knocked down NF1 in MPNST724 and STS26T cells using specific siRNA constructs (**Fig. 26B**); Neurofibromin loss resulted in increased apoptosis in response to HDACi. Together, these data demonstrate a potential role for NF1 loss in MPNST sensitivity to the pro-apoptosis effects of HDACis.



### Section 3: Aim 2: (Macro)Autophagy as a mechanism of HDACi resistance in MPNST

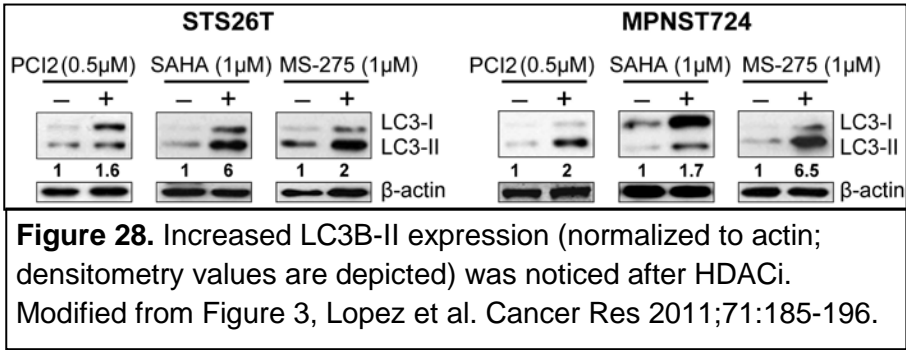
#### 3.1 HDACis induce autophagosome accumulation in MPNST cells

It is critical to determine the potential mechanisms contributing to the observed tolerance of some MPNST cells to HDAC inhibitors in order to develop more effective HDACi-based therapeutic combinations. To evaluate structural changes in “resistant” cells induced by HDACi, transmission electron microscopy (TEM) was utilized. Many, autophagosomal structures of various size were observed in PCI2 treated cells, with



no morphological features indicative of apoptosis or necrotic cell death (**Fig. 27**). The

presence of HDACi-induced autophagosome accumulation was further established when western blotting for the presence of LC3B conversion and the expression of LC3B-II. An increased expression of LC3B-II is indicative of an increase in autophagosome number; all three HDACis enhanced LC3B-II expression (**Fig. 28**). STS26T and MPNST724 were stably transduced to express GFP-LC3 and these were treated with HDACi and monitored via fluorescent microscopy. HDACi treatment induced an increase in GFP-LC3 puncta, representative of autophagosome accumulation (**Fig. 29**). HDACi-induced autophagosomal accumulation was also



observed *in vivo*.  
GFP-LC3 transduced  
MPNST cells were  
injected s.c. into

SCID mice and when tumors reached 1 cm, mice were treated with PCI2 for 4 days. On the 5<sup>th</sup> day a final dose was administered and tumors were collected after 2, 4, and 6 h. Western blot analysis of the tumor samples showed increased LC3B-II conversion in a time-dependent manner (**Fig. 30**). Furthermore, TEM identified autophagosome accumulation in tumor cells *in vivo* after treatment with PCI2 (**Fig. 30**). Interestingly, TEM analyses have demonstrated the potential accumulation of autophagosomes in NF1-associated, HDACi sensitive, MPNST cells in response to therapy. However, in contrast to resistant cells, signs of apoptosis were noted in these cells on TEM (chromatin condensation, membrane blebbing, etc.). Additional assays,

as per above, confirmed autophagosome accumulation in this MPNST cell line cohort (Fig. 31, 32).

Together, these experiments demonstrated that HDACi-induced autophagosomal accumulation occurs in all tested MPNST cell lines. Autophagosome accumulation is not necessarily a mark of induced autophagy as it can signify either enhanced autophagic flux or blocked, incomplete autophagy. Multiple additional experiments are required in order to determine the implications of the above observations.

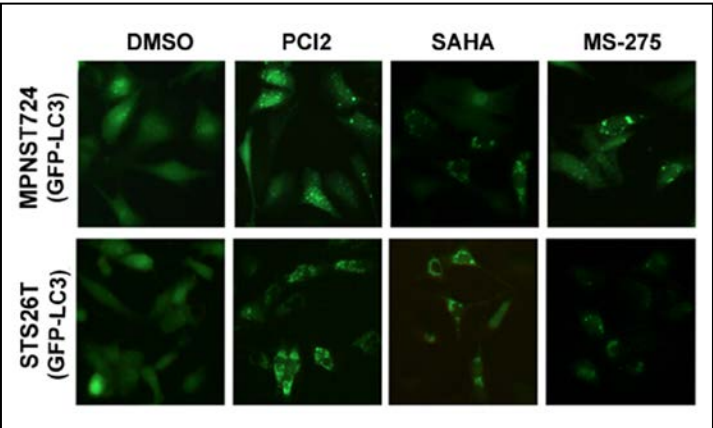


**Figure 29.** Cells stably transduced to express GFP-LC3 exhibited increased GFP puncta in response to HDACis. Modified from Figure 3, Lopez et al. Cancer Res 2011;71:185-196.

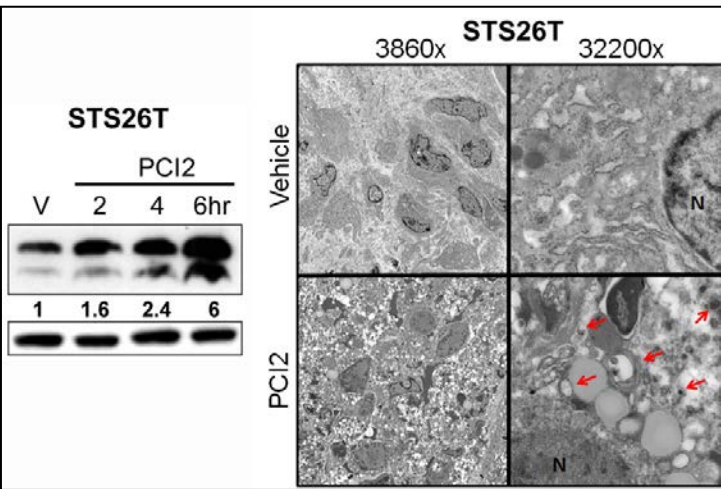


**Figure 30.** WB of STS26T xenografts' protein treated with PCI2 (50 mg/kg/d) harvested 2, 4, and 6 h after final dose showed a time-dependent increase in LC3B-II expression. TEM images showing autophagosomal structures in STS26T xenografts. Samples used for the experiments shown here are from the same *in vivo* therapeutic experiment.

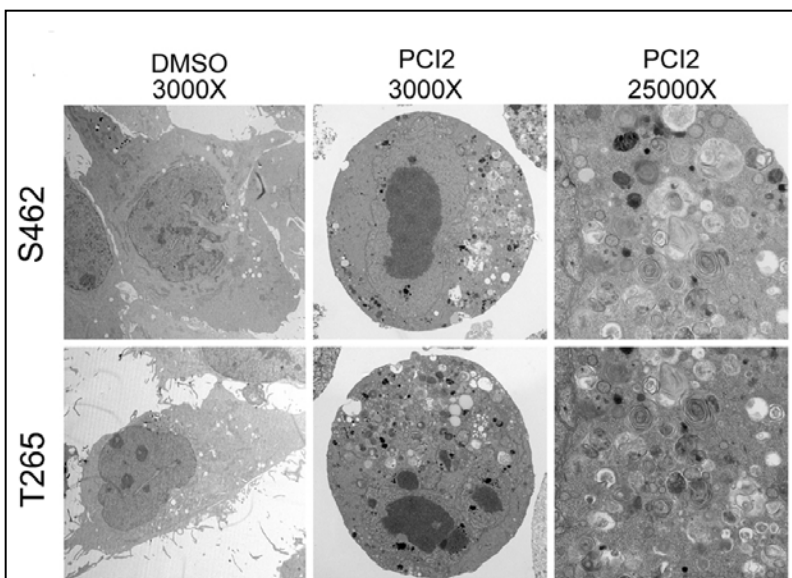


**Figure 31.** TEM images showing ultrastructural changes in NF1-associated MPNST cells in response to PCI2 (0.5 $\mu$ M/24 h). As seen in “resistant” cells (**Fig. 28**) a large number of autophagic vesicles can be found after HDACi treatment. However, prominent features of apoptosis such as chromatin condensation and loss of nuclear membranes are also evident. Modified from Figure S3, Lopez et al. Cancer Res 2011;71:185-196.

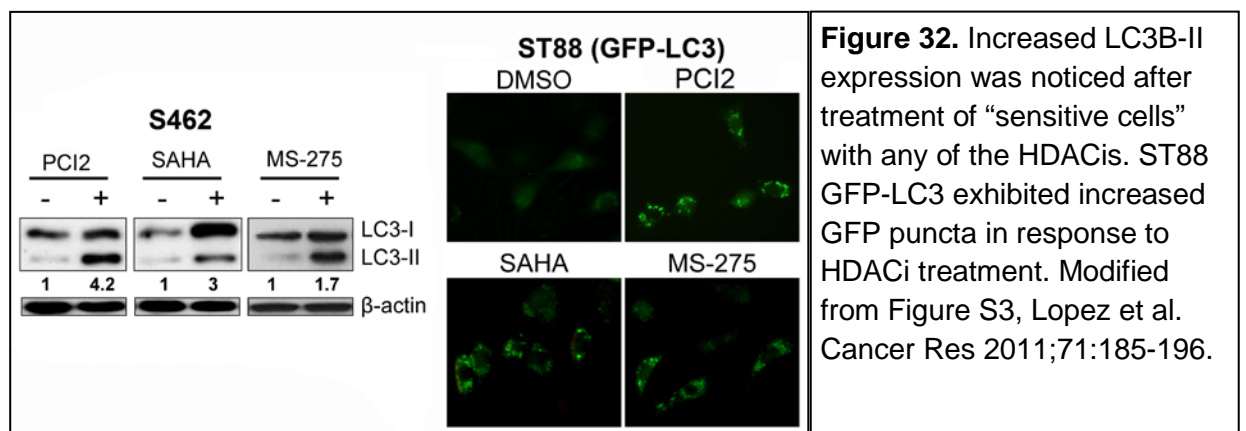


**Figure 32.** Increased LC3B-II expression was noticed after treatment of “sensitive cells” with any of the HDACis. ST88 GFP-LC3 exhibited increased GFP puncta in response to HDACi treatment. Modified from Figure S3, Lopez et al. Cancer Res 2011;71:185-196.

### 3.2 HDACis induce productive autophagy in MPNST cells in vitro and in vivo

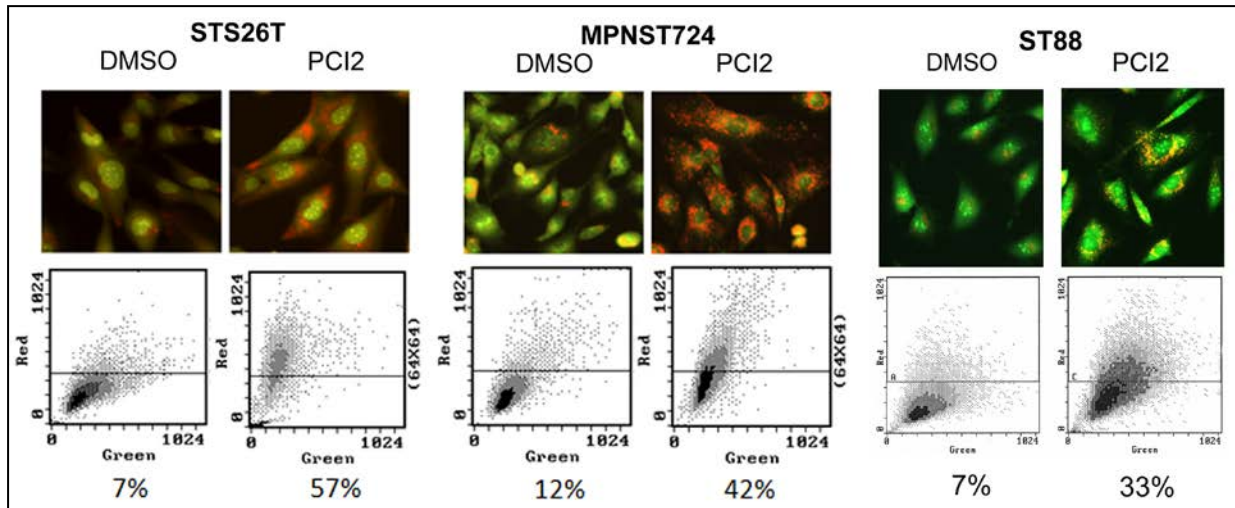


**Figure 33.** AO staining demonstrated increased AVOs in PCI2 treated (0.5uM/24 h) sporadic and NF1-associated MPNST cells compared to control treated cells, as was further confirmed via FACS analysis. Modified from Figure 3 and S3, Lopez et al. Cancer Res 2011;71:185-196.

As stated above, additional assays are required to distinguish between enhanced autophagic flux (productive autophagy) and blocked autophagy. First, staining with the lysotropic compound acridine orange revealed an increase in acidic vesicular organelles in PCI2 treated cells compared to control DMSO treated cells; microscopy and FACS analysis both confirmed this observation (**Fig. 33**).



Increased acridine orange staining was seen in both “resistant” and “sensitive” cells suggesting enhanced productive autophagy in response to treatment. This assay, however, is not sufficient to conclusively determine productive autophagy and additional experiments using inhibitors of the final stages of autophagy (Bafilomycin A1 [BFA] and chloroquine [CQ]) are usually needed. Pretreatment (1 h) of MPNST cells with either lysosome inhibitor followed by PCI2 for 24 h resulted in a higher expression of LC3B-II compared to control, BFA or CQ alone, and PCI2 alone, providing evidence for enhanced productive autophagy in response to PCI2 (**Fig. 34**). Those effects were noted in both “resistant” (**Fig. 34A**) and “sensitive” (**Fig. 34B**) MPNST cell lines. Similarly, when GFP-LC3 transduced cells were treated with BFA or CQ, HDACi, and BFA/CQ combined with HDACi, an increase of GFP cleavage from LC3B was observed in PCI2 treated cells compared to other treatments (**Fig. 35A**).

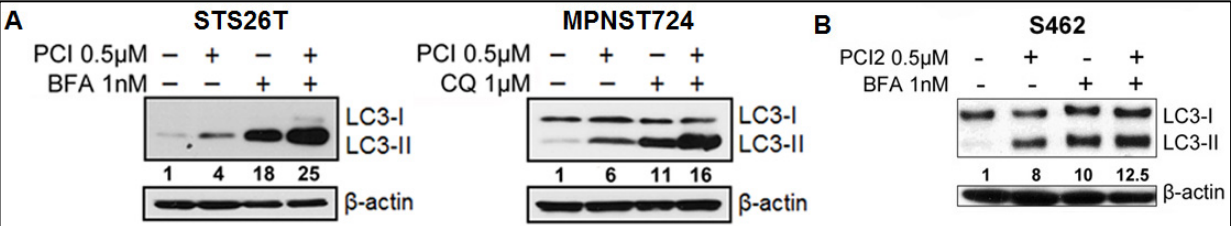
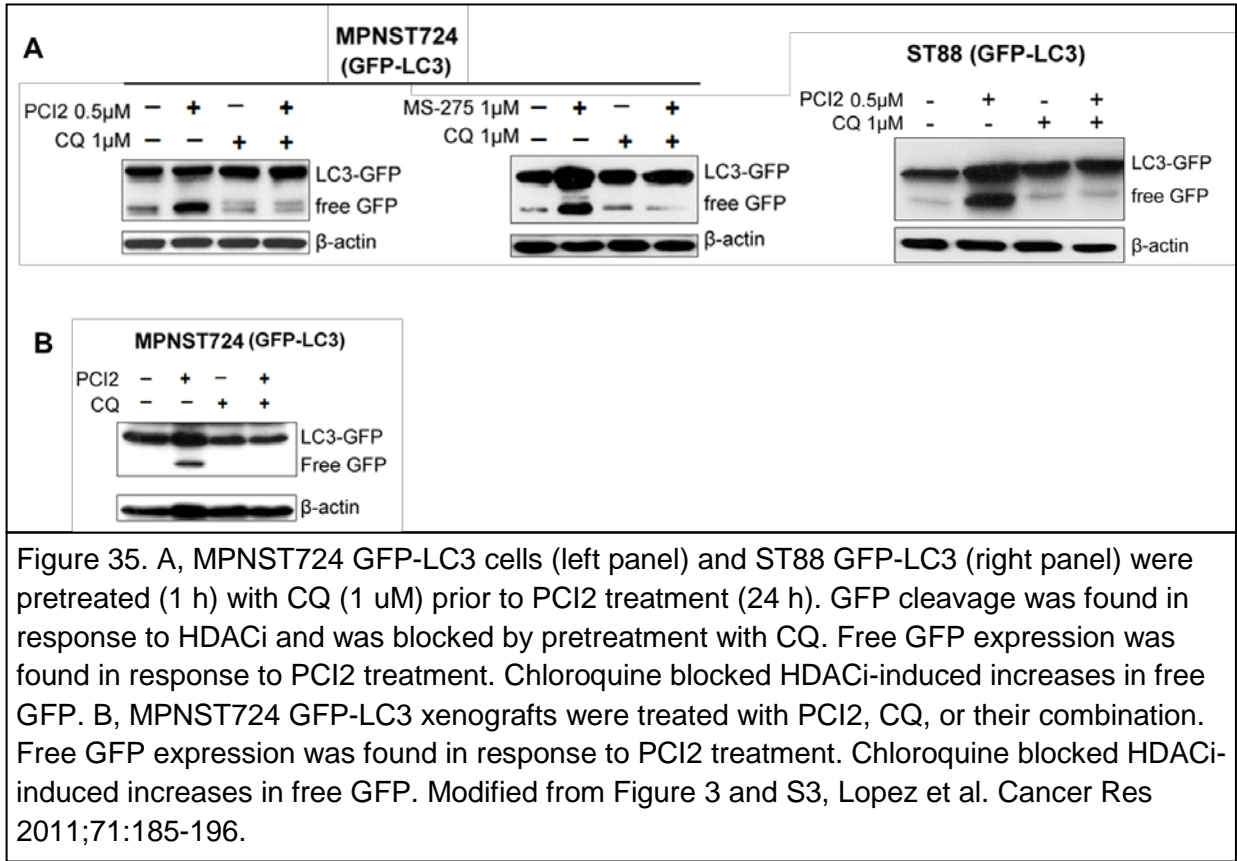


Figure 34. Sporadic (panel A) and NF1-associated MPNST cells (panel B) were pretreated (1 h) with low doses of the inhibitors BFA (1 nM) or CQ (1 μM) prior to PCI2 treatment (24 h). Additional increased LC3B-II expression in response to PCI2 was noticed in the presence of these inhibitors. Modified from Figure 3 and S3, Lopez et al. Cancer Res 2011;71:185-196.



Together, these assays support HDACi-induced productive autophagy in MPNST cells *in vitro*. GFP-LC3 xenografts were also treated with PCI2, chloroquine, and the combination (mice were treated with chloroquine 1 day prior to combining with PCI2). Western blot analysis of the tumor samples showed an increase cleaved GFP in PCI2 treated mice whereas pretreatment with CQ inhibited PCI2-induced GFP cleavage (**Fig. 35B**). This data revealed that HDACi-induced autophagy can be recapitulated *in vivo*.



### 3.3 Autophagy is a mechanism of therapeutic resistance in MPNST

The role of drug-induced autophagy in cancer remains controversial, whether this process contributes to cell death or is a mechanism of resistance might be a cell-context, -compound, -specific consequence (93, 94). To evaluate the role of HDACi-induced autophagy in MPNST we evaluated the impact of autophagy blockade by genetic (i.e. siRNA) and pharmacological inhibition on the HDACi therapeutic response. Knockdown of beclin 1, ATG5, and ATG7, genes essential for the induction of autophagy, was combined with PCI2. Knockdown of these genes, as expected, inhibited PCI2-induced LC3B conversion (i.e. autophagy) and most importantly resulted in enhanced apoptosis compared to knockdown or PCI2 treatment alone (**Fig. 36-38**). Enhanced apoptosis was noted in both “resistant” and “sensitive” MPNST cell lines; a lower PCI dose was used for the later.

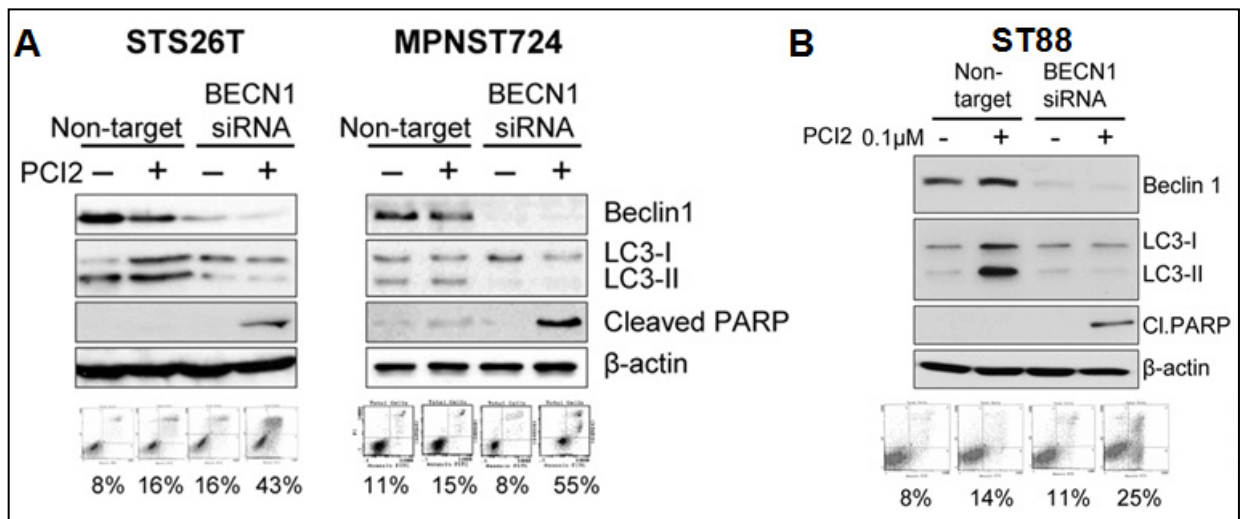


Figure 36. Anti-Beclin siRNA (20 nM pool) knockdown in sporadic (A) and NF1-associated MPNST cells (B) was confirmed by WB and autophagy blockade was validated using LC3B-II WB. Enhanced apoptosis in response to PCI2 (sporadic cells 0.5  $\mu$ M/24 h; NF1-associated cells 0.1  $\mu$ M/24 h) was determined by PARP cleavage and Annexin-V/PI FACS analysis. Modified from Figure 4 and S3, Lopez et al. Cancer Res 2011;71:185-196.

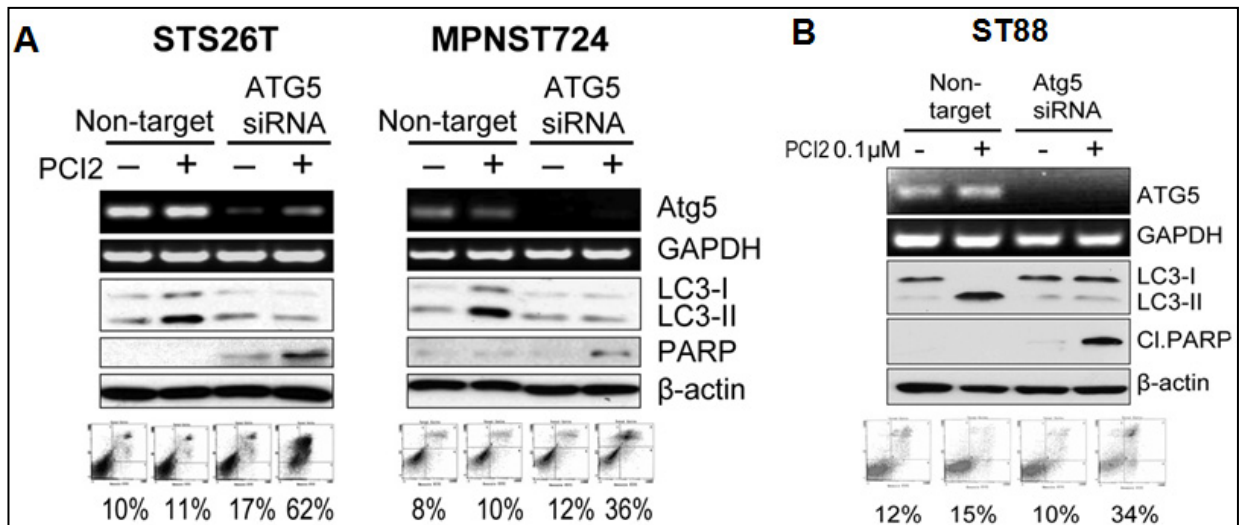
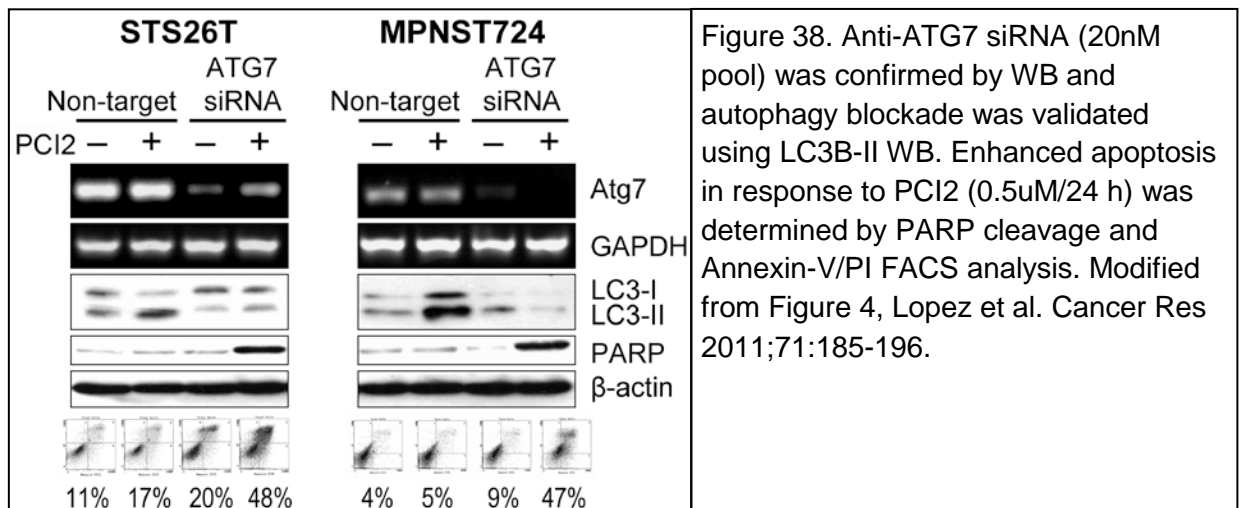


Figure 37. Anti-ATG5 siRNA (20nM pool) knockdown in sporadic (A) and NF1-associated MPNST cells (B) was confirmed by RT-PCR and autophagy blockade was validated using LC3B-II WB. Enhanced apoptosis in response to PCI2 (sporadic cells 0.5uM/24h; NF1-associated cells (0.1uM/24 h) was determined by PARP cleavage and Annexin-V/PI FACS analysis. Modified from Figure 4 and S3, Lopez et al. Cancer Res 2011;71:185-196.



We next evaluated the effect of pharmacological inhibition of autophagy combined with HDACi. Again, we used BFA and/or CQ to inhibit lysosomal-mediated degradation of HDACi-induced autophagosome content. Monotherapy with BFA/CQ and PCI2 had no effect on the clonogenic potential of MPNST cell lines, but combination of these compounds resulted in a significant reduction in colony forming capacity (**Fig. 39**).

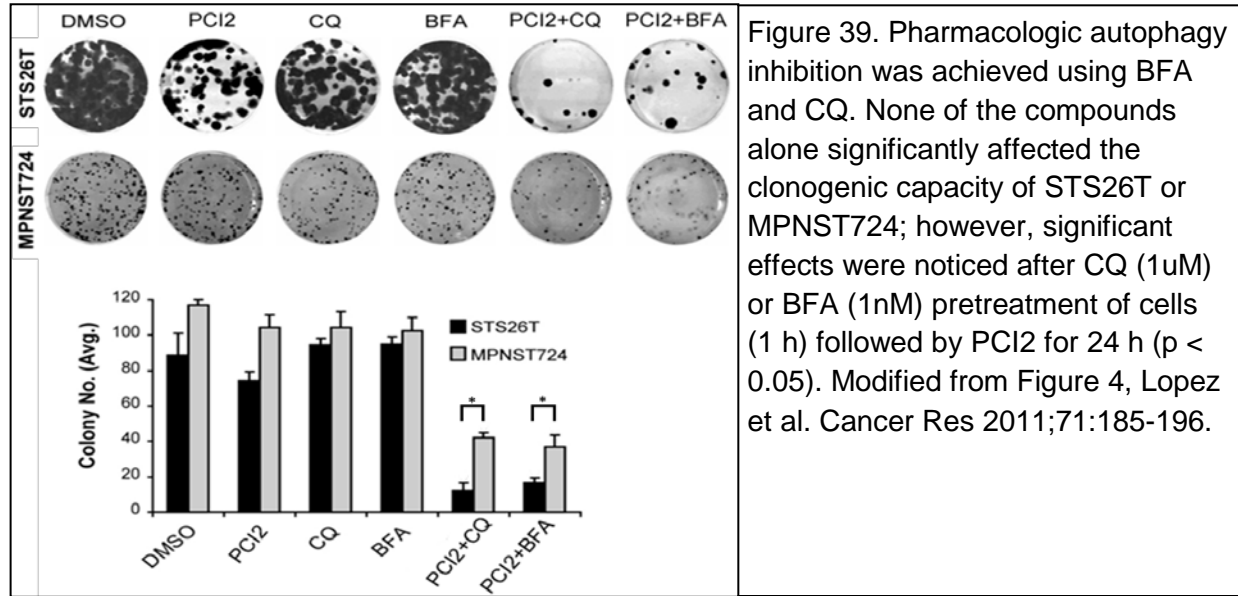
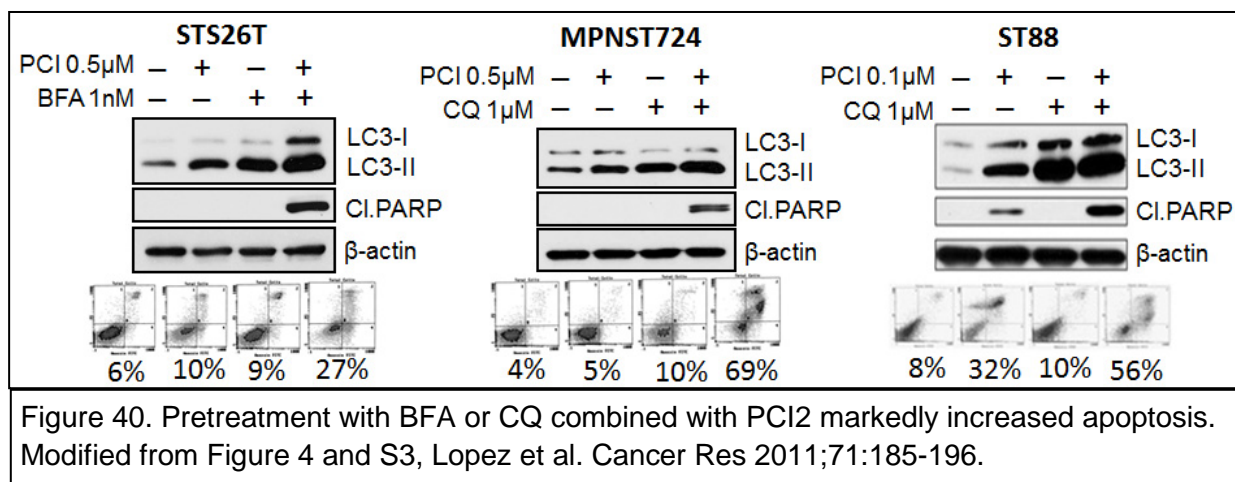


Figure 39. Pharmacologic autophagy inhibition was achieved using BFA and CQ. None of the compounds alone significantly affected the clonogenic capacity of STS26T or MPNST724; however, significant effects were noticed after CQ (1uM) or BFA (1nM) pretreatment of cells (1 h) followed by PCI2 for 24 h ( $p < 0.05$ ). Modified from Figure 4, Lopez et al. Cancer Res 2011;71:185-196.

Combination therapy also resulted in enhanced apoptosis compared to BFA/CQ and PCI2 alone (**Fig. 40**). These effects were noted in both “resistant” and “sensitive” MPNST cell lines; a lower PCI2 dose was utilized for the later. Taken together, our data strongly demonstrates that autophagy blockade enhances the pro-apoptotic effects of HDACis in MPNST. This occurs in both cells that are relatively resistant to HDACi-induced apoptosis as well as cells that are sensitive to these effects. In the later scenario, combining autophagy blockade with even low doses of HDACis induces marked cell death.



While the above results are highly promising, all of these observations were made using cells growing in culture. At this stage it was thus critical if superior effects of HDACi/autophagy blockade can be recapitulated *in vivo*. To that end, mice harboring STS26T and MPNST724 xenografts were allocated into 4 treatment arms when tumors reached ~5 mm<sup>3</sup>: vehicle, CQ, PCI2, CQ combined with PCI2. In the combination treatment, mice were treated with CQ 24 hr prior to combining with PCI2. As in previously described experiments (see **Fig. 25**), the efficacy of PCI2 as monotherapy was minimal as compared to vehicle control. Similarly, Chloroquine alone did not significantly impact tumor growth. However, combination therapy resulted in significant tumor growth inhibition in both xenograft models compared to vehicle or either compound alone (**Fig. 41**). MPNST724 xenograft volumes and weights at study termination were: control 1576.1 mm<sup>3</sup> ±573.6 and 1.3 g ±0.2; PCI2 1131.1 mm<sup>3</sup> ±257.7 and 1.24 g ±0.1; Chloroquine 925.3 mm<sup>3</sup> ±201.8 and 1.1 g ±0.1; and combination 209.2 mm<sup>3</sup> ±44.8 and 0.25 g ±0.1 respectively. STS26T tumor volumes and weight at study termination were: control 1242.8 mm<sup>3</sup> ±120 and 1.4 g

$\pm 0.2$ ; PCI2  $985.5 \text{ mm}^3 \pm 143.8$  and  $1.1 \text{ g} \pm 0.1$ ; Chloroquine  $1030.3 \text{ mm}^3 \pm 144$  and  $1.2 \text{ g} \pm 0.2$ ; and combination  $171.7 \text{ mm}^3 \pm 123$  and  $0.24 \text{ g} \pm 0.1$  respectively.

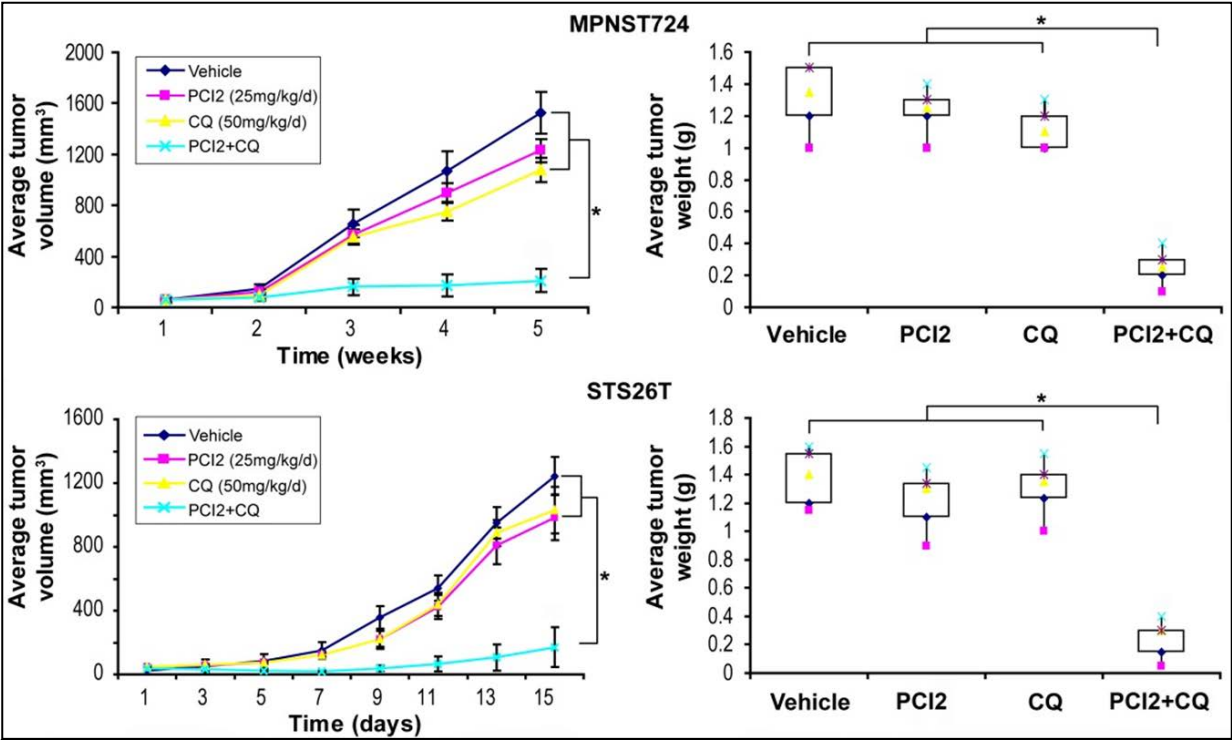


Figure 41. Tumor growth curves/weight bars showing a significant impact of PCI2 + CQ combination on MPNST724 and STS26T growth ( $p = 0.04$  and  $p = 0.03$ , respectively). No significant effect was noted after either compound alone. \*, statistically significant effects;  $p < 0.05$ . Modified from Figure 5, Lopez et al. Cancer Res 2011;71:185-196.

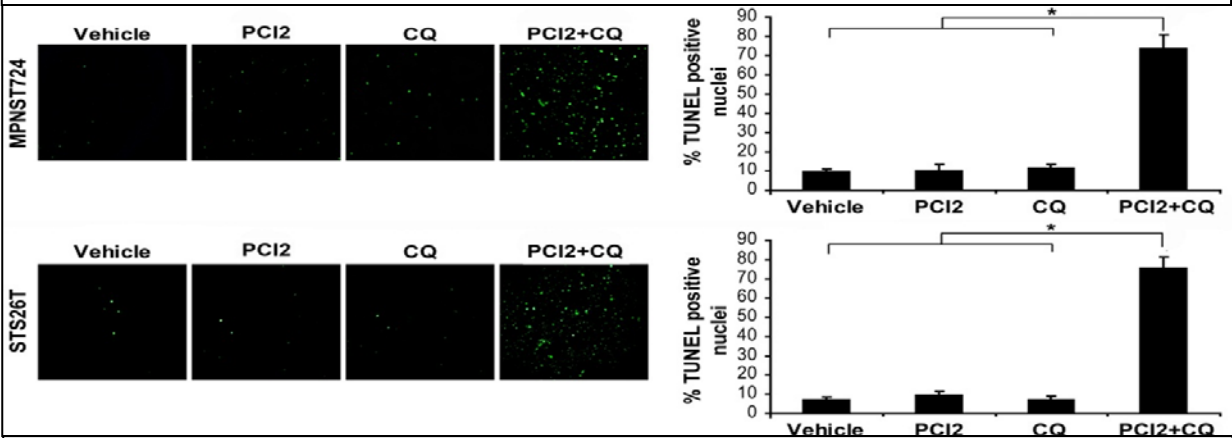


Figure 42. TUNEL assay of samples from Fig. 43. Significant increase in apoptosis (TUNEL staining) was observed in combination-treated xenografts ( $p < 0.05$ ). \*, statistically significant effects;  $p < 0.05$ . Modified from Figure 5, Lopez et al. Cancer Res 2011;71:185-196.

Immunohistochemical analysis revealed that combination treated tumors had a significant increase in TUNEL positive cells compared to vehicle or either compound alone (**Fig. 42**).

While the above experiment evaluated the effects of treatment on local MPNST xenograft growth it is critical to assess if this therapeutic regiment affects MPNST lung metastasis growth. Limited by the lack of spontaneous MPNST lung metastasis mouse models, we utilized an experimental model where STS26T cells are injected i.v. into the tail vein. Established lung metastasis develop within 2 weeks after injection, thus treatment was initiated at that time. Similar to the local growth xenograft models, combination of CQ with PCI2 significantly inhibited the growth of STS26T lung metastases compared to either drug alone (**Fig. 43**). All mice in this therapeutic experiment had observable macroscopic lung metastases, however, the number of macroscopic lesions was severely reduced in combination therapy mice compared to vehicle, PCI2 and Chloroquine alone. The average number of macroscopic lung metastases were: Vehicle  $9.6 \pm 1.8$ , PCI2  $8.2 \pm 1.7$ , Chloroquine  $8.5 \pm 1.7$ , combination  $2.1 \pm 1.1$ . This difference between vehicle, PCI2 and Chloroquine alone compared to combination was highly significant ( $p > 0.001$ ). Average lung weights from each group also depicted these significant differences: Vehicle  $0.6 \text{ g} \pm 0.1$ , PCI2  $0.4 \text{ g} \pm 0.1$ , Chloroquine  $0.4 \text{ g} \pm 0.1$ , combination  $0.2 \text{ g} \pm 0.1$ . Cumulatively, these data confirm that autophagy blockade sensitizes MPNST xenografts to the pro-apoptotic effects of HDACi *in vivo*.

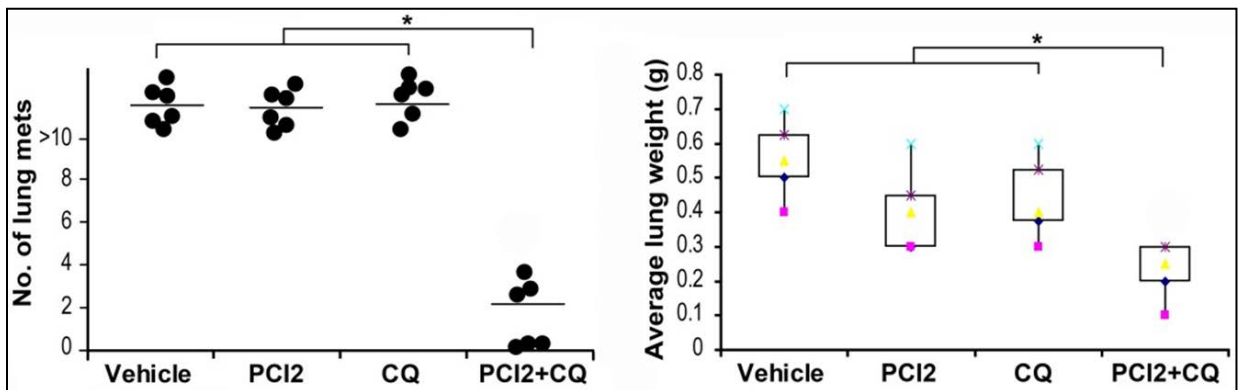


Figure 43. STS26T lung metastases bearing mice were treated with PCI2, CQ, or their combination. A significant decrease in number of visible metastasis (left graph) and average lung weight (right graph) were found in the combination therapy group ( $p < 0.05$ ) but not after treatment with either agent alone. \*, statistically significant effects;  $p < 0.05$ . Modified from Figure 5, Lopez et al. Cancer Res 2011;71:185-196.



## *Section 4: Aim 2: Molecular mechanisms underlying HDACi induced autophagy in MPNST*

### *4.1 Autophagy gene array results and confirmation*

Unraveling the molecular mechanisms underlying the development of productive autophagy in response to HDACi are highly important. This information can not only enhance our current knowledge of the autophagy process but can hopefully result in the identification of molecules that can be targeted in combination with HDACi to achieve improved anti-MPNST therapeutic effects. This is especially critical when realizing that Chloroquine is not exclusively an autophagy inhibitor, having multiple “off target” effects. To identify potential molecules contributing to HDACi-induced autophagy, we used a focus PCR-based autophagy array (this platform consists of primers targeting 84 genes known to play a role in autophagy, 56). RNA was extracted from MPNST cells treated with PCI2 (0.5uM, 24 h) or with DMSO alone and autophagy related gene expression changes were determined. Treatment with PCI2 induced the overexpression of 4 genes and the downregulation of 5 genes in all 4 cell lines tested. Overexpressed genes *CXCR4*, *TMEM74*, and *IRGM* and downregulated *NF-kB* were chosen for array validation. Quantitative RTPCR demonstrated a dose-dependent increase or decrease in the RNA expression of the selected genes after treatment with PCI2 (**Fig. 44**). These PCI2-induced changes in RNA expression also occurred in samples obtained from *in vivo* therapeutic experiments (**Fig. 45**). This data identified a

variety of HDACi-modified genes potentially important in HDACi-induced autophagy, warranting additional study.

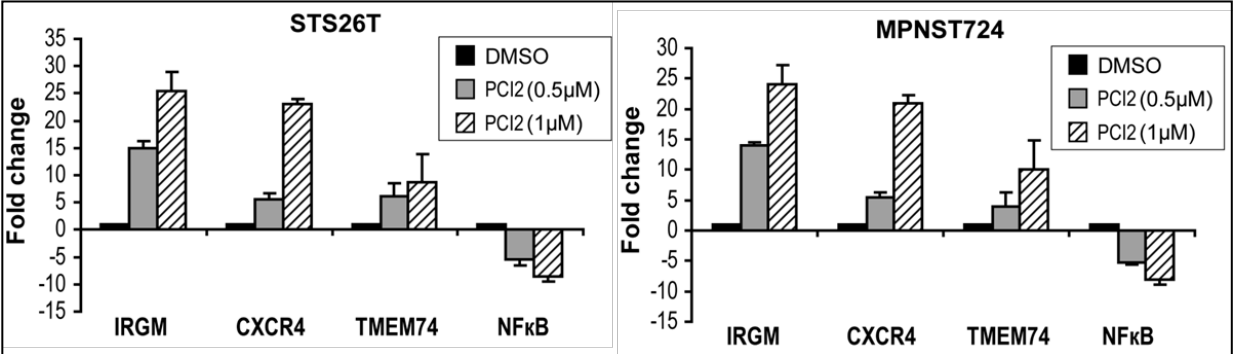


Figure 44. A focused autophagy PCR array identified several genes to be reproducibly deregulated in response to PCI2 (0.5uM/24 h). A concordant dose-dependent increase/decrease in corresponding RNA expression levels was identified (qRTPCR) in both cell lines after treatment with PCI2 (24 h). Modified from Figure 6, Lopez et al. Cancer Res 2011;71:185-196.

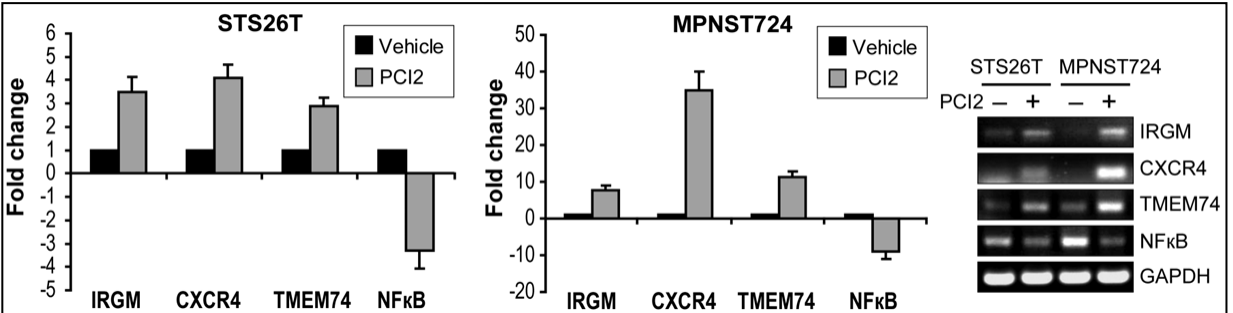


Figure 45. An increase in *IRGM*, *CXCR4*, and *TMEM74* mRNA and a decrease in *NF-kB* mRNA levels were identified by qRTPCR and RTPCR in xenograft tissues retrieved from experiments described earlier. Modified from Figure 6, Lopez et al. Cancer Res 2011;71:185-196.

#### 4.2 IRGM as an HDACi target enhancing

Among the genes selected for validation, *IRGM* exhibited the highest increase in HDACi-induced RNA expression, and was thus chosen for further evaluation of its potential role in HDACi-induced autophagy. To determine whether the observed increase in *IRGM* is PCI2 specific or is a more general response to HDACi in our cells we evaluated its expression in response to SAHA and MS-275; both compounds enhanced the expression of this gene. WB analysis further demonstrated that the effects on *IRGM* mRNA were also recapitulated in protein expression levels (**Fig. 46**).

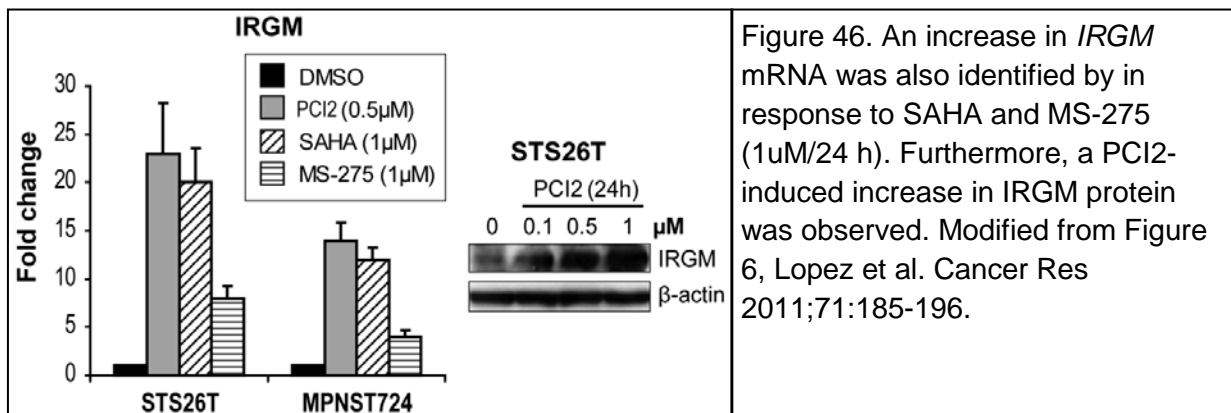


Figure 46. An increase in *IRGM* mRNA was also identified by in response to SAHA and MS-275 (1uM/24 h). Furthermore, a PCI2-induced increase in *IRGM* protein was observed. Modified from Figure 6, Lopez et al. Cancer Res 2011;71:185-196.

Next, the impact of *IRGM* on HDACi-induced autophagy was evaluated. *IRGM* was knocked down in MPNST cells using siRNA constructs; KD was confirmed by RTPCR. These cells as well as cells transfected with non-targeting siRNA constructs (used as controls) were treated with PCI2. WB analyses confirmed that *IRGM* KD inhibited LC3 conversion and LC3-II expression in MPNST cells in response to PCI2. Most importantly, *IRGM* KD induced apoptosis in MPNST cells in response to HDAC inhibition (**Fig. 47**). Together, we found that HDACi-induced expression of *IRGM*

enhances productive autophagy and inhibition of this protein enhances the pro-apoptotic effects of the drug.

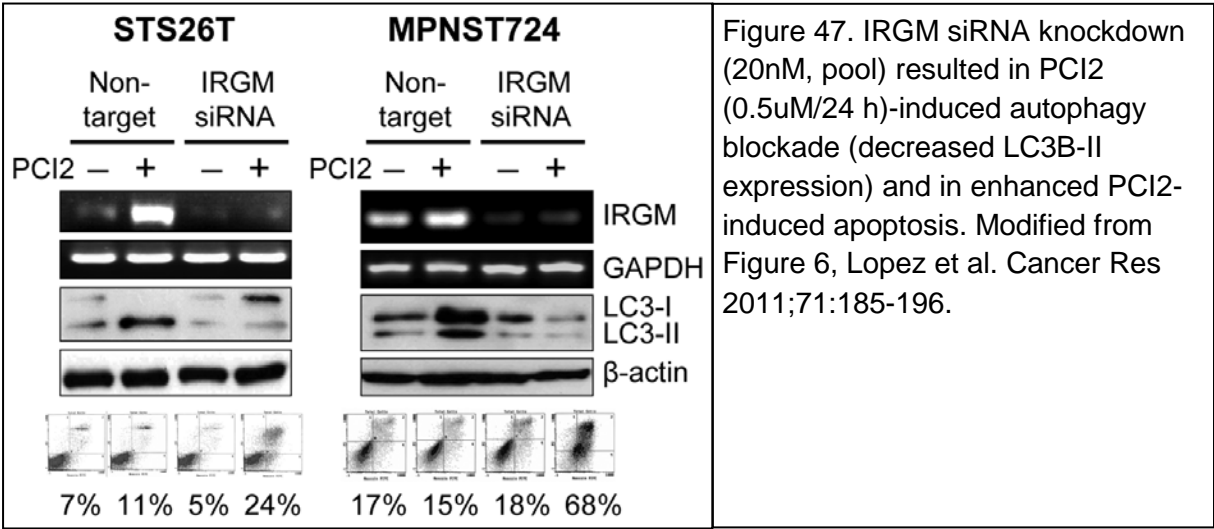


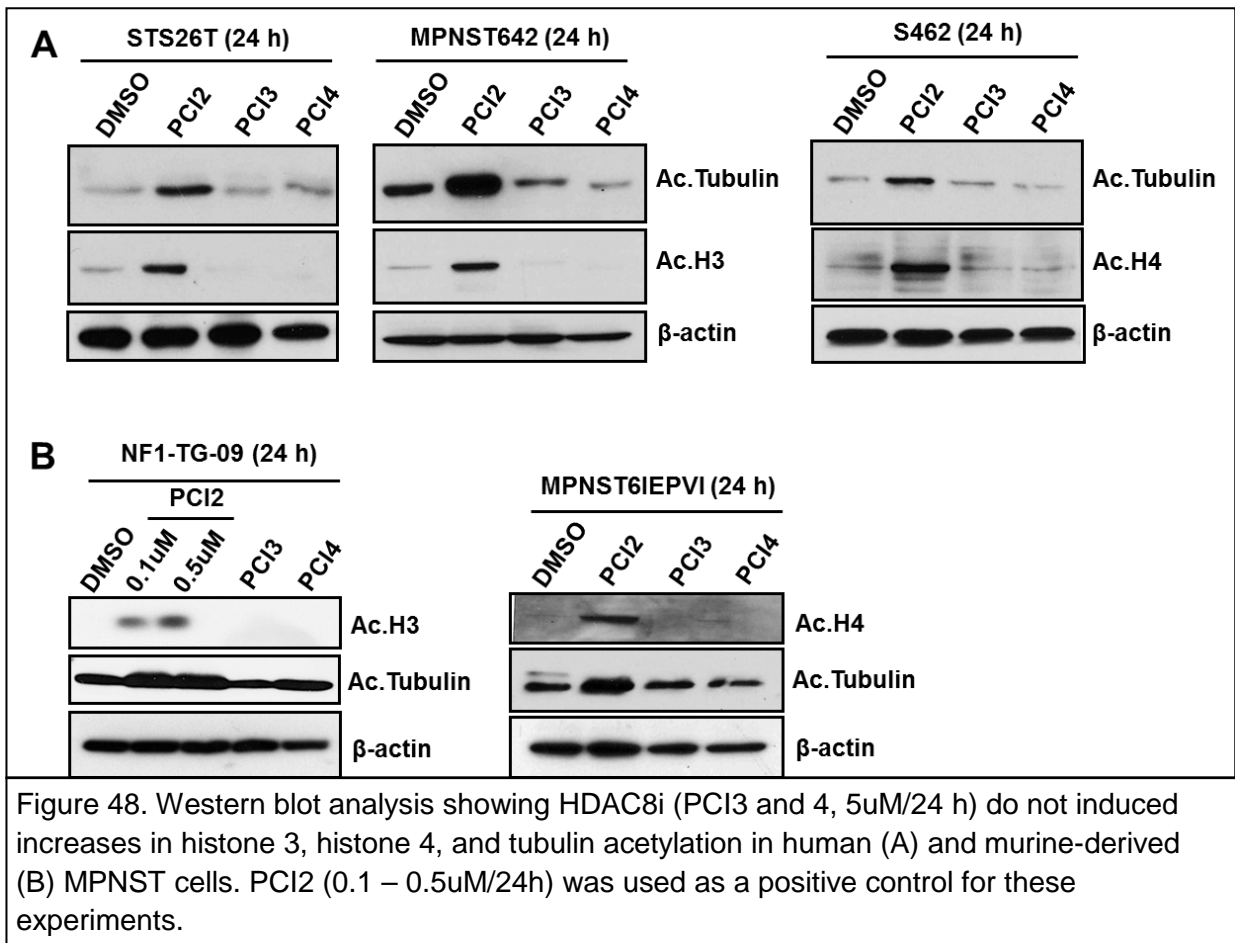
Figure 47. IRGM siRNA knockdown (20nM, pool) resulted in PCI2 (0.5uM/24 h)-induced autophagy blockade (decreased LC3B-II expression) and in enhanced PCI2-induced apoptosis. Modified from Figure 6, Lopez et al. Cancer Res 2011;71:185-196.

## Section 5: Aim 3: Effects of HDAC8 inhibition on MPNST

### 5.1 Effects of HDAC8is on human and murine MPNST cells *in vitro*

Collectively, we have shown that MPNSTs are highly sensitive to the effects of pan-HDACi when administered as single agents or in combination with autophagy inhibitors. However, data stemming from clinical studies suggest that pan-HDACi have a narrow therapeutic window due to toxicity. Development of HDAC isoform-specific inhibitors might increase this therapeutic window by eliminating unwarranted side effects elicited by blocking multiple HDAC enzymes. While no specific inhibitors are currently available for HDACs 1, 2, or 3, recently, highly selective compounds blocking the activity of the forth isoform, HDAC8, have been developed. In these final set of experiments, we sought to evaluate the effects of such inhibitors: PCI-34051 and its derivative PCI-48012; the later a little less selective but having better PK/PD properties making it ideal for *in vivo* studies. For these studies, in addition to testing the effects on our panel of human MPNST cell lines, we have also utilized several murine MPNST cell lines derived from tumors spontaneously developed in the MPNST GEM model (cis NF1<sup>-/+</sup>/p53<sup>-/+</sup>). Two such cell lines (MPNST6IEP4 and MPNST6IEP) were provided by Dr. Luis Parada (UT Southwestern, Dallas, TX) and two additional ones (NF1-TG-05 and NF1-TG-09) were developed in our laboratory. HDAC8 inhibition, unlike the inhibition of other HDACs, was previously demonstrated to not induce the acetylation of histones and/or tubulin. To confirm that PCI3 and PCI4 do not inhibit other HDACs we evaluated the expression of acetylated histones and tubulin via WB. As shown in **Fig. 48**, induction of histones 3 and 4 and tubulin acetylation was observed in human

as well as murine MPNST cells after PCI2 treatment but not in response to PCI3 or PCI4.



This data confirms with previously published data demonstrating that histone 3 and 4 and tubulin are not deacetylation targets of HDAC8, at least in certain cellular models (66, 68). Despite these results, HDAC8 has been shown to deacetylate core histone proteins (61, 63, 64). KrennHrubec et al. showed that compound 2, a ‘linkerless’ hydroxamate-derived compound with high affinity to HDAC8, when used at high doses (100 $\mu$ M) induced the expression of acetylated histone 4 and  $\alpha$ -tubulin in HeLa and HEK293 cells. Importantly, compound 2 at 0.8 $\mu$ M was shown to have minimal

inhibition of HDAC6, a HDAC known to specifically deacetylate tubulin (70). Our data using PCI3/4 suggests, at least in our MPNST models, that HDAC8 may serve in a role independent of histone modification. Similar to the work done by Krennhrubec and colleagues, it will be important to identify if PCI3/4 can induce histone and tubulin acetylation in our MPNST cells at higher doses than currently used. Of note, Balasubramanian et al., showed that PCI-34051 (PCI3) did not induce the acetylation of histones or tubulin in Jurkat cells at doses < 25uM (68). Next, we proceeded to determine whether HDAC8 inhibitors exhibit any effects on the growth of MPNST cells. MTS assays (96 h) demonstrated a dose-dependent growth inhibitory effect of PCI3/4 on human and murine-derived MPNST using doses in the micromolar range (**Fig 49**).

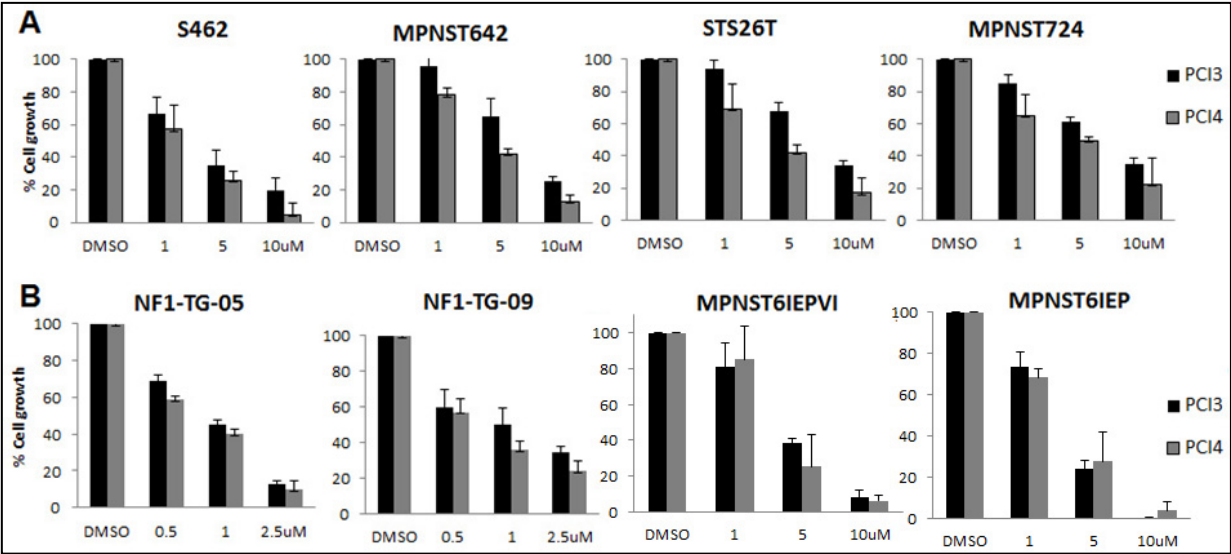
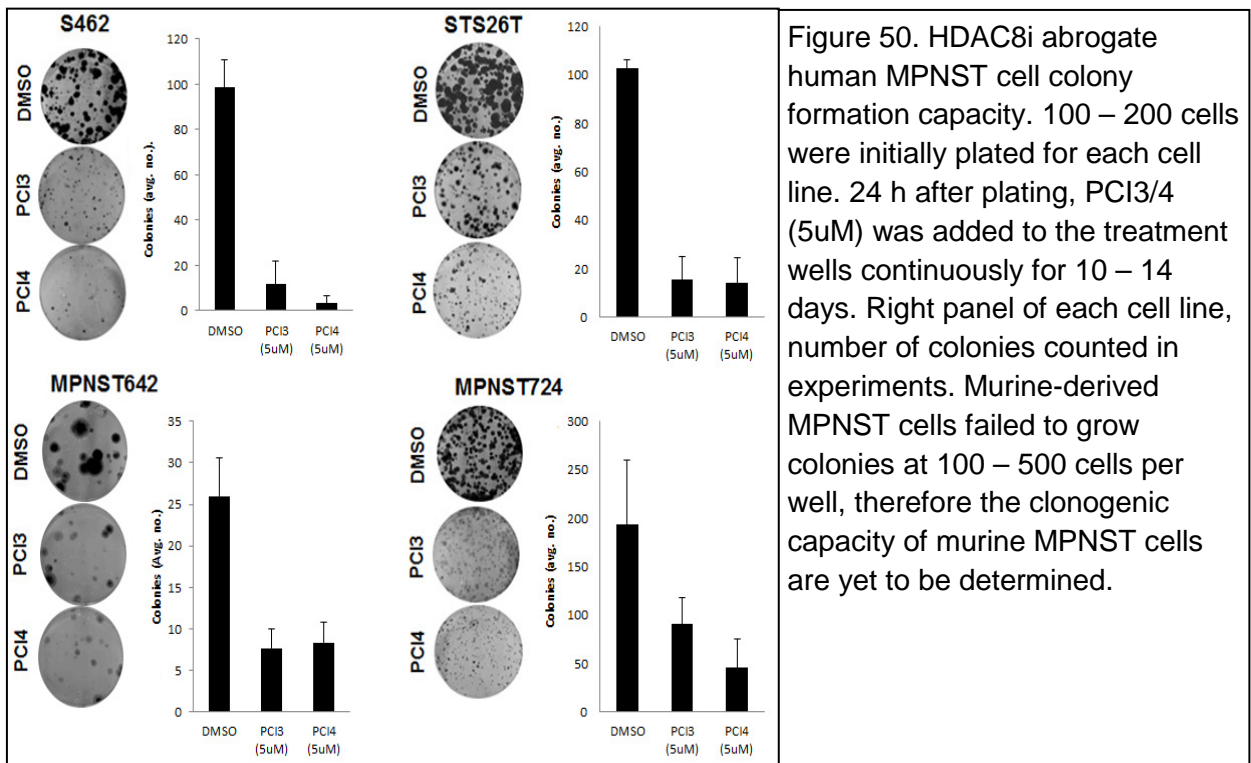


Figure 49. MTS assays demonstrating the effect of HDAC8 inhibition (96 h) on human (A) and murine-derived (B) MPNST cell growth. Murine-derived MPNST cells exhibited marked sensitivity to both HDAC8i compared to human MPNST cell lines. Murine MPNST cell growth was abrogated with lower doses compared to human MPNST cell. Although STS cell growth inhibition was seen with both agents, a more significant response to PCI2 was observed in cells tested (as previously demonstrated). Black bars depict PCI3, grey bars depict PCI4.

Effective doses of PCI3 were similar to previously reported effective doses in T-cell-derived leukemia cell lines (68). Interestingly, PCI3 was not shown to induce cytotoxicity in solid tumor cell lines of various histology at doses equal or less than 5uM (68). However, Compound 2 was shown to abrogate the growth of neuroblastoma cell lines (69, 71). Notably, both neuroblastoma and MPNST originate from neural crest cells. Similarly to the pattern noticed with pan-HDACis, NF1-associated cells, at least S462, was more sensitive to both HDAC8is compared to sporadic MPNST cell lines independent of p53 mutational status or growth rate. S462 had a 50% reduction in cell growth at dose ranges of 1-5uM for both HDAC8i compounds. MPNST642 and STS26T both had a 50% reduction in cell growth at dose ranges of 5-10uM and 1-5uM for PCI3 and PCI4, respectively. MPNST724 had a 50% reduction in cell growth at dose ranges of 5-10uM for both HDAC8i compounds (**Fig. 49A**). Among human and murine MPNST, the murine MPNST cells were more sensitive to HDAC8is compared to human MPNST and required lower doses of both compounds (**Fig. 49B**). This pattern seen in human MPNST cells was recapitulated using a clonogenic assay (**Fig. 50**). The clonogenic capacity of murine-derived MPNST cells was very low where colonies would not form when 100-500 cells per well (in a 6-well culture plate) were plated and cultured for >10 days. For human MPNST cells, approximately 100 cells are all that are required to successfully grow colonies. Due to this unforeseen characteristic of murine-derived MPNST cells, clonogenic assays were not conducted. The variation of effect between PCI3 and PCI4 may possibly be due to the nominal affinity of PCI4 has to HDAC6 compared to PCI3 (data not shown). Overall, these data





demonstrate human and murine-derived MPNST growth inhibition in response to the pharmacological inhibition of HDAC8.

To further investigate the role of HDAC8 inhibition on MPNST growth, we next tested the effect of both compounds on MPNST cell cycle. To evaluate PCI3/4 effect on cell cycle without the potential marked increase in sub-G1 fractionation, the MPNST cells (human and murine) were tested with 5uM of both compounds for 48h. From here on, these preliminary studies utilized 2 human MPNST cell lines (one NF1-associated and one sporadic cell line) and 2 murine-derived MPNST cell lines (NF1-TG-09 developed in our laboratory and MPNST6IEPVI developed by Dr. Luis Parada). PCI2 (used as control) did not induce an increase in S-phase, but rather a decrease compared to PCI3/4. PCI2 induced an increase in G1 and G2 in S462 and a marked increase in G2 in STS26T cells. PCI2 induced a modest increase in G1 and G2 in MPNST6IEPVI

cells. Interestingly, cell cycle analysis revealed a common pattern of HDAC8i-induced S-phase cell cycle arrest, regardless of p53, NF1 status, and species (**Fig. 51**).

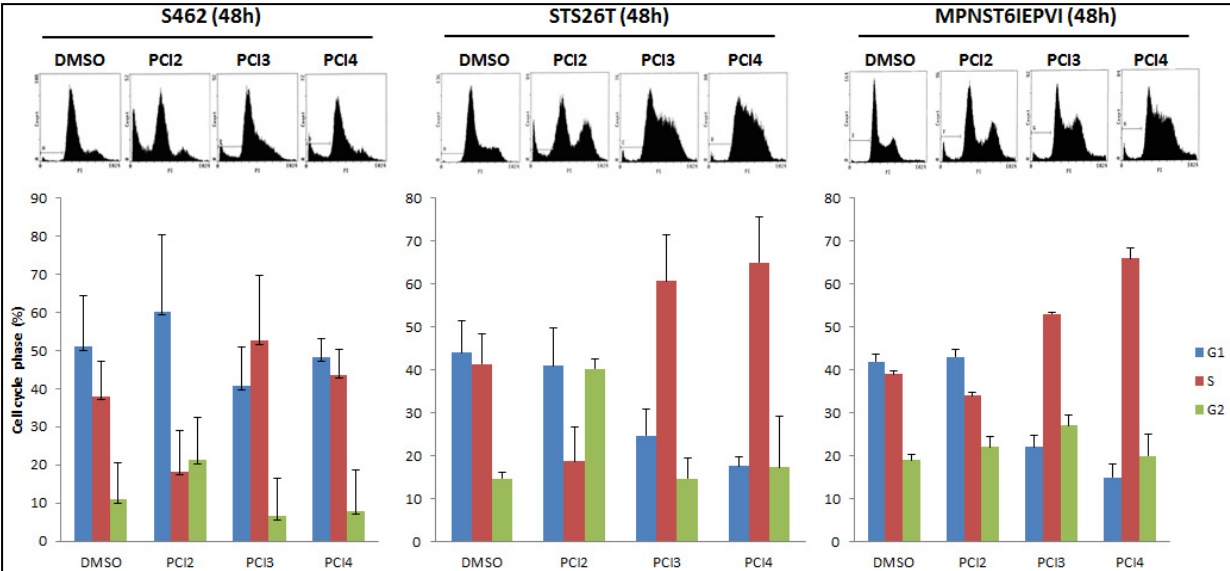


Figure 51. PI staining/FACS analyses showing the effect of HDACis (PCI2 0.5uM/48 h, PCI3/4 5uM/48 h) on human and murine-derived MPNST cell cycle progression. PCI2 reduced S-phase with a modest increase in G1 and G2 in S462 cells. STS26T exhibited a PCI2-induced G2 arrest. The effect of PCI2 on murine-derived MPNST cells was modest. All 3 MPNST cell lines exhibited S-phase arrest when treated with either HDAC8i. Additionally, an increase in sub G1 population is observed (depicted in the respective histograms), suggesting cell death.

STS26T exhibited the greatest increase in PCI3/4-induced S-phase arrest with reductions in both G1 and G2 fractions. Despite the marked PCI3/4-induced increase in the S-phase fraction in STS26T, this increase was not statistically significant ( $p = 0.1$  and  $0.09$  for PCI3 and 4, respectively). In the cell lines tested, PCI4 was shown to induce a slightly higher increase in the S-phase fraction compared to PCI3. Both HDAC8is and especially PCI2 induced an increase in the sub-G1 fraction in NF1-associated cells with a modest effect in sporadic MPNST cells. Since the sub-G1 fraction potentially indicates apoptosis, we next evaluated the effect of both compounds on apoptosis. PCI3/4 induced marked apoptosis in human MPNST and murine-derived MPNST cells (**Fig. 52**)

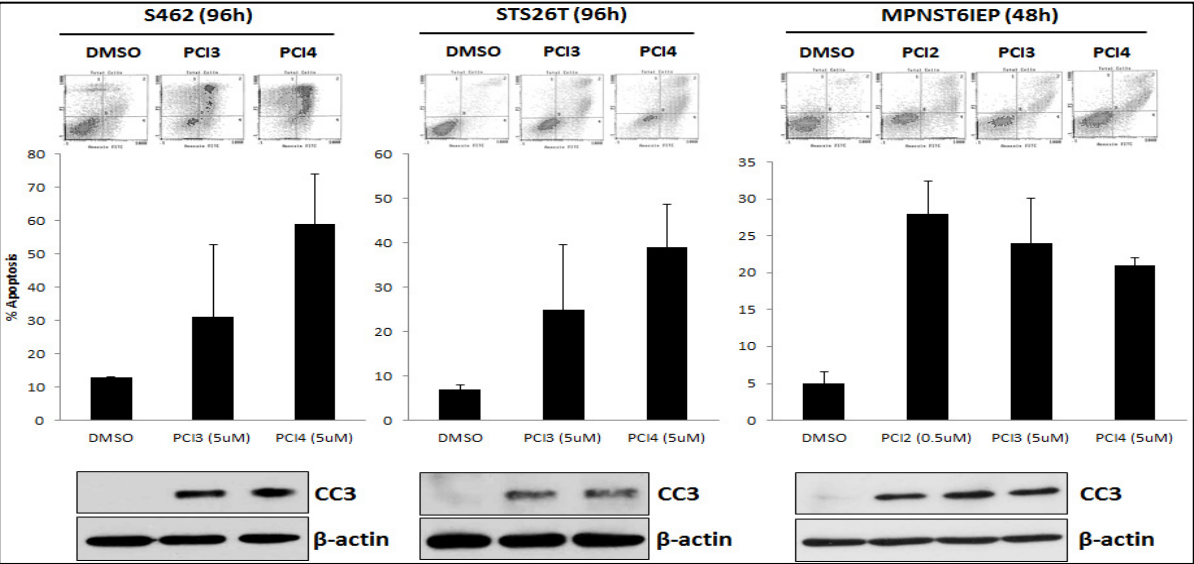


Figure 52. HDAC8i (PCI3/4 5uM/96 h) induced human MPNST cell apoptosis (Annexin V/PI staining FACS analyses). Similar to the “sensitive” and “resistant” pattern observed in Figure 23, NF1-associated cell line S462 showed marked HDAC8i-induced apoptosis while these effects were lower in sporadic cell lines. The response of these cell lines to HDAC8i-induced apoptosis was recapitulated and further confirmed via WB for cleaved caspase 3 (CC3). Due to the higher sensitivity toward HDAC8i compared to human MPNST cell lines, murine MPNST cells were treated for 48 h. PCI2 (0.5uM/48 h) and both HDAC8i (PCI3/4 5uM/48 h) induced marked apoptosis in murine-derived MPNST cells (Annexin V/PI staining FACS analyses, CC3 WB).

PCI3 and PCI4 enhanced annexin V positive cells S462, where PCI4 had a significantly higher effect than PCI3 ( $p=0.29$  and  $p=0.03$  for PCI3 and 4, respectively). This enhancement of PCI3/4-induced apoptosis was confirmed via an increase in cleaved caspase 3 (CC3). PCI3 induced an increase in annexin V positive STS26T cells ( $p=0.18$ ) but a significant increase in annexin V positive STS26T cells ( $p=0.03$ ) was observed with PCI4 treatment. PCI3/4-induced apoptosis in STS26T cells was demonstrated when immunoblotting for cleaved caspase 3 (CC3). Murine-derived MPNST cells exhibited PCI2-induced as well as PCI3/4-induced apoptosis (48 h). All three drugs induced significant apoptosis in MPNST6IEP cells as depicted using Annexin V FACS analysis (PCI2, PCI3, and PCI4,  $p<0.05$ ) and cleaved caspase 3 (CC3) WB.

These promising *in vitro* data supports the role of HDAC8 in MPNST warranting further investigation.

## 5.2 Effects of PCI4 on the growth of human and murine MPNST *in vivo*

To investigate the role of HDAC8 inhibition *in vivo*, we utilized our only human NF1-associated MPNST model using MPNST642 cells. This experiment was conducted as mentioned above (Section 2.1 and ref. 56) while utilizing PCI4 (20 mg/kg BID) instead of PCI2. During the course of this therapeutic experiment, there was no discernible xenograft growth variation between the vehicle and PCI4-treated groups as tumors from both groups grew in parallel (**Fig. 53**). No noticeable drug-induced toxicities occurred as the mice remained in relatively good well-being with no weight loss. At

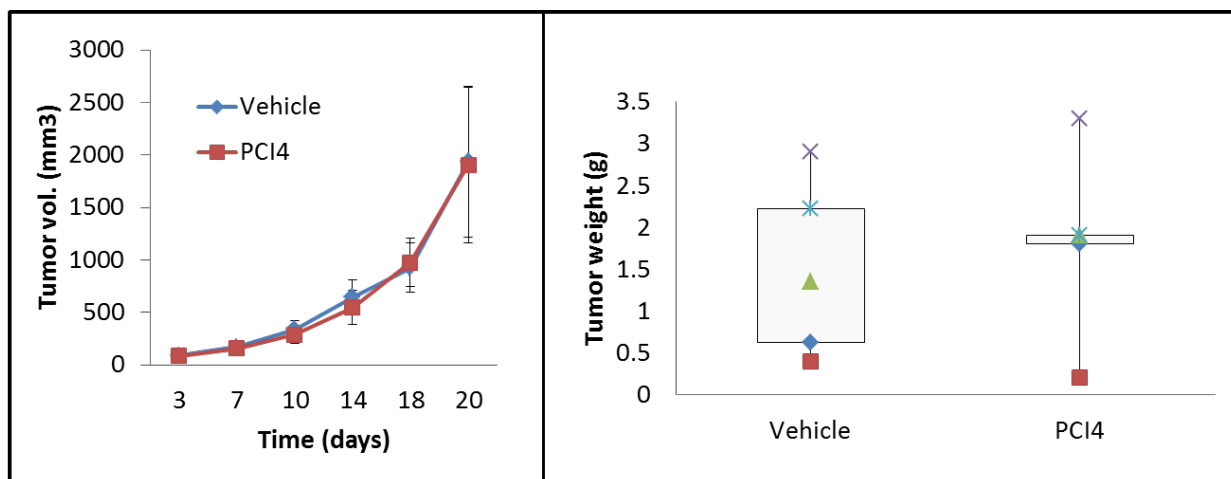
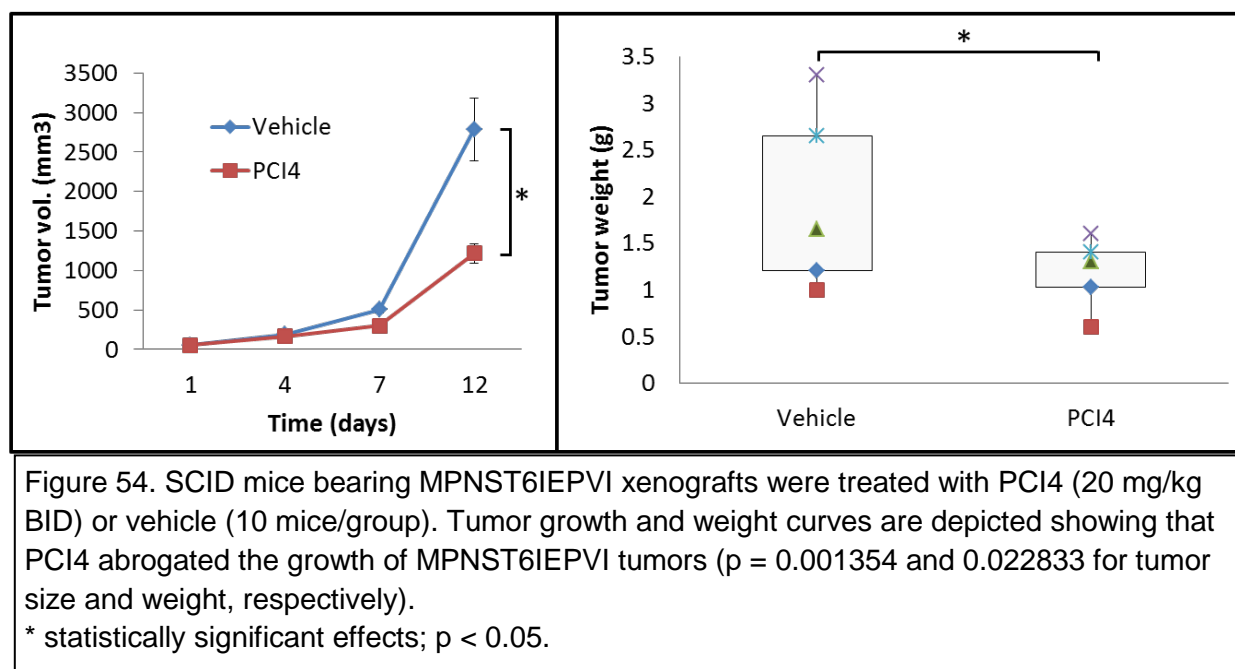


Figure 53. SCID mice bearing MPNST642 xenografts were treated with PCI4 (PCI4; 20 mg/kg BID) or vehicle (5-6 mice/group). Tumor growth and weight curves are depicted showing that PCI4 had no effect on the growth of MPNST642 tumors. Tumors were processed for H&E. Serum and tumors were saved for PD/PK studies to identify drug concentration circulating in the mice and tumor.

termination of this experiment, tumor volumes and weights were surprisingly marginally higher in PCI4-treated mice compared to vehicle-treated mice (PCI4-treated mice average tumor volume and weight:  $1906.4 \text{ mm}^3 \pm 594.8$  and  $1.96 \text{ g} \pm 0.52$ , respectively; vehicle-treated mice average tumor volume and weight:  $1679.1 \text{ mm}^3 \pm 648.5$  and  $1.48 \text{ g} \pm 0.43$ , respectively). To test if the lack of effect might be related to problems with drug accessibility plasma and tissue was collected and saved for future PK/PD analysis. This therapeutic experiment was repeated using the murine-derived MPNST6IEPVI cell line. This study was conducted similar to the previous experiment. Treatment with PCI4 began when palpable tumors reached an average diameter of ~5mm. The growth rate of the MPNST6IEPVI xenografts was fast and thus treatment occurred for 12 days. Of note, two mice from the vehicle group and one mouse from the PCI4 treatment began to take on a thin appearance despite the absence of weight

loss. The abdomen of these thinning mice appeared larger than that of their litter mates. Aside from these three above-mentioned thin mice, all other mice in both groups appeared to be in good well-being. During the course and at termination of this experiment tumors from PCI4 therapy were noticeably small than vehicle-treated tumors (**Fig. 54**).



PCI4 treatment significantly abrogated tumor volume and weight compared to vehicle ( $p = 0.001$  and  $p = 0.02$ , respectively). At the end of this experiment the average tumor volume and weight for vehicle-treated mice was  $2786.1 \text{ mm}^3 \pm 396$  and  $1.96 \text{ g} \pm 0.28$ , respectively; and average tumor volume and weight for PCI4-treated mice was  $1215.1 \text{ mm}^3 \pm 125$  and  $1.21 \text{ g} \pm 0.11$ , respectively. When tumors were collected, each mouse was dissected to evaluate potential spontaneous metastases. The stomach and intestine of both thin mice from the vehicle group and one thin mouse from the PCI4

group had numerous metastatic nodules of varying size. The lungs of these mice were also inspected during the dissection and were suspect of metastasis. Abdominal tumors and lungs from these mice were processed for H&E slides.

This significant *in vivo* experiment supports further investigation and the attempt for an additional *in vivo* experiment utilizing a human MPNST cell line.

## Chapter VII: Discussion

These studies revealed important findings with great therapeutic potential. In these studies we showed the efficacy of pan-HDACi alone and in combination with conventional chemotherapy in genetically complex STS of various histologies *in vitro* and *in vivo*. Our findings supported the initiation of a clinical trial where PCI-24781 will be combined with doxorubicin for patients with advanced sarcoma (clinicaltrials.gov). Our focus then shifted to single histology, MPNST, where we demonstrated pan-HDACi to have marked anti-MPNST effects in a cohort of NF1-associated MPNST cells lines *in vitro* and *in vivo*. In this study we also identified that our sporadic MPNST cell lines were relatively “resistant” to the pro-apoptotic effects of HDAC inhibition. HDACi-induced productive autophagy was identified as a mechanism of resistance in these cells, and when autophagy blockade was supplemented with HDAC inhibition, the cells succumbed to HDACi-induced apoptosis *in vitro* and *in vivo*. Among the HDACis currently tested clinically, they inhibit multiple HDAC isoforms, mainly class I HDACs. Despite their promise, the therapeutic index of these compounds is relatively low, given their wide spectrum of toxicities (95). By targeting a single, biologically relevant, HDAC isoform, our expectation was to improve therapeutic efficacy by reducing the toxicities associated with inhibition of multiple HDAC isoforms. Toward that end, we used HDAC8-specific inhibitors and tested their potential efficacy on human and murine-derived MPNST. Our initial data suggests a tumorigenic role HDAC8 in MPNST. We showed that, similar to T-cell derived leukemia (68) and



neuroblastoma cells (71), our human and murine-derived MPNST cells were sensitive to HDAC8 inhibition (doses around 5uM). Both human and murine NF1-associated MPNST exhibited more sensitivity to HDAC8 inhibition compared to human sporadic MPNST cells; an observation we previously reported with pan-HDAC inhibitors (56). Uniquely, all MPNST cell lines tested (both human and murine) exhibited HDAC8i-induced S-phase cell cycle arrest. Most importantly, we demonstrated that HDAC8 inhibition induced significant murine-derived MPNST xenograft growth inhibition *in vivo*. As these studies continue to expand, various aspects of these studies harbor intriguing queries.

Similar to data in our study (50), the synergism among various HDACis combined with several anti-cancer compounds have been well documented in a variety of histologically diverse cancers. The synergistic effect usually depends on the sequencing of the compounds, where pre-treatment with an HDACi sensitizes tumors cells to the pro-apoptotic effects of chemotherapy. This sequencing enhanced the anti-STS effects of doxorubicin and cisplatin in both our *in vitro* and *in vivo* studies. Currently, there are more than 100 clinical trials evaluating the effects of HDACis combined with a variety of chemotherapies ([www.clinicaltrials.gov](http://www.clinicaltrials.gov)).

The HDACi-induced impairment of the double-strand break repair mechanism supplemented with DNA damaging compounds has been shown to have a synergistic role (96, 97). HDACis have been shown to inhibit HR repair, a potential mechanism

contributing to chemoresistance in some malignancies (96-98). Previously, our lab has shown the high expression of Rad51 is high in a variety of clinical and cell line STS subtypes. This overexpression of Rad51, a protein that plays a crucial role in HR, in STS potentially plays a role in their chemoresistant nature. When we knocked down (siRNA) Rad51, the STS cells tested succumbed to the pro-apoptotic effects of doxorubicin (85). Adimoolam and colleagues (98) have previously showed that PCI-24781 reduced the expression of Rad51 in a colorectal carcinoma cell line (HCT116). PCI2-induced down-regulation of Rad51 inhibited HR and radiosensitized these colorectal carcinoma cells as well as lung carcinoma cell lines (NCI-H460, A549) to irradiation.

In our study, we showed that PCI2 reduced the mRNA and protein expression of *Rad51* in STS cells of different histology. We showed the PCI2-induced transcriptional repression of *Rad51* to be mediated through increased binding of E2F1 to the *Rad51* proximal promoter. E2F1 has been shown to primarily act as a transcriptional activator, where E2F4 acts as a negative transcriptional regulator. Interestingly, Bindra and Glazer (99) have shown that during hypoxic conditions, E2F4/p103 complexes binds to the *Rad51* promoter resulting in its downregulation. A negative regulatory role for E2F1 has also been described in a variety of genes (100-102). Possibly, E2F binding partners influence the positive or negative role on transcription, where HDACi can impact the construction of the E2F complexes. HDACis may also induce the acetylation of E2F proteins, thus enhancing their binding to their respective binding sites on various promoters (103). Despite these intriguing pre-clinical findings, DNA

damage repair does not solely depend on Rad51, as this dynamic mechanism utilizes numerous other molecules.

Other genes (i.e. *CHK1*, *CTGF*) identified from our initial gene array may possibly contribute to the chemoresistant nature of STS. Gene array analysis showed that *CTGF* increased by an average of 16-fold and *CHK1* decreased by an average of 6-fold after PCI2 treatment. The PCI2-induced reduction of RNA and protein were confirmed for both genes. Lee et al. previously showed that SAHA induced DNA breaks in both normal as well as transformed cells, where normal cells retained the ability to repair the HDACi-induced DNA breaks (81). They showed that when *CHK1* was inhibited *in vitro* and *in vivo* in normal cells, the cells succumbed to the pro-apoptotic effects of HDACi. The role of *CHK1* on chemoresistance has been supplemented in a variety of studies combining *CHK1* inhibition, either by genetic or chemical inhibition, with a variety of targeted therapies and chemotherapeutic compounds (104-106). Furthermore, cells with non-functional *CHK1* have been shown to be sensitive to a vast range of DNA damaging compounds or replication inhibitors (107).

Regarding the role of *CTGF*, there is evidence that *CTGF* regulates cancer cell migration, invasion, angiogenesis, and anoikis. However, *CTGF* has been associated with a favorable as well as unfavorable prognosis (108-111). Alterations of *CTGF* expression in tumor cells suggests that it may be regulated by epigenetic modifications of the DNA. Most array data did not suggest *CTGF* to be regulated by HDACs,

whereas a variable degree of up-regulation was observed in certain hepatoma cell lines (112) as well as our STS cell lines. Komorowsky et al. reported upregulation of CTGF in renal cell carcinoma cell lines and Hep3B cells upon treatment with various types of HDACis (113). These observations indicate that, in addition to the acetylation status of the histones, CTGF expression will be determined by cell type-specific transcription factors, which are direct or indirect targets of HDACs (114).

CTGF has also been shown to serve a tumor suppressor. It can induce apoptosis in human breast cancer cells (108) and suppress cell proliferation in non-small cell lung cancer cells (109) and human oral squamous cell carcinoma-derived cells (110).

Furthermore, studies have shown that lower CTGF expression was negatively associated with survival and mortality in lung adenocarcinoma and colorectal cancer (115, 111). Again, the biological function of CTGF seems to be cell type specific and it is probably due to the complex contextual interactions within a specific tumor environment (114).

The basis for the selective toxicity of cancer cells to HDACis is not known. If aberrant gene expression were the primary method for HDACi-induced apoptosis, then it would be expected both normal cells and tumor cells to be equally sensitive to HDACis. As a matter of fact, providing that the disruption of apoptotic pathways is a critical occurrence in tumorigenesis, it would be anticipated that normal cells would be much more sensitive to HDACi-induced cell death than cancer cells. If HDACi-induced cell death is associated with aberrant mitosis, then the circumstance where cancer cells

generally lose their cell cycle checkpoints can make these cancer cells more sensitive to HDAC inhibition (117). The failure to activate two cell-cycle checkpoints that are present in normal cells is responsible for the tumor-selective action of HDACi (117).

In the context of sensitivity to HDACis, we previously showed that NF1-associated MPNST are relatively more sensitive to HDACi compared to sporadic MPNST cells. In the natural history of MPNST, the loss of NF1 is a hallmark of the disease. This Ras-GAP protein regulates the activity of various Ras isoforms (K-, H-, and N-Ras). The loss of this gene results in higher Ras activity consequentially promoting tumor survival and progression. In our study, we showed that NF1-associated MPNST cells were more sensitive to the pro-apoptotic effects of HDACis compared to sporadic MPNST cell lines. Sporadic MPNST can manifest in the presence or somatic loss of NF1 (24). Currently, the precise occurrence and importance of the somatic loss of NF1 in sporadic MPNST progression is unknown. We showed that both sporadic cells, STS26T and MPNST724 had NF1. Using a Ras activity assay, STS26T had no Ras activity, however, despite the presence of NF1, Ras activity was enhanced in MPNST724. Despite the Ras activity in one sporadic cell lines and not the other, knockdown of NF1 in both cell lines sensitized the cells to the pro-apoptotic effects of HDACi. The tumor suppressive role of NF1 is well documented, however, at least in our study, its loss sensitizes sporadic MPNST cells to HDAC inhibition. Interestingly, enhanced Ras activity has been shown to sensitize STAT1-deficient cells to pan-HDACi-induced apoptosis (118). However, regardless of enhanced Ras activity in MPNST724, the cells succumbed to HDACi-induced apoptosis with NF1 knock down,

suggesting a potential protective role of NF1 outside of its regulatory role in Ras activation. In a non-Ras-GAP role, NF1 overexpression has been shown to induce an increase in the expression levels of the focal adhesion kinase (FAK), and changes in the activation mitogen-activated protein kinases proteins (MAPKs) (119). This suggests the presence of a Ras-independent NF1-dependent pathway able to modify the levels of expression of FAK and the levels of activation of MAPKs. Because FAK and many proteins recently found to bind NF1 have a role in the cytoskeleton, this pathway may involve rearrangement of cytoskeletal components that assist in anchorage independence (120). NF1 knockout has been shown to activate the Rho-ROCK-LIMK2-cofillin pathway to modify the actin cytoskeleton reorganization and stimulate cell motility, invasiveness, and cell-cell adhesion, thus leading to the formation of large cell aggregates. This phenotype is suggestive toward the multiple neurofibroma formations in NF1 patients (120). From this, it would be interesting to identify if this pathway is constitutively active in our NF1-associated compared to our sporadic MPNST cell lines. Activation of this pathway may also explain the presence of potential spontaneous metastases observed in our MPNST6IEPVI *in vivo* model. Identifying the potential activation of this pathway in NF1-associated MPNST and correlating its activation with metastases may rationalize novel combination therapeutic strategies for metastatic disease in NF1 patients.

Where a majority of cancer cells tested exhibit sensitivity to pan-HDACis, normal cells show resistance. As briefly mentioned before, the accumulation of reactive oxygen species (ROS) is among the many mechanisms of HDACi-induced sensitivity in cancer

cells (121-123). Unlike cancer cells, normal cells exhibit a higher expression of thioredoxin, a natural scavenger of ROS; potentially playing a role in their resistance to pan-HDACi-induced oxidative stress. This cytoprotective role of thioredoxin to pan-HDACi was established where knockdown of thioredoxin sensitized normal cells to the pro-apoptotic effects of pan-HDACi (124). Certain cancer cells overexpress thioredoxin, potentially giving them a survival advantage toward HDACi-induced oxidative stress (125, 126). Similar to the effects observed in normal cells, inhibition or knockdown of this antioxidant in these cancers can enhance the efficacy of pan-HDACis, potentially making this combination therapy ideal in cancer exhibiting resistance to HDACis. Pre-clinical screening of tumors with an up-regulation of thioredoxin would likely denote their probable response to HDACi. As of note, Subramanian et al., showed that Bax<sup>-/-</sup> embryonic murine fibroblasts to be resistant to pan-HDAC inhibition (127).

Other mechanisms of resistance toward HDACis have been documented and summarized by Fantin and Richon (128). One such mechanism of therapeutic resistance is therapy-induced autophagy.

In our study, we identified HDACi-induced productive macroautophagy (herein “autophagy”) as a mode of resistance in MPNST cells *in vitro* and *in vivo*.

Autophagy is an intracellular, catabolic process used to degrade and recycle cellular components via the lysosomal system (129). Autophagy is a dynamic process that plays an integral role in normal processes maintaining cellular homeostasis. Various

forms of autophagy have been identified. The bulk, lysosomal-mediated degradation of long-lived proteins and long-lived/damaged organelles occurs through macroautophagy. Where macroautophagy is the most studied mechanism, other forms of autophagy exist: microautophagy is the direct engulfment of cellular constituents by the lysosome; chaperone-mediated autophagy occurs where only proteins that possess a certain peptidic consensus sequence are identified by a chaperone complex and moved to the lysosome. Numerous forms of selective autophagy have also been identified: pexophagy (selective degradation of peroxisomes), mitophagy (selective degradation of mitochondria), aggrephagy (selective degradation of protein aggregates), xenophagy (selective degradation of foreign bodies; i.e. bacteria, viruses) are among the various forms of selective autophagy (130).

When studying autophagy, the detection of autophagosome accumulation does not translate to an increase in autophagic flux. Klionsky et al., have emphasized the utility of “multiple assays” to properly identify the presence of autophagy as well as the functionality of this process (79).

Autophagic flux or productive autophagy refers to the complete, unperturbed process of autophagy beginning with the development of a horseshoe-shaped double membranous phagophore, which develops around an area of cytoplasmic contents enclosing the contents in an autophagosome which is then fused with a lysosome at which the autophagosomal contents are degraded where these degraded components can be reused by the cell (129). Aside from the homeostatic role of autophagy in normal cell physiology, autophagic cell death (ACD, type II cell death) was previously



suggested as a mode of cell death (131, 132). ACD has been suggested as a misnomer (133) where cell death with autophagy is the likely occurrence notwithstanding, the archival evidence recently brought forth by Clarke and Puyal that *bone fide* autophagic cell death (cell death promoted via autophagy, independent from apoptosis or necrosis) occurs in some contexts (134). Shao and colleagues showed that HDAC inhibitors SAHA and butyrate induced cell death that had morphological features of autophagy, independent of caspase activation in Apaf-1 KO MEF cells, HeLa cells overexpressing Bcl-XL, and cells treated with caspase inhibitor Z-VAD-FMK (122). In our studies, we demonstrated that NF1-associated MPNST cells succumbed to HDACi-induced apoptosis. In the apoptotic bodies of these cells, numerous autophagosomal structures were identified, suggesting, at least in our model, that HDAC inhibition induces apoptosis in the presence of autophagy. Although not yet attempted in our studies, it would be interesting to investigate the outcome of apoptosis inhibition combined with HDAC inhibition in our MPNST models (e.g. caspase inhibitor Z-VAD-FMK combined with HDACi). The cross-talk among the autophagic and cell death pathways is well established (135). For instance, Pyo and colleagues showed that ATG5, a protein important during formation of the extending autophagosomal membrane, interacts with Fas-Associated protein with Death Domain (FADD) to induce interferon- $\gamma$ -mediated cell death in HeLa cells (136). Furthermore, Yousefi et al. demonstrated that ATG5 can be cleaved in a calpain-dependent manner, resulting in a “switch” from autophagy to apoptosis (137). Although not yet studied in our NF1-associated MPNST model, the presence of numerous autophagosomal

structures in HDACi-induced apoptotic bodies (**Fig. 32**) suggests the aforementioned cross-talk among these dynamic processes; NF1-associated cells were succumbing to HDACi-induced apoptosis in the presence of autophagy, rather than dying of autophagic cell death.

While the controversy between ACD and the therapy-induced protective role remains, a majority of studies have pointed out that anti-cancer therapy-induced autophagy serves in the survival of cancer cells (138-140).

The deregulation of autophagy-related genes has been shown to augment tumorigenesis in some malignancies (141). In the case of many breast-related malignancies, *BECN1* is monoallelically deleted resulting in deregulated autophagy (142, 143), indicating the tumor suppressive role of autophagy. Tumor cells with functional autophagic machinery can circumvent cell death potentially manifested in the form of anti-cancer therapy or bio-energetic stress (144).

As in the case with our work in MPNST, a wide variety of studies have shown tumor growth inhibition and the augmentation of cell death when therapies that induce autophagy are initially supplemented with the inhibition of autophagy (145-147).

A variety of methods, either being genetic or pharmacological inhibition are used to study the effects of autophagy inhibition. With current methods, autophagy can be inhibited at induction or the early steps of the formation of the autophagosome and at the stage of lysosomal-mediated degradation. Tumors cells that use therapy-induced autophagy as a mode of resistance; inhibition at either of the abovementioned stages

of autophagy enhances tumor cell growth inhibition and cell death. We showed that regardless of autophagic stage inhibition, either by inhibiting induction with Beclin1 or ATG5/7 siRNA or by inhibiting lysosomal-mediated degradation with chloroquine or BFA, the pro-apoptotic effects of HDACi in MPNST were enhanced *in vitro* and *in vivo*. Our data enhanced the current knowledge and importance of therapy resistance mediated through therapy-induced autophagy, and further complements the impetus toward the inhibition of autophagy in the clinical setting. Among the compounds used to inhibit autophagy, chloroquine and its derivatives are currently the only autophagy inhibitors used in the clinic. While chloroquine has been used for the treatment of malaria and is currently being used in clinical trials as an autophagy inhibitor, this compound has some off- target effects outside of autophagy (147). The lack of autophagy-specific inhibitors for clinical use warrants the development and/or identification of novel inhibitors which may support the role of autophagy in the context of cancer therapy. The identification/development of novel autophagy inhibitors can potentially lead to the clinically relevant development of novel combination therapies beyond the current, sole use of chloroquine. It is important to form an understanding regarding the selective manipulation of autophagy in therapeutically specific circumstances. In our studies we showed that HDACi induces the expression of *IRGM*, *TMEM74*, and *CXCR4* potentially contributing the HDACi-induced autophagy observed in our MPNST cells. While the role of autophagy in these proteins has been identified (148-150), their individual role in the autophagic machinery and contribution toward HDACi-induced autophagy and chemoresistance remains to be discovered. As a proof

of concept, we showed that when *IRGM* was genetically inhibited by siRNA, HDACi-induced autophagy was blocked leading to the increase of HDACi-induced apoptosis. As this initial pre-clinical data is forthcoming, it will be important to expand these studies further with the hopes of potentially identifying “druggable” targets in a novel manner to inhibit autophagy.

It will also be important to identify the role of HDAC inhibition on these inducible targets; which individual HDAC or combination of HDAC isoforms induces autophagy, and which of these scenarios induce the expression of certain genes (i.e. *IRGM*, *TMEM74*, *CXCR4*) that induce autophagy? Identifying these specificities will broaden the current, yet limited knowledge on the aforementioned subject with efforts geared toward clinical practicality.

Where we showed the significant anti-STS and anti-MPNST effects exerted by pan-HDACis, we also began initial studies observing the effects by inhibiting individual HDAC isoforms, namely HDAC8. In the milieu of normal human tissues, HDAC8 has been shown to be exclusively expressed by cells showing smooth muscle differentiation, including visceral and vascular smooth muscle cells, myoepithelial cells, and myofibroblasts, and is mainly detected in the cytosol (66). Waltregny et al. showed that HDAC8 overexpression in murine fibroblasts formed cytoplasmic stress fiber-like structures that co-localized with the smooth muscle cytoskeleton protein smooth muscle  $\alpha$ -actin.

HDAC8 has also been shown to potentially be a more sensitive marker than desmin and h-caldesmon in epithelioid smooth muscle tumors, where HDAC8 detection may be useful in serving in the differential diagnosis of uterine-derived mesenchymal tumors (67). As these studies have identified the practical use of HDAC8 clinically, little is known about molecular contributions in normal and cancer cells. The identification of acetylated targets of HDAC8 has been very minimal. Recently, Karolczak-Bayatti and colleagues showed HDAC8 can interact with Hsp20 to affect its acetylation (151). In their study they used a HDAC8 inhibitor that augmented Hsp20 acetylation with no increase of histone acetylation or discernible global gene expression changes. The effects they observed were associated with significant inhibition of spontaneous and oxytocin-augmented contractions of *ex vivo* human myometrial tissue strips. A possible mechanism by which Hsp20 acetylation can affect myometrial activity is by the liberation of cofilin, which will regulate contraction in smooth muscle cells (151). A notable observation in our study was HDAC8i-induced increase in the S-phase in human and murine-derived MPNST cells regardless of their NF1 and p53 status. This unique cell cycle arrest occurred with both HDAC8 inhibitors (PCI3 and PCI4) whereas pan-HDACi induced either G1- or G2-cell cycle arrest in sporadic and human and murine-derived NF1-associated MPNST cells.

S-phase checkpoint has been shown to be mediated by ATR and Chk2 in human cells in response to DNA damage and replication-stress conditions (152). The S-phase

checkpoint can be categorized into three checkpoints: replication, S-M, and intra-S-phase checkpoint. The replication checkpoint initiates when the replication forks get stalled due to a stress (i.e. depletion of dNTP pools, inhibition of DNA polymerases, DNA damage). S-M checkpoint certifies that cells won't attempt to divide before the whole genome becomes duplicated. DNA double-strand breaks which are created just outside the active replicon activate the intra-S-phase checkpoint. Unlike the other two S-phase checkpoints, this checkpoint does not get activated in response to disruption at the replication fork.

Notably, none of the S-phase checkpoints require p53 (153, 154) for their activation. As we have yet identified a role for HDAC8 during S-phase of the cell cycle, Deardorff and colleagues recently reported that structural maintenance of chromosomes 3 (SMC3) is a deacetylation target of HDAC8 in HeLa cells (155). SMC3 is a member of the SMC family of proteins (156, 158). This protein is a vital component of a multi-protein cohesin complex that holds sister chromatids together during mitosis, facilitating proper segregation of the chromosome (156). Acetylation of SMC3 has been shown to occur and play an essential role during S-phase in both yeast and human systems (158). Where we have shown possible S-phase arrest after treatment with PCI3/4, Deardorff et al., showed unaltered cell cycle progression in HeLa cells in the presence of HDAC8 inhibition (i.e. inhibition of HDAC8 was performed using siRNA and/or 25uM, PCI-34051). Identification of this HDAC8-SMC3 interaction among other potential HDAC8 regulated S-phase proteins will enhance current

knowledge on the role of HDAC8 in cell cycle progression. It will also be essential to determine the effect of HDAC8 inhibition on the cell cycle progression of normal cells. If HDAC8 inhibition induces *bona fide* S-phase arrest in MPNST cells, it may be ideal to combine HDAC8 inhibition with antimetabolitic compounds (e.g. 5-fluorouracil, cytarabine, gemcitabine, etc.), which exert their cytotoxic effects during S-phase.

This is but one aspect on the role of HDAC8 in genetically complex STS as we plan to continue to develop our basic knowledge on this subject. This study has led to invaluable information that not only enhances current knowledge on the biology of genetically complex STS, namely MPNST, but also the impetus for novel therapies for patients with these malignancies.

## Chapter VIII: Conclusions and future directions

In this work we have shown the therapeutic efficacy of pan-HDACis in combination with chemotherapy for the treatment of complex karyotypic STS. Our initial study (Lopez et al. 2009) helped support the rationale that led to a clinical trial combining PCI2 with conventional chemotherapy for patients with high grade STS. Similar to the anti-STS effect of pan-HDACis in STS cells of various histology, pan-HDACis were shown to have a significant anti-MPNST effect in NF1-associated, but not in sporadic MPNST. This dichotomy among the NF1-associated and sporadic MPNST cohorts led us to the identification of HDACi-induced productive autophagy; an implied mechanism of therapeutic resistance observed in a variety of pre-clinical and clinical settings. Inhibition of HDACi-induced productive autophagy enhanced the pro-apoptotic effects of HDACi *in vitro* and *in vivo*. These data opened a variety of current and future avenues exploring the vast role HDAC inhibition and the contribution toward anti-STS effects. One such avenue was to identify the role of individual HDAC isoforms in STS. The unique pattern of “sensitivity” and “resistance” to pan-HDACi in our MPNST model led us to further dissect this distinction based on the contribution of class I HDAC isoforms. Of the class I HDAC isoforms, due to its unique catalytic structure compared to other HDACs of this class (i.e. HDAC1, 2, 3), HDAC8-specific inhibitors have been developed. To elucidate the contribution of individual HDACs in MPNST we utilized HDAC8-specific inhibitors *in vitro* and *in vivo*. Initial data demonstrated that both HDAC8 inhibitors abrogated human and murine-derived MPNST cell growth by uniquely inducing S-phase arrest and inducing cell



death *in vitro*. Most importantly, HDAC8 inhibition significantly abrogated murine-derived MPNST xenograft growth *in vivo*.

Future studies will be to identify the expression of HDAC8 in normal nerve, neurofibroma, and MPNST clinical samples (TMA) to distinguish a possible correlation with the progression of the disease. HDAC8 has been reported to be a nuclear as well as cytoplasmic protein. As briefly mentioned above, knowledge of its role in either cellular compartment is limited and is cell context specific. Determining the sub-cellular localization of HDAC8 in clinical samples as well as tumor cells lines will be translationally pertinent. Preliminary effects reported in this study using the HDAC8 inhibitors will be supplemented with the utility of siRNA, specific for HDAC8. Taking into consideration of future studies, inhibiting HDAC8 with either siRNA or compound may yield variations in biological outcome. Pharmacological inhibition of HDAC8 will inhibit the enzymes ability to deacetylate its targets, however, this inhibitory method may not disrupt functional multi-protein complex potentially containing HDAC8. siRNA targeting HDAC8 would not only inhibit deacetylation of its targets, but it would also disrupt multi-protein complexes where HDAC8 plays a role. With the aforementioned scenario in mind, the potential identification of binding partners and acetylation targets of HDAC8 will also be explored using both siRNA and PCI3/4 in high throughput experiments. This method will be carried out by isolating acetylated proteins after HDAC8 inhibition followed by mass spectrometry analysis. Furthermore, gene expression patterns correlating with therapeutic response will be established. To

further complement the experiments proposed above and identify potential gene expression signatures predictive of HDAC8 inhibition response as well as HDAC8 inhibition-induced gene expression changes that might correlate with enhanced therapeutic response gene array analysis on control and HDAC8-inhibition-treated cells (siRNA and PCI3/4) will be performed.

Potential studies mentioned above will hopefully demonstrate significant efficacy of HDAC8 inhibitors in MPNST preclinical models, thus forming a basis for design of 'smart' personalized, and future STS clinical trials. HDAC8 is an understudied HDAC isoform; comprehensive investigation to determine HDAC8 expression, localization, function and molecular driven mechanisms is unequivocally warranted.

## References

1. Pisters P, Weiss M, Maki R. Soft-Tissue Sarcoma. Cancer Management: 14<sup>th</sup> Edition. 2011.
2. Lahat G, Lazar AJ, Lev D. Sarcoma Epidemiology and Etiology: Potential Environmental and Genetic Factors. Surg Clin N Am 2008;88:451–481.
3. Surveillance, Epidemiology, and End Results (SEER) Program. Available at: [www.seer.cancer.gov](http://www.seer.cancer.gov). Accessed September 15, 2007.
4. Malkin D, Li FP, Strong LC, Fraumeni JF, Kim DH, Kassel J, Gryka A, Bischoff FZ, Tainsky MA. Germ line p53 mutations in a familial syndrome of breast cancer, sarcomas, and other neoplasms. Science 1990;250:1233–8.
5. Varley JM, McGown G, Thorncroft M, Santibanez-Koref MF, Kelsey AM, Tricker KJ, Evans DG, Birch JM. Germ-line mutations of TP53 in Li-Fraumeni families: an extended study of 39 families. Cancer Res 1997;57:3245–52.
6. Reissmann PT, Simon MA, Lee WH, Slamon DJ. Studies of the retinoblastoma gene in human sarcomas. Oncogene 1989;4:839-43.
7. Bookstein R, Lee EY, To H, Young LJ, Sery TW, Hayes RC, Friedmann T, Lee WH. Human retinoblastoma susceptibility gene: genomic organization and analysis of heterozygous intragenic deletion mutants. PNAS 1988;85:2210-4.
8. Evans DG, Baser ME, McGaughan J, Sharif S, Howard E, Moran A. Malignant peripheral nerve sheath tumours in neurofibromatosis. J Med Genet 2002;39:311–4.
9. Tucker T, Wolkenstein P, Revuz J, Zeller J, Friedman JM. Association between benign and malignant peripheral nerve sheath tumors in NF1. Neurology 2005;65:205–11.

10. Riad S, Biau D, Holt GE, Werier J, Turcotte RE, Ferguson PC, Griffin AM, Dickie CI, Chung PW, Catton CN, O'Sullivan, Wunder JS. The clinical and functional outcome for patients with radiation-induced soft tissue sarcoma. *Cancer* 2012;118:2682-92.
11. Kenney RJ, Cheney R, Stull MA, Kraybill W. Soft Tissue Sarcomas: Current Management and Future Directions. *Surg Clin N Am* 2009;89:235–247.
12. Gadd MA, Casper ES, Woodruff JM, McCormack PM, Brennan MF. Development and treatment of pulmonary metastases in adult patients with extremity soft tissue sarcoma. *Ann Surg* 1993;218:705-12.
13. Welter S, Grabellus F, Bauer S, Schmid KW, Stamatis G, Totsch M. Growth patterns of lung metastases from sarcomas. *Virchows Arch* 2011;459:213-9.
14. Grimer R, Judson I, Peake D, Seddon B. Guidelines for the Management of Soft Tissue Sarcomas. *Sarcoma* 2010:506182.
15. Clark MA, Fisher C, Judson I, Thomas JM. Soft-Tissue Sarcomas in Adults. *N Engl J Med* 2005;353:701-11.
16. Grobmyer SR, Brennan MF. Predictive variables detailing the recurrence rate of soft tissue sarcomas. *Current Opinion in Oncology* 2003;15(4): 319–326.
17. Blay JY, van Glabbeke M, Verweij J, van Oosterom AT, Le Cesne A, Oosterhuis JW, Judson I, Nielsen OS. Advanced soft tissue sarcoma: a disease that is potentially curable for a subset of patients treated with chemotherapy. *European Journal of Cancer* 2003;39:64–69.
18. Van Glabbeke M, van Oosterom AT, Oosterhuis JW, Mouridsen H, Crowther D, Somers R, Verweij J, Santoro A, Buesa J, Tursz T. Prognostic factors for the outcome of chemotherapy in advanced soft tissue sarcoma: an analysis of

- 2,185 patients treated with anthracycline- containing first-line regimens—an European organization for research and treatment of cancer soft tissue and bone sarcoma group study. *J Clin Onc* 1999;17:150–157.
19. Pisters P, Leung DH, Woodruff J, Shi W, Brennan MF. Analysis of prognostic factors in 1,041 patients with localized soft tissue sarcomas of the extremities. *J Clin Oncol* 1996;14:1679–89.
  20. Stoeckle E, Coindre JM, Bonvalot S, Kantor G, Terrier P, Bonichon F, Nguyen Bui B, French Federation of Cancer Centers Sarcoma Group. Prognostic factors in retroperitoneal sarcoma: a multivariate analysis of a series of 165 patients of the French Cancer Center Federation Sarcoma Group. *Cancer* 2001;92:359–68.
  21. Ducatman BS, Scheithauer BW, Piepgras DG, Reiman HM, Ilstrup DM. Malignant peripheral nerve sheath tumors. A clinicopathologic study of 120 cases. *Cancer* 1986;57:2006–21.
  22. Evans DG, Baser ME, McGaughan J, Sharif S, Howard E, Moran A. Malignant peripheral nerve sheath tumours in neurofibromatosis. *J Med Genet* 2002;39:311–4.
  23. Perry A, Roth KA, Banerjee R, Fuller CE, Gutmann DH. NF1 deletions in S-100 protein-positive and negative cells of sporadic and neurofibromatosis 1 (NF1)-associated plexiform neurofibromas and malignant peripheral nerve sheath tumors. *Am J of Path* 2001;159:57-61.
  24. Bottillo I, Ahlquist T, Brekke H, Danielsen SA, van den Berg E, Mertens F, Lothe RA, Dallapiccola B. Germline and somatic NF1 mutations in sporadic and

- NF1-associated malignant peripheral nerve sheath tumours. *J of Path* 2009;217:693-701.
25. Katz D, Lazar AJ, Lev D. Malignant peripheral nerve sheath tumour (MPNST): the clinical implications of cellular signalling pathways. *Expert Reviews* 2009;11:e30.
26. Gutmann DH, Alyswoth A, Carey JC, Korf B, Marks J, Pyeritz RE, Rubenstein A, Viskochil D. The diagnostic evaluation and multidisciplinary management of neurofibromatosis 1 and neurofibromatosis 2. *JAMA* 1997;278:51-57.
27. Woodruff JM. Pathology of the major peripheral nerve sheath neoplasms. *Monographs in Pathology* 1996; 38:129-161.
28. Zou C, Smith KD, Liu J, Lahat G, Myers S, Wang WL, Zhang W, McCutcheon IE, Slopis JM, Lazar AJ, Pollock RE, Lev D. Clinical, pathological, and molecular variables predictive of malignant peripheral nerve sheath tumor outcome. *Ann Surg* 2009;249:1014–22.
29. Anghileri M, Miceli R, Fiore M, Mariani L, Ferrari A, Mussi C, Lozza L, Pollini P, Olmi P, Casali PG, Pilotti S, Gronchi A. Malignant peripheral nerve sheath tumors: prognostic factors and survival in a series of patients treated at a single institution. *Cancer* 2006;107:1065–74.
30. Wong WW, Hirose T, Scheithauer BW, Schild SE, Gunderson LL. Malignant peripheral nerve sheath tumor: analysis of treatment outcome. *Int J Radiat Oncol Biol Phys* 1998;42:351–60.
31. Carli M, Ferrari A, Mattke A, Zanetti I, Casanova M, Bisogno G, Cecchetto G, Alaggio R, De Sio L, Koscielniak E, Sotti G, Treuner J. Pediatric malignant

- peripheral nerve sheath tumor: the Italian and German soft tissue sarcoma cooperative group. *J Clin Onc* 2005; 23:8422-8430.
32. Gallinari P, Di Marco S, Jones P, Pallaoro M, Steinkuhler C. HDACs, histone deacetylation and gene transcription: from molecular biology to cancer therapeutics. *Cell Res* 2007;17:195-211.
33. De Ruijter AJ, van Gennip AH, Carson HN, Kemp S, van Kuilenburg AB. Histone deacetylases (HDACs): characterization of the classical HDAC family. *Biochem J.* 2003;370: 737-749.
34. Dokmanovic M, Clarke C, Marks PA. Histone deacetylase inhibitors: overview and perspectives. *Mol. Cancer Res* 2007;5(10):981–9.
35. Suzuki T. Explorative Study on Isoform-Selective Histone Deacetylase Inhibitors. *Chem Pharm Bull* 2009;57:897—906.
36. Friend C, Scher W, Holland JG, Sato T. Hemoglobin synthesis in murine virus-induced leukemic cells in vitro: stimulation of erythroid differentiation by dimethyl sulfoxide. *PNAS* 1971;68:378-382.
37. Yoshida M, Kijima M, Akita M, Beppu T. Potent and specific inhibition of mammalian histone deacetylase both in vivo and in vitro by trichostatin A. *J Biol Chem* 1990;265:17174-9.
38. Richon VM, Emiliani S, Verdin E, Webb Y, Breslow R, Rifkind RA, Marks PA. A class of hybrid polar inducers of transformed cell differentiation inhibits histone deacetylases. *PNAS* 1998;95:3003–3007.
39. Richon VM, Webb Y, Merger R, Sheppard T, Jursic B, Ngo L, Civoli F, Breslow R, Rifkind RA, Marks PA. Second generation hybrid polar compounds are potent inducers of transformed cell differentiation. *PNAS* 1996;93:5705–8.

40. Marks PA, Breslow R. Dimethyl sulfoxide to vorinostat: development of this histone deacetylase inhibitor as an anticancer drug. *Nat Biotechnol* 2007;25:84–90.
41. Duvic M, Talpur R, Ni X, Zhang C, Hazarika P, Kelly C, Chiao JH, Reilly JF, Ricker JL, Richon VM, Frankel SR. Phase 2 trial of oral vorinostat (suberoylanilide hydroxamic acid, SAHA) for refractory cutaneous T-cell lymphoma (CTCL). *Blood* 2007;109:31–9
42. Jaboin J, Wild J, Hamidi H, Khanna C, Kim CJ, Robey R, Bates SE, Thiele CJ. MS-27-275, an inhibitor of histone deacetylase, has marked in vitro and in vivo antitumor activity against pediatric solid tumors. *Cancer Res* 2002;62:6108-15.
43. Ito T, Ouchida M, Morimoto Y, Yoshida A, Jitsumori Y, Ozaki T, Sonobe H, Inoue H, Shimizu K. Significant growth suppression of synovial sarcomas by the histone deacetylase inhibitor FK228 in vitro and in vivo. *Cancer Lett.* 2005;224:311-9.
44. Lubieniecka JM, de Bruijn DR, Su L, van Dijk AH, Subramanian S, van de Rijn M, Poulin N, van Kessel AG, Nielsen TO. Histone deacetylase inhibitors reverse SS18-SSX-mediated polycomb silencing of the tumor suppressor early growth response 1 in synovial sarcoma. *Cancer Res.* 2008;68:4303-10.
45. Nguyen A, Su L, Campbell B, Poulin N, Nielsen TO. Synergism of heat shock protein 90 and histone deacetylase inhibitors in synovial sarcoma. *Sarcoma.* 2009;2009:794901.
46. Su L, Cheng H, Sampaio AV, Nielsen TO, Underhill TM. EGR1 reactivation by histone deacetylase inhibitors promotes synovial sarcoma cell death through the PTEN tumor suppressor. *Oncogene.* 2010;29:4352-61.



47. Mühlenberg T, Zhang Y, Wagner AJ, Grabellus F, Bradner J, Taeger G, Lang H, Taguchi T, Schuler M, Fletcher JA, Bauer S. Inhibitors of deacetylases suppress oncogenic KIT signaling, acetylate HSP90, and induce apoptosis in gastrointestinal stromal tumors. *Cancer Res.* 2009;69:6941-50.
48. Kutko MC, Glick RD, Butler LM, Coffey DC, Rifkind RA, Marks PA, Richon VM, LaQuaglia MP. Histone deacetylase inhibitors induce growth suppression and cell death in human rhabdomyosarcoma in vitro. *Clin Cancer Res* 2003;9:5749-5755.
49. Gastaldi T, Bonvini P, Sartori F, Marrone A, Iolascon A, Rosolen A. Plakoglobin is differentially expressed in alveolar and embryonal rhabdomyosarcoma and is regulated by DNA methylation and histone acetylation. *Carcinogenesis* 2006;27:1758-67.
50. Lopez G, Liu J, Ren W, Wei W, Wang S, Lahat G, Zhu Q, Bornmann WG, McConkey DJ, Pollock RE, Lev D. Combining PCI-24781, a novel histone deacetylase inhibitor, with chemotherapy for the treatment of soft tissue sarcoma. *Clin Cancer Res* 2009;15:3472-83.
51. Blattmann C, Oertel S, Ehemann V, Thiemann M, Huber PE, Bischof M, Witt O, Deubzer HE, Kulozik AE, Debus J, Weber KJ. Enhancement of radiation response in osteosarcoma and rhabdomyosarcoma cell lines by histone deacetylase inhibition. *Int J Radiat Oncol Biol Phys* 2010;78:237-45.
52. Ailenberg A, Silverman M. Differential effects of trichostatin A on gelatinase A expression in 3T3 fibroblasts and HT-1080 fibrosarcoma cells: implications for use of TSA in cancer therapy. *Biochem Biophys Res Commun* 2003;302:181-5.

53. Shim JS, Kim DH, Kwon HJ. Plakoglobin is a new target gene of histone deacetylase in human fibrosarcoma HT1080 cells. *Oncogene* 2004;23:1704-11.
54. Sampson ER, Amin V, Schwarz EM, O'Keefe RJ, Rosier RN. The histone deacetylase inhibitor vorinostat selectively sensitizes fibrosarcoma cells to chemotherapy. *J Orthop Res* 2011;29:623-32.
55. Hrzenjak A, Moinfar F, Kremser ML, Strohmeier B, Petru E, Zatloukal K, Denk H. Histone deacetylase inhibitor vorinostat suppresses the growth of uterine sarcomas in vitro and in vivo. *Mol Cancer* 2010;9:49.
56. Lopez G, Torres KE, Liu J, Hernandez B, Young E, Belousov R, Bolshakov S, Lazar AJ, Slopis JM, McCutcheon IE, McConkey D, Lev D. Autophagic survival in resistance to histone deacetylase inhibitors: novel strategies to treat malignant peripheral nerve sheath tumors. *Cancer Res* 2011;71:185-96.
57. Lopez G, Torres KE, Lev D. Autophagy blockade enhances HDAC inhibitors' pro-apoptotic effects: potential implications for the treatment of a therapeutic-resistant malignancy. *Autophagy* 2011;7:440-1.
58. Park SY, Jun JA, Jeong KJ, Heo HJ, Sohn JS, Lee HY, Park CG, kang J. Histone deacetylases 1, 6 and 8 are critical for invasion in breast cancer. *Oncol Rep* 2011;25:1677-81.
59. Vannini A, Volpari C, Filocamo G, Casavola EC, Brunetti M, Renzoni D, Chakravarty P, Paolini C, De Francesco R, Gallinari P, Steinkuhler C, Di Marco S. Crystal structure of a eukaryotic zinc-dependent histone deacetylase, human HDAC8, complexed with a hydroxamic acid inhibitor. *PNAS* 2004;101:15064-9.

60. Lee H, Rezai-Zadeh N, Seto E. Negative regulation of histone deacetylase 8 activity by cyclic AMP-dependent protein kinase A. *Mol Cell Biol* 2004;24:765-73.
61. Hu E, Chen Z, Fredrickson T, Zhu Y, Kirkpatrick R, Zhang GF, Johanson K, Sung CM, Liu R, Winkler J. Cloning and characterization of a novel human class I histone deacetylase that functions as a transcription repressor. *J Biol Chem* 2000;275:15254-64.
62. de Ruijter AJ, van Gennip AH, Caron HN, Kemp S, van Kuilenburg AB. Histone deacetylases (HDACs): characterization of the classical HDAC family. *Biochem J* 2003;370:737-49.
63. Buggy JJ, Sideris ML, Mak P, Lorimer DD, McIntosh B, Clark JM. Cloning and characterization of a novel human histone deacetylase, HDAC8. *Biochem J* 2000;350:199-205.
64. Lee H, Rezai-Zadeh N, Seto E. Negative regulation of histone deacetylase 8 activity by cyclic AMP-dependent protein kinase A. *Mol Cell Biol* 2004;24:765-73.
65. Wilson BJ, Tremblay AM, Deblois G, Sylvain-Drolet G, Giguère V. An acetylation switch modulates the transcriptional activity of estrogen-related receptor alpha. *Mol Endocrinol* 2010;24:1349-58.
66. Waltregny D, Glénisson W, Tran SL, North BJ, Verdin E, Colige A, Castronovo V. Histone deacetylase HDAC8 associates with smooth muscle alpha-actin and is essential for smooth muscle cell contractility. *FASEB J* 2005;19:966-8.
67. de Leval L, Waltregny D, Boniver J, Young RH, Castronovo V, Oliva E. Use of histone deacetylase 8 (HDAC8), a new marker of smooth muscle differentiation,

- in the classification of mesenchymal tumors of the uterus. *Am J Surg Pathol* 2006;30:319-27.
68. Balasubramanian S, Ramos J, Luo W, Sirisawad M, Verner E, Buggy JJ. A novel histone deacetylase 8 (HDAC8)-specific inhibitor PCI-34051 induces apoptosis in T-cell lymphomas. *Leukemia* 2008;22:1026-34.
69. Oehme I, Deubzer HE, Wegener D, Pickert D, Linke JP, Hero B, Kopp-Schneider A, Westermann F, Ulrich SM, von Deimling A, Fischer M, Witt O. Histone deacetylase 8 in neuroblastoma tumorigenesis. *Clin Cancer Res* 2009;15:91-9.
70. Krennhrubec K, Marshall BL, Hedglin M, Verdin E, Ulrich SM. Design and evaluation of 'Linkerless' hydroxamic acids as selective HDAC8 inhibitors. *Bioorg Med Chem Lett* 2007;17:2874-8..
71. Oehme I, Deubzer HE, Lodrini M, Milde T, Witt O. Targeting of HDAC8 and investigational inhibitors in neuroblastoma. *Expert Opin Investig Drugs* 2009;18:1605-17.
72. Miller SJ, Rangwala F, Williams J, Ackerman P, Kong S, Jegga AG, Kaiser S, Aronow BJ, Frahm S, Kluwe L, Mautner V, Upadhyaya M, Muir D, Wallace M, Hagen J, Quelle DE, Watson MA, Perry A, Gutman DH, Ratner N. Large-scale molecular comparison of human schwann cells to malignant peripheral nerve sheath tumor cell lines and tissues. *Cancer Res* 2006;66:2584-91.
73. Casella GT, Wieser R, Bunge RP, Margitich IS, Katz J, Olson L, Wood PM. Density dependent regulation of human Schwann cell proliferation. *Glia* 2000;30:165-177.

74. Jin Z, Lahat G, Korchin B, Nguyen T, Zhu Q, Wang X, Lazar AJ, Trent J, Pollock RE, Lev D. Midkine enhances soft-tissue sarcoma growth: a possible novel therapeutic target. *Clin Cancer Res* 2008;14:5033–42.
75. Zhu Q, Ren W, Korchin B, Lahat G, Dicker A, Lu Y, Mills G, Pollock RE, Lev D. Soft tissue sarcoma cells are highly sensitive to AKT blockade: A role for p53-independent up-regulation of GADD45 $\alpha$ . *Cancer Res* 2008;68:2895–903.
76. Liu J, Zhan M, Hannay JA, Das P, Bolshakov S, Kotilingam D, Yu D, Lazar AJ, Pollock RE, Lev D. Wild-type p53 inhibits nuclear factor-kappaB-induced matrix metalloproteinase-9 promoter activation: implications for soft tissue sarcoma growth and metastasis. *Mol Cancer Res* 2006;4:803-10.
77. Takeuchi H, Kondo Y, Fujiwara K, Kanzawa T, Aoki H, Mills GB, Kondo S. Synergistic augmentation of rapamycin-induced autophagy in malignant glioma cells by phosphatidylinositol 3-kinase/protein kinase B inhibitors. *Cancer Res* 2005;65:3336-46.
78. Zou C, Smith KD, Zhu Q, Liu J, McCutcheon IE, Slopis JM, Meric-Bernstam F, Peng Z, Bornmann WG, Mills GB, Lazar AJ, Pollock RE, Lev D. Dual targeting of AKT and mammalian target of rapamycin: a potential therapeutic approach for malignant peripheral nerve sheath tumor. *Mol Cancer Ther* 2009;8:1157-68.
79. Klionsky DJ, Abeliovich H, Agostinis P, Agrawal DK, Aliev G, Askew DS, Baba M, Baehrecke EH, Bahr BA, Ballabio A, Bamber BA, Bassham DC, Bergamini E, Bi X, Biard-Piechaczyk M, Blum JS, Bredesen DE, Brodsky JL, Brumell JH, Brunk UT, Bursch W, Camougrand N, Cebollero E, Cecconi F, Chen Y, Chin LS, Choi A, Chu CT, Chung J, Clarke PG, Clark RS, Clarke SG, Clavé C, Cleveland JL, Codogno P, Colombo MI, Coto-Montes A, Cregg JM, Cuervo AM,

Debnath J, Demarchi F, Dennis PB, Dennis PA, Deretic V, Devenish RJ, Di Sano F, Dice JF, Difiglia M, Dinesh-Kumar S, Distelhorst CW, Djavaheri-Mergny M, Dorsey FC, Dröge W, Dron M, Dunn WA Jr, Duszenko M, Eissa NT, Elazar Z, Esclatine A, Eskelinen EL, Fésüs L, Finley KD, Fuentes JM, Fueyo J, Fujisaki K, Galliot B, Gao FB, Gewirtz DA, Gibson SB, Gohla A, Goldberg AL, Gonzalez R, González-Estévez C, Gorski S, Gottlieb RA, Häussinger D, He YW, Heidenreich K, Hill JA, Høyer-Hansen M, Hu X, Huang WP, Iwasaki A, Jäättelä M, Jackson WT, Jiang X, Jin S, Johansen T, Jung JU, Kadowaki M, Kang C, Kelekar A, Kessel DH, Kiel JA, Kim HP, Kimchi A, Kinsella TJ, Kiselyov K, Kitamoto K, Knecht E, Komatsu M, Kominami E, Kondo S, Kovács AL, Kroemer G, Kuan CY, Kumar R, Kundu M, Landry J, Laporte M, Le W, Lei HY, Lenardo MJ, Levine B, Lieberman A, Lim KL, Lin FC, Liou W, Liu LF, Lopez-Berestein G, López-Otín C, Lu B, Macleod KF, Malorni W, Martinet W, Matsuoka K, Mautner J, Meijer AJ, Meléndez A, Michels P, Miotto G, Mistiaen WP, Mizushima N, Mograbi B, Monastyrska I, Moore MN, Moreira PI, Moriyasu Y, Motyl T, Münz C, Murphy LO, Naqvi NI, Neufeld TP, Nishino I, Nixon RA, Noda T, Nürnberg B, Ogawa M, Oleinick NL, Olsen LJ, Ozpolat B, Paglin S, Palmer GE, Papassideri I, Parkes M, Perlmutter DH, Perry G, Piacentini M, Pinkas-Kramarski R, Prescott M, Proikas-Cezanne T, Raben N, Rami A, Reggiori F, Rohrer B, Rubinsztein DC, Ryan KM, Sadoshima J, Sakagami H, Sakai Y, Sandri M, Sasakawa C, Sass M, Schneider C, Seglen PO, Seleverstov O, Settleman J, Shacka JJ, Shapiro IM, Sibirny A, Silva-Zacarin EC, Simon HU, Simone C, Simonsen A, Smith MA, Spanel-Borowski K, Srinivas V, Steeves M, Stenmark H, Stromhaug PE, Subauste CS, Sugimoto S, Sulzer D, Suzuki T,

- Swanson MS, Tabas I, Takeshita F, Talbot NJ, Tallóczy Z, Tanaka K, Tanaka K, Tanida I, Taylor GS, Taylor JP, Terman A, Tettamanti G, Thompson CB, Thumm M, Tolkovsky AM, Tooze SA, Truant R, Tumanovska LV, Uchiyama Y, Ueno T, Uzcátegui NL, van der Klei I, Vaquero EC, Vellai T, Vogel MW, Wang HG, Webster P, Wiley JW, Xi Z, Xiao G, Yahalom J, Yang JM, Yap G, Yin XM, Yoshimori T, Yu L, Yue Z, Yuzaki M, Zabirnyk O, Zheng X, Zhu X, Deter RL. Guidelines for the use and interpretation of assays for monitoring autophagy in higher eukaryotes. *Autophagy* 2008;4:151-75.
80. Ren W, Korchin B, Lahat G, Wei C, Bolshakov S, Nguyen T, Merritt W, Dicker A, Lazar AJ, Sood A, Pollock RE, Lev D. Combined vascular endothelial growth factor receptor/epidermal growth factor receptor blockade with chemotherapy for treatment of local, uterine, and metastatic soft tissue sarcoma. *Clin Cancer Res* 2008;14:5466–75.
81. Lee JH, Choy ML, Ngo L, Foster SS, Marks PA. Histone deacetylase inhibitor induces DNA damage, which normal but not transformed cells can repair. *PNAS* 2010;107:14639–44.
82. Fuino L, Bali P, Wittmann S, Donapaty S, Guo F, Yamaguchi H, Wang HG, Atadja P, Bhalla K. Histone deacetylase inhibitor LAQ824 down-regulates Her-2 and sensitizes human breast cancer cells to trastuzumab, taxotere, gemcitabine, and epothilone B. *Mol Cancer Ther* 2003;2:971–84.
83. Pauer LR, Olivares J, Cunningham C, Williams A, Grove W, Kraker A, Olson S, Nemunaitis J. Phase I study of oral CI-994 in combination with carboplatin and paclitaxel in the treatment of patients with advanced solid tumors. *Cancer Invest* 2004;22:886–96.

84. Banuelos CA, Banath JP, MacPhail SH, Zhao J, Reitsema T, Olive PL.  
Radiosensitization by histone deacetylase inhibitor PCI-24781. *Clin Cancer Res* 2007;13:6816–26.
85. Hannay JA, Liu J, Zhu Q, Bolshakov S, Li L, Pisters P, Lazar AJ, Yu D, Pollock RE, Lev D. Rad51 overexpression contributes to chemoresistance in human soft tissue sarcoma cells: a role for p53/activator protein 2 transcriptional regulation. *Mol Cancer Ther* 2007;6:1650-60.
86. Shinohara A, Ogawa H, Ogawa T. Rad51 protein involved in repair and recombination in *S. cerevisiae* is a RecA-like protein. *Cell* 1992;69:457-70.
87. Baumann P, West SC. Role of the human RAD51 protein in homologous recombination and double-stranded-break repair. *Trends Biochem Sci* 1998;23:247-51.
88. Rocchi P, Tonelli R, Camerin C, Purgato S, Fronza R, Bianucci F, Guerra F, Pession A, Ferreri AM. p21Waf1/Cip1 is a common target induced by short-chain fatty acid HDAC inhibitors (valproic acid, tributyrin and sodium butyrate) in neuroblastoma cells. *Oncol Rep* 2005;13:1139-44.
89. Hasselbach L, Haase S, Fischer D, Kolberg HC, Sturzbecher HW.  
Characterization of the promoter region of the human DNA-repair gene Rad51. *Eur J Gynaecol Oncol* 2005;26:589–98.
90. Zhao Y, Lu S, Wu L, Chai G, Wang H, Chen Y, Sun J, Yu Y, Zhou W, Zheng Q, Wu M, Otterson GA, Zhu WG. Acetylation of p53 at lysine 373/382 by the histone deacetylase inhibitor depsipeptide induces expression of p21Waf1/Cip1. *Mol Cell Bio* 2006;26:27827–90.



91. Menon AG, Anderson KM, Riccardi VM, Chung RY, Whaley JM, Yandell DW, Farmer GE, Freiman RN, Lee JK, Li FP. Chromosome 17p deletions and p53 gene mutations associated with the formation of malignant neurofibrosarcomas in von Recklinghausen neurofibromatosis. *PNAS* 1990;87:5435–9.
92. Taylor BS, Barretina J, Socci ND, DeCarolis P, Ladanyi M, Meyerson M, Singer S, Sander C. Functional Copy-Number Alterations in Cancer. *PLOS One* 2008;3(9):e3179.
93. Levine B, Yuan J. Autophagy in cell death: an innocent convict? *J Clin Invest* 2005;115:2679–88.
94. Kondo Y, Kanzawa T, Sawaya R, Kondo S. The role of autophagy in cancer development and response to therapy. *Nat Rev Cancer* 2005;5:726–34.
95. McKinsey TA. Isoform-selective HDAC inhibitors: closing in on translational medicine for the heart. *J Mol Cell Cardiol* 2011;51:491-6.
96. Yaneva M, Li H, Marple T, Hasty P. Non-homologous end joining, but not homologous recombination, enables survival for cells exposed to a histone deacetylase inhibitor. *Nucleic Acids Res* 2005;33:5320–30.
97. Munshi A, Tanaka T, Hobbs ML, Tucker SL, Richon VM, Meyn RE. Vorinostat, a histone deacetylase inhibitor, enhances the response of human tumor cells to ionizing radiation through prolongation of  $\gamma$ -H2AX foci. *Mol Cancer Ther* 2006;5:1967–74.
98. Adimoolam S, Sirisawad M, Chen J, Thiemann P, Ford JM, Buggy JJ. HDAC inhibitor PCI-24781 decreases RAD51 expression and homologous recombination. *PNAS* 2007;104:19482–7.

99. Bindra RS, Glazer PM. Repression of RAD51 gene expression by E2F4/p130 complexes in hypoxia. *Oncogene* 2007;26:2048-57.
100. Koziczak M, Krek W, Nagamine Y. Pocket protein-independent repression of urokinase-type plasminogen activator and plasminogen activator inhibitor 1 gene expression by E2F1. *Mol Cell Biol* 2000;20:2014–22.
101. Croxton R, Ma Y, Song L, Haura EB, Cress WD. Direct repression of the Mcl-1 promoter by E2F1. *Oncogene* 2002;21:1359–69.
102. Crowe DL, Nguyen DC, Tsang KJ, Kyo S. E2F-1 represses transcription of the human telomerase reverse transcriptase gene. *Nucleic Acids Res* 2001;29:2789–94.
103. Marzio G, Wagener C, Gutierrez MI, Cartwright P, Helin K, Giacca M. E2F family members are differentially regulated by reversible acetylation. *J Biol Chem* 2000;275:10887–92.
104. Tao ZF, Lin NH. Chk1 inhibitors for novel cancer treatment. *Anticancer Agents Med Chem* 2006;6:377-88.
105. Ma CX, Janetka JW, Piwnicka-Worms H. Death by releasing the breaks: CHK1 inhibitors as cancer therapeutics. *Trends Mol Med* 2011;17:88-96.
106. Dent P, Tang Y, Yacoub A, Dai Y, Fisher PB, Grant S. CHK1 inhibitors in combination chemotherapy: thinking beyond the cell cycle. *Mol Interv* 2011;11:133-40.
107. Meuth M. Chk1 suppressed cell death. *Cell Div* 2010;5:21.
108. Hishikawa K, Oemar BS, Tanner FC, Nakaki T, Lüscher TF, Fujii T. Connective

- tissue growth factor induces apoptosis in human breast cancer cell line MCF-7. *J Biol Chem* 1999;274:37461-6.
109. Chien W, Yin D, Gui D, Mori A, Frank JM, Said J, Kusuanco D, Marchevsky A, McKenna R, Koeffler HP. Suppression of cell proliferation and signaling transduction by connective tissue growth factor in non-small cell lung cancer cells. *Mol Cancer Res* 2006;4:591-8.
110. Moritani NH, Kubota S, Nishida T, Kawaki H, Kondo S, Sugahara T, Takigawa M. Suppressive effect of overexpressed connective tissue growth factor on tumor cell growth in a human oral squamous cell carcinoma-derived cell line. *Cancer Lett* 2003;192:205-14.
111. Lin BR, Chang CC, Che TF, Chen ST, Chen RJ, Yang CY, Jeng YM, Liang JT, Lee PH, Chang KJ, Chau YP, Kuo ML. Connective tissue growth factor inhibits metastasis and acts as an independent prognostic marker in colorectal cancer. *Gastroenterology* 2005;128:9-23.
112. Chiba T, Yokosuka O, Arai M, Tada M, Fukai K, Imazeki F, Kato M, Seki N, Saisho H. Identification of genes up-regulated by histone deacetylase inhibition with cDNA microarray and exploration of epigenetic alterations on hepatoma cells. *J Hepatol* 2004;41:436-45.
113. Komorowsky C, Ocker M, Goppelt-Struebe M. Differential regulation of connective tissue growth factor in renal cells by histone deacetylase inhibitors. *J Cell Mol Med* 2009;13:2353-64.
114. Cicha I, Goppelt-Struebe M. Connective tissue growth factor: context-dependent

- functions and mechanisms of regulation. *Biofactors* 2009;35:200-8.
115. Chang CC, Shih JY, Jeng YM, Su J, Lin BZ, Chen ST, Chau YP, Yang P, Kuo ML. Connective tissue growth factor and its role in lung adenocarcinoma invasion and metastasis. *J Natl Cancer Inst* 2004;96:364-75.
116. Johnstone RW, Licht JD. Histone deacetylase inhibitors in cancer therapy: is transcription the primary target? *Cancer Cell* 2003;4:13-8.
117. Warrener R, Beamish H, Burgess A, Waterhouse NJ, Giles N, Fairlie D, Gabrielli B. Tumor cell-selective cytotoxicity by targeting cell cycle checkpoints. *FASEB J* 2003;17:1550-2.
118. Klampfer L, Huang J, Shirasawa S, Sasazuki T, Augenlicht L. Histone deacetylase inhibitors induce cell death selectively in cells that harbor activated kRasV12: The role of signal transducers and activators of transcription 1 and p21. *Cancer Res* 2007;67:8477-85.
119. Corral T, Jiménez M, Hernández-Muñoz I, Pérez de Castro I, Pellicer A. NF1 modulates the effects of Ras oncogenes: evidence of other NF1 function besides its GAP activity. *J Cell Physiol* 2003;197:214-24.
120. Larizza L, Gervasini C, Natacci F, Riva P. Developmental abnormalities and cancer predisposition in neurofibromatosis type 1. *Curr Mol Med* 2009;9:634-53.
121. Miller CP, Singh MM, Rivera-Del Valle N, Manton CA, Chandra J. Therapeutic strategies to enhance the anticancer efficacy of histone deacetylase inhibitors. *J Biomed Biotechnol* 2011;2011:514261.
122. Shao Y, Gao Z, Marks PA, Jiang X. Apoptotic and autophagic cell death induced

- by histone deacetylase inhibitors. PNAS 2004;101:18030-5.
123. Rosato RR, Grant S Histone deacetylase inhibitors: insights into mechanisms of lethality. Expert Opin Ther Targets 2005;9:809-24.
124. Ungerstedt JS, Sowa Y, Xu WS, et al. Role of thioredoxin in the response of normal and transformed cells to histone deacetylase inhibitors. PNAS 2005;102:673-8.
125. Lincoln DT, Ali Emadi EM, Tonissen KF, Clarke FM. The thioredoxin-thioredoxin reductase system: over-expression in human cancer. Anticancer Res 2003;23:2425-33.
126. Shao L, Diccianni MB, Tanaka T, Gribi R, Yu AL, Pullen JD, Camitta BM, Yu J. Thioredoxin expression in primary T-cell acute lymphoblastic leukemia and its therapeutic implication. Cancer Res 2001;61:7333-8.
127. Subramanian C, Opiari AW, Bian X, Castle VP, Kwok RP. Ku70 acetylation mediates neuroblastoma cell death induced by histone deacetylase inhibitors. PNAS 2005;102:4842-7.
128. Fantin VR, Richon VM. Mechanisms of resistance to histone deacetylase inhibitors and their therapeutic implications. Clin Cancer Res 2007;13:7237-42.
129. Klionsky DJ. Autophagy. Curr Biol 2005;15:R282-3.
130. Johansen T, Lamark T. Selective autophagy mediated by autophagic adapter proteins. Autophagy 2011;7:279-96.
131. Schwartz LM, Smith SW, Jones ME, Osborne BA. Do all programmed cell deaths occur via apoptosis?. PNAS 1993;90:980–984.

132. Shen S, Kepp O, Michaud M, Martins I, Minoux H, Metivier D, Maiuri MC, Kroemer RT, Kroemer G. Association and dissociation of autophagy, apoptosis and necrosis by systematic chemical study. *Oncogene* 2011;30:4544-56.
133. Kroemer G, Levine B. Autophagic cell death: the story of a misnomer. *Nat Rev Mol Cell Biol* 2008;9:1004-10.
134. Clarke PG, Puyal J. Autophagic cell death exists. *Autophagy* 2012;8:867-9.
135. Gordy C, He YW. The crosstalk between autophagy and apoptosis: where does this lead? *Cell* 2012;3:17-27.
136. Pyo JO, Jang MH, Kwon YK, Lee HJ, Jun JI. Essential roles of Atg5 and FADD in autophagic cell death: dissection of autophagic cell death into vacuole formation and cell death *J Biol Chem* 2005;280:20722-9.
137. Yousefi S, Perozzo R, Schmid I, Ziemiecki A, Schaffner T, Scapozza L, Brunner T, Simon HU. Calpain-mediated cleavage of Atg5 switches autophagy to apoptosis. *Nat Cell Biol* 2006;8:1124-32.
138. Chen and Karantza-Wadsworth. Role and regulation of autophagy in cancer. *Biochim Biophys Acta* 2009;1516–1523.
139. Carew JS, Nawrocki ST, Kahue CN, Zhang H, Yang C, Chung L, Houghton JA, Huang P, Giles FL, Cleveland JL. Targeting autophagy augments the anticancer activity of the histone deacetylase inhibitor SAHA to overcome Bcr-Abl-mediated drug resistance. *Blood* 2007;33:313–322.
140. Apel, I.Herr, H. Schwarz, H.P. Rodemann, A.Mayer, Blocked autophagy sensitizes resistant carcinoma cells to radiation therapy. *Cancer Res*

2008;68:1485–1494.

141. Qu X, Yu J, Bhagat G, Furuya N, Hibshoosh H, Troxel A, Rosen J, Eskelinen EL, Mizushima N, Ohsumi Y, Cattoretti G, Levine B. Promotion of tumorigenesis by heterozygous disruption of the beclin 1 autophagy gene. *J Clin Invest* 2003;112:1809–1820.
142. Aita VM, Liang XH, Murty VV, Pincus DL, Yu W, Cayanis E, Kalachikov S, Gilliam TC, Levine B. Cloning and genomic organization of beclin 1, a candidate tumor suppressor gene on chromosome 17q21. *Genomics* 1999;59:59–65.
143. Liang XH, Jackson S, Seaman M, Brown K, Kempkes B, Hibshoosh H, Levine B. Induction of autophagy and inhibition of tumorigenesis by beclin 1. *Nature* 1999;402:672–676.
144. Lum JJ, Bauer DE, Kong M, Harris MH, Li C, Lindsten T, Thompson CB. Growth factor regulation of autophagy and cell survival in the absence of apoptosis. *Cell* 2005;120:237–248.
145. Carew JS, Medina EC, Esquivel JA, Mahalingam D, Swords R, Kelly K, Zhang H, Huang P, Mita AC, Mita MM, Giles FJ, Nawrocki ST. Autophagy inhibition enhances vorinostat-induced apoptosis via ubiquitinated protein accumulation. *J Cell Mol Med* 2010;14:2448-59.
146. Gammoh N, Marks PA, Jiang X. Curbing autophagy and histone deacetylases to kill cancer cells. *Autophagy* 2012;8(10).
147. Chen N, Debnath J. Autophagy and tumorigenesis. *FEBS Lett* 2010;584:1427–

35.

148. Singh SB, Davis AS, Taylor GA, Deretic V. Human IRGM induces autophagy to eliminate intracellular mycobacteria. *Science* 2006;313:1438–41.
149. Yu C, Wang L, Lv B, Lu Y, Zeng L, Chen Y, Ma D, Shi T, Wang L. TMEM74, a lysosome and autophagosome protein, regulates autophagy. *Biochem Biophys Res Commun* 2008;369:622–9.
150. Espert L, Denizot M, Grimaldi M, Robert-Hebmann V, Gay B, Varbanov M, Codogno P, Biard-Piechaczyk M. Autophagy is involved in T cell death after binding of HIV-1 envelope proteins to CXCR4. *J Clin Invest* 2006;116:2161–72.
151. Karolczak-Bayatti M, Sweeney M, Cheng J, Edey L, Robson SC, Ulrich SM, Treumann A, Taggart MJ, Europe-Finner GN. Acetylation of heat shock protein 20 (Hsp20) regulates human myometrial activity. *J Biol Chem* 2011;286:34346-55.
152. Segurado M, Tercero JA. The S-phase checkpoint: targeting the replication fork. *Biol Cell* 2009;101:617-27.
153. Bartek J, Lukas J. Mammalian G1- and S-phase checkpoints in response to DNA damage. *Curr Opin Cell Biol* 2001;13:738-47.
154. Bartek J, Lukas J. Chk1 and Chk2 kinases in checkpoint control and cancer. *Cancer Cell* 2003;3:421-9.
155. Deardorff MA, Bando M, Nakato R. HDAC8 mutations in Cornelia de Lange syndrome affect the cohesin acetylation cycle. *Nature* 2012;489:313-7.
156. Nasmyth K. Cohesin: a catenase with separate entry and exit gates? *Nat Cell Biol*



2011;13:1170-7.

158. Zhang J, Shi X, Li Y, Kim BJ, Jia J, Huang Z, Yang T, Fu X, Jung SY, Wang Y, Zhang P, Kim ST, Pan X, Qin J. Acetylation of Smc3 by Eco1 is required for S phase sister chromatid cohesion in both human and yeast. *Mol Cell* 2008;31(1):143-51.

## **Vita**

Gonzalo Lopez Jr was born in Kingsville, Texas on August 3, 1978, the son of Emelda Lopez and Gonzalo Lopez Sr. Upon graduating from HM King High School in Kingsville, Texas, he enrolled at Texas A&M University – Kingsville in his same home town. He received a Bachelor of Science degree in Biology from Texas A&M University – Kingsville in 2002. He then entered the Masters program in Chemistry at Texas A&M University – Kingsville while working as a graduate researcher at the Natural Toxins Research Center under the guidance of Dr. John C. Perez. He received a Masters of Science in Chemistry in 2006 from Texas A&M University – Kingsville. During his time at Texas A&M University – Kingsville, he was a co-author on a few manuscripts studying the biomedical aspects of peptides derived from snake venom. In 2006, he enrolled in the Graduate School of Biomedical Science program at UT MD Anderson.

Permanent address:

1906 John

Kingsville, Texas 78363